Experimental and Numerical Investigations of Forming Behavior in Ti-6Al-4V Alloy at Elevated Temperatures

THESIS

Submitted in partial fulfilment
of the requirements for the degree of
DOCTOR OF PHILOSOPHY

by

NITIN RAMESH KOTKUNDE
ID No 2012PHXF542H

Under the Supervision of
Dr. AMIT KUMAR GUPTA

BIRLA INSTITUTE OF TECHNOLOGY AND SCIENCE, PILANI
2015

BIRLA INSTITUTE OF TECHNOLOGY AND SCIENCE, PILANI

CERTIFICATE

This is to certify that the thesis entitled "**Experimental and Numerical Investigations of Forming Behavior in Ti-6Al-4V Alloy at Elevated Temperatures**" and submitted by Mr. **Nitin Ramesh Kotkunde ID No: 2012PHXF542H** for award of Ph.D. Degree of the Institute embodies original work done by him under my supervision.

Signature of the Supervisor :

Name in capital letters : **Dr. Amit Kumar Gupta**

Designation : **Associate Professor**

Date :

ACKNOWLEDGEMENTS

I would like to express my gratitude to my supervisor Prof. **Amit Kumar Gupta** for his strong support, patience and constant availability for technical discussions. I feel motivated and encouraged after technical discussions with him. I would like to thank him for being my inspiration and well-wisher. This thesis is the outcome of the kind co-operation, good-will, and technical and moral support extended by **Dr. Swadesh Kumar Singh**, Professor in Mechanical Engineering Department, GRIET, Hyderabad. He provided me an opportunity to use the lab facility available at GRIET

I am highly indebted to the **Department of Science and Technology (DST)**, Govt. of India for their project grant ***SERB-DST, SR/FTP/ETA-0056/2011***, which helped in procuring the test facilities and raw material to conduct this research.

I am grateful to my doctoral advisory committee members, **Prof. Daseswara Rao Yendluri** (Head of Department, Mechanical Engineering) and **Prof. N Suresh Kumar Reddy** for their valuable advices during semester reviews. I am grateful to them for their suggestions in bringing this thesis into final form. I also take this opportunity to thank **Prof. B. N. Jain**, Vice – Chancellor, BITS-Pilani and **Prof. V.S. Rao**, Director, BITS-Pilani, Hyderabad Campus for providing a research environment.

Co-authors in the my published papers deserve very special thanks. The valuable inputs from them really helpful for publishing the papers in the reputed international journals and conferences.

I am thankful to few of my colleagues, Dr. Sandip Deshmukh, Dr. Pramod Salunkhe, Dr. Syed Mujahed Hussaini, Dr. Akhlad Iqbal, Mr. Kurra Suresh, Mr.

Khalid Anwar, Mr. G. Pavan Kumar, who supported me during my difficult time. I am extremely grateful to all the faculty and staff of Mechanical Engineering Department. I owe special thanks to Workshop staff for providing me the unstinted cooperation and help whenever required. Also, I would like to thank the technical staff at GRIET for their corporation and help during the experimentation there.

I would like to thank several colleagues beyond BITS-Pilani University who in one way or another contributed in this research. I would like to express my particular gratitude to **Dr.V. V. Kutumba Rao**, Former Professor, IIT BHU for sharing part of his invaluable knowledge in fractography area. I would like to thank **Prof. Jeong-Whan Yoon** form Deakin University in Australia who openly answered my questions and doubts in the area of material models. In addition, I would like to thank **Prof. K. Narasimhan, IIT Mumbai** for a valuable technical suggestions on Forming Limit Diagram. Also, I would express my gratitude towards **Hyderabad Central University** and **BHEL**, **Hyderabad** for providing me the facility to do the Scanning Electron Microscope (SEM) analysis.

Most of all I would like to thank my wife **Piyusha** for her unyielding devotion and love, support, encouragement and quiet patience. My deepest appreciation also goes to my **parents** and only sister **Mrs. Dipali** for their faith in me and allowing me to be as ambitious as I wanted. Also I would like to thank my close friends and other family members for their constant support and guidance.

Nitin Ramesh Kotkunde

ABSTRACT

In this thesis work, experimental and numerical investigations on forming behavior of Ti-6Al-4V alloy at elevated temperatures have been carried out. Accurate determination of material properties and flow stress behavior is an essential prerequisite for developing required material model in order to analyze the forming behavior of a material. The material properties and flow stress behavior have been studied from room temperature to 400^0C at an interval of 50^0C and wide range of strain rates (10^{-5}, 10^{-4}, 10^{-3} and 10^{-2} s^{-1}) using uniaxial tensile tests. Additionally, fractography study of failed tensile test specimens revealed microvoids and shallow dimples which indicated predominantly ductile failure in Ti-6Al-4V alloy at elevated temperatures.

Formability of Ti-6Al-4V alloy has been evaluated using deep drawing process from room temperature to 400^0C at an interval of 50^0C. Ti-6Al-4V alloy is difficult to draw up to 150^0C and within the experimental range the maximum LDR of 1.86 is obtained at 400^0C. It indicates poor formability of Ti-6Al-4V at elevated temperatures. Failures in the deep drawn cups have been identified in two regions namely, initial (neck) and final (wall) failure. The fractography in neck region revealed failure due to excessive tensile stresses. However, in wall region, failure has been observed due to excessive shear stresses. The quality of successfully drawn cups has been evaluated based on thickness distribution and earing profile. The uniform thickness distribution is obtained at higher temperature with optimum blank diameter and a predominant earing tendency with four ears has been observed in all the deep drawn cups at elevated temperatures. Forming Limit Curve (FLC) has been determined experimentally for Ti-6Al-4V alloy at 400^0C by conducting a Nakazima test. The various qualitative aspects of

stretching process such as LDH diagram, thickness distribution of stretched specimens have been investigated at 400^0C.

For theoretical and numerical analysis, various advanced anisotropic yield criteria namely, Hill 1948, Barlat 1989, Barlat 1996, Barlat 2000 and Cazacu Barlat have been developed at elevated temperatures. Cazacu Barlat yield criterion is found to be the most suited model for Ti-6Al-4V alloy among the developed anisotropic yield criteria, since anisotropy in yielding and stress asymmetry resulted in excellent validation of yield function with experimental data points. Additionally, different constitutive models viz., *m-FB*, *JC*, *m-Arr*., *m-ZA* and *MTS* have been developed from room temperature to 400^0C at an interval of 50^0C and wide range of strain rates (10^{-5}, 10^{-4}, 10^{-3} and 10^{-2} s^{-1}). Among all the considered models, *MTS* model is preferred for prediction of flow stress of Ti-6Al-4V alloy.

Theoretical FLCs have been determined using Marciniak Kuczynski (M-K) theory incorporating the developed yield criteria and constitutive models. The effect of yield model is more pronounced than the effect of constitutive model for theoretical FLCs prediction. The Cazacu Barlat yield criterion with *m-Arr.* constitutive model is found to be the best in predicting the theoretical FLC of Ti-6Al-4V alloy at 400^0C. The experimental and theoretical results of deep drawing and stretching process have been validated with FE analysis. The important formability aspects such as thickness distribution, earing profile, LDH and FLC have been investigated. FE analysis with Cazacu Barlat yield criterion is found to be in the best agreement with the experimental and theoretical results of forming behavior of Ti-6Al-4V alloy at elevated temperatures.

Keywords: Formability, Ti-6Al-4V Alloy, Anisotropic Yield Criteria, Constitutive Models, FLC, M-K Theory, FE Analysis.

TABLE OF CONTENTS

ACKNOWLEDGEMENTS iii

ABSTRACT v

TABLE OF CONTENTS vii

LIST OF TABLES xi

LIST OF FIGURES xiii

LIST OF ABBREVIATIONS xvii

LIST OF SYMBOLS xviii

CHAPTER 1: INTRODUCTION 1

1.1 Introduction to Ti-6Al-4V Alloy 2

1.2 Fundamental of Sheet Metal Forming Process 4

1.3 Material Models for Numerical Analysis of Sheet Metal Forming Processes 6

1.4 Finite Element Analysis of Sheet Metal Forming Processes 8

1.5 Methodology Adopted for the Study 10

1.6 Organization of the Thesis 12

CHAPTER 2: LITERATURE REVIEW 15

2.1 Introduction 15

2.2 Fundamental of Deep Drawing Process 17

2.3 Mechanical Properties 20

2.4 Material Models for Numerical Analysis of Sheet Metal Forming Processes 26

2.4.1 Yield Criteria 27

2.4.2 Constitutive Models 32

2.5 Forming Limit Diagram (FLD) 34

2.6 Finite Element Analysis of Sheet Metal Forming Process 38

2.7 Objectives of the Study 40

2.8 Summary of Literature Review 41

CHAPTER 3: EXPERIMENTAL INVESTIGATIONS OF FORMING BEHAVIOR FOR TI-6AL-4V ALLOY 42

3.1 Material Properties 42

3.2 Microstructure and Fractography Study 54

3.3 Experimental Investigation on Deep Drawing of Ti-6Al-4V Alloy 58

3.3.1 Experimental Set up for Deep Drawing Process 58

3.3.2 Failure Study in Deep Drawing Cups 62

3.3.3 Formability Study 66

3.4 Summary 70

CHAPTER 4: MATERIAL MODELS FOR NUMERICAL ANALYSIS OF SHEET METAL FORMING PROCESS 71

4.1. Yield Criteria 71

4.1.1 Hill 1948 Yield Criterion 72

4.1.2 Barlat 1989 Yield Criterion 72

4.1.3 Baralt 1996 Yield Criterion 74

4.1.4 Barlat 2000 Yield Criterion 75

4.1.5 Cazacu Barlat Yield Criterion 77

4.1.6 Comparison of Yield Criteria 79

4.2 Constitutive models 82

4.2.1 Modified Fields-Backofen Model 82

4.2.2 Johnson Cook Model 84

4.2.3 Modified Arrhenius Model 85
4.2.4 Modified Zerilli Armstrong Model 87
4.2.5 Mechanical Threshold Stress model 88
4.2.6 Comparison of constitutive models 90
4.3 Summary 94
CHAPTER 5: EXPERIMENTAL AND THEORETICAL STUDIES OF FORMING LIMIT DIAGRAM 95
5.1 Introduction to Forming Limit Diagram 95
5.2 Experimental Forming Limit Curve 98
5.3 Fractography Study 102
5.4 Theoretical Analysis for Forming Limit Curve 104
5.5 Results and Discussion 109
5.6 Summary 115
CHAPTER 6: FINITE ELEMENT ANALYSIS OF SHEET METAL FORMING PROCESS 116
6.1 Introduction to Finite Element Analysis for Sheet metal Forming Process 116
6.2 Pre-processing of Deep Drawing Process 120
6.3 Finite Element Analysis of Deep Drawing Process 125
6.3.1 Failure Study 125
6.3.2 Thickness Distribution 127
6.3.3 Earing Profile 129
6.4 Finite Element Analysis of Stretching Process 131
6.4.1 Thickness Distribution 132
6.4.2 Limiting Dome Height 134
6.4.3 Forming Limit Curve 136

6.5 Summary 139

CHAPTER 7: CONCLUSIONS 140

7.1 Salient Conclusions 140

7.2 Specific Contributions to the Research 143

7.3 Further Scope of Work 144

REFERENCES 145

LIST OF PUBLICATIONS 159

BRIEF BIOGRAPHY OF THE SUPERVISOR 163

BRIEF BIOGRAPHY OF THE CANDIDATE 164

LIST OF TABLES

Table 3.1: Chemical composition of as received Ti–6Al–4V alloy 42

Table 3.2: Strain hardening exponent (*n*) and strain rate sensitivity (*m*) at various temperatures 48

Table 3.3: Anisotropic coefficient (*r*) for Ti-6Al-4V alloy at various temperatures..... 51

Table 3.4: Variation of yield strength (σ_y), ultimate tensile strength (σ_{ut}) and % ductility at various temperatures..... 52

Table 3.5: Biaxial material properties and compressive yield stress for Ti-6Al-4V alloy.... 53

Table 3.6: Technical specifications of experimental test rig..... 60

Table 3.7: LDR at various temperatures..... 67

Table 4.1: The material constants of Barlat 1989 yield criterion for Ti-6Al-4V alloy 73

Table 4.2: The material constants of Barlat 1996 yield criterion for Ti-6Al-4V alloy 75

Table 4.3: The material constants of Barlat 2000 yield criterion for Ti-6Al-4V alloy 77

Table 4.4: The material constants of Cazacu-Barlat yield criterion for Ti-6Al-4V alloy..... 78

Table 4.5: Mechanical tests required for various considered yield criteria..... 81

Table 4.6: Material constants for modified Fields–Backofen (*m-FB*) constitutive model.... 84

Table 4.7: Material constants for Johnson Cook (*JC*) constitutive model 85

Table 4.8: Material constants for modified Arrhenius (*m-Arr*.) model..... 87

Table 4.9: Coefficients of Equation β with Zener-Hollomon parameter (*Z*)..... 87

Table 4.10: Material constants for modified Zerilli Armstrong (*m-ZA*) model 88

Table 4.11: Material constants for Mechanical Threshold Stress (*MTS*) model..... 90

Table 4.12: Comparison of various constitutive models based on statistical measures and number of material constants 92

Table 5.1: Final f_0 values used for the various theoretical FLC predictions 110

Table 5.2: Fréchet Distance between FLC predictions 114

Table 6.1: Material properties as an input for FE analysis..... 122

Table 6.2: Physical properties for Ti-6Al-4V alloy at room temperature 123

Table 6.3: Physical properties for Ti-6Al-4V alloy at various temperatures 123

Table 6.4: Variation of coefficient of friction value with temperature 123

Table 6.5: Average absolute error for experimental thickness..... 129

Table 6.6: Total CPU time taken for simulation 130

Table 6.7: Average absolute error for experimental thickness..... 134

LIST OF FIGURES

Fig.1.1: Common applications of sheet metal forming processes 2

Fig.1.2:Sheet metal forming applications for Ti-6Al-4V alloy 3

Fig.1.3: Schematic of circular deep drawing process 4

Fig.1.4: Parameters influencing sheet metal formability 5

Fig.1.5: Methodology adopted for the present work..... 11

Fig.1.6: Organization of thesis..... 14

Fig.2.1: Four different zones in deep drawing 20

Fig.2.2: Forces in deep drawing of a cylindrical cup 20

Fig.2.3: Important influencing factors affecting the experimental FLD 36

Fig.2.4: Various theoretical models available for FLD prediction 36

Fig.3.1: Dimension of tensile test specimen as per *ASTM E8/E8M-11* sub-sized standard 43

Fig.3.2: Computerized UTM with magnified view of high temperature contact type extensometer 44

Fig.3.3: 3-zone split furnace attached to UTM for high temperature tensile testing 45

Fig.3.4: Representative broken tensile test specimen after tests at various temperatures ... 45

Fig. 3.5: Representative true stress-strain curves at various temperatures (a) 10^{-5} s^{-1} strain rate (b) 10^{-2} s^{-1} strain rate 46

Fig. 3.6: Representative true stress vs true strain curves at various strain rates (a) 100^0C (b) 400^0C 46

Fig. 3.7: Specimen orientations with respect to the sheet rolling direction..... 50

Fig. 3.8: Dimensions of specimen used for anisotropic coefficient (*r*) calculation..... 50

Fig.3. 9: Optical micrographs showing the key micro-constituents in Ti-6Al-4V alloy at 200X magnification..... 54

Fig.3.10: Representative fractography images of fracture tensile specimens over the range of magnification..... 56

Fig.3.11: EDS analysis of inclusion portion show in Fig. 3.10 (f) 57

Fig. 3.12: Basic geometry in a simple cup drawing process..... 58

Fig. 3.13: Experimental test rig for deep drawing process 59

Fig. 3.14: Induction heating coil arrangement for deep drawing process up to 400^0C..... 60

Fig. 3.15: Dimensions of tooling geometry used for deep drawing process..... 61

Fig.3.16: Type of failures occurred during experimentation (a) neck failure at 50^0 C (b) neck failure at 100^0 C (c) fracture at upper wall at 400^0C 63

Fig.3.17: SEM fractography images of neck region at room temperature..... 65

Fig.3.18: SEM fractography images of neck region at 100^0C..... 65

Fig.3.19: SEM fractography images of wall region at 400^0C..... 65

Fig. 3.20: Successfully drawn cups at various temperatures (a) 200^0C (b) 300^0C (c) 400^0C..... 67

Fig. 3.21: Representative thickness distribution with variation of (a) temperature (b) blank diameter 68

Fig. 3.22: Representative punch vs. load displacement for 52 mm blank diameter with variation of temperature 68

Fig. 3.23: Representative earing profile of 54 mm blank diameter at 400^0C 69

Fig.4.1:Representative yield loci for Ti-6Al-4V alloy at 400^0C..... 80

Fig.4.2: Representative planer distribution of variation (a) yield stress (b) anisotropy coefficient..... 81

Fig.4.3: Representative flow stress prediction using various constitutive model prediction..... 91

Fig.4.4: Correlation coefficient for various constitutive models..... 93

Fig.5.1: Forming limit diagram as defined by Keeler and Goodwin 96

Fig.5.2: Forming limit diagram for necking and fracture 97

Fig.5.3: FLD test setup as per *ASTM E2218* standard 98

Fig.5.4: Dimension of specimens used for experimental FLC 99

Fig.5.5: Experimental FLC for Ti-6Al-4V alloy at 400^0C..... 100

Fig.5.6: LDH diagram for Ti-6Al-4V alloy at 400^0C 101

Fig.5.7: Representative thickness distribution at various widths of specimen 101

Fig.5.8: Representative SEM images (a & b) uniaxial tension region (*120 mm×30 mm*) (c & d) plane strain region (*120 mm×80 mm*) (e & f) biaxial tension region (*120 mm × 120 mm*) 103

Fig.5.9: Geometric imperfection of the Marciniak Kuczinsky (M-K) model..... 105

Fig.5.10: Flow chart of algorithm for plotting theoretical FLCs 109

Fig.5.11: Variation of f_0 value for FLC prediction 111

Fig.5.12: Theoretical FLC using various yield criteria..... 113

Fig.6.1: Schematic representation of step used in FE analysis 117

Fig.6.2: Mesh adaptivity (a) blank (b) after some deformation..... 119

Fig.6.3: Axisymmetric model for deep drawing process..... 121

Fig.6.4: Representative experimental and FE validation of punch load vs. punch disp. at 400^0C 124

Fig.6.5: Comparison of neck failure at experimentation and FE analysis 126

Fig.6.6: Comparison of chipping of material at experimentation and FE analysis..... 126

Fig.6.7: Representative successfully drawn cups at 400^0C using various yield criteria.... 128

Fig.6.8: Representative thickness distribution using various yield criteria at 400^0C 129

Fig.6.9: Representative earing profile of experimental and simulated cup at 400^0C 130

Fig.6.10: Preprocessing model of stretching setup 132

Fig.6.11: Representative thickness distribution of successfully stretched specimens (a) *120 mm × 120 mm* (b) *120 mm × 80 mm* (c) *120 mm × 30 mm*..... 133

Fig.6.12: Representative thickness at dome using various yield criteria..... 135

Fig.6.13: LDH using various yield criteria 135

Fig.6.14: Representative simulated specimens at plane strain condition..... 137

Fig.6.15: Failure strain in simulated FLDs using various yield criteria 138

LIST OF ABBREVIATIONS

HCP	: Hexagonal close packed crystal structure
BCC	: Body centered cubic crystal structure
FCC	: Face centered cubic crystal structure
ASTM	: American Society for Testing and Materials
UTM	: Universal testing machine
CNC	: Computerized numerical control
LDR	: Limiting draw ratio
RT	: Room temperature
FLD	: Forming limit diagram
FLC	: Forming limit curve
SEM	: Scanning electron microscope
EDS	: Energy dispersive spectroscopy
M-K	: Marciniak-Kuaynski
m-FB	: Modified Fields- Backofen model
JC	: Johnson Cook model
m-Arr.	: Modified Arrhenius model
m-ZA	: Modified Zerilli Armstrong model
MTS	: Mechanical threshold model
COF	: Coefficient of friction
LDH	: Limiting dome height

LIST OF SYMBOLS

n	: Strain hardening exponent
K	: Strength coefficient
r	: Anisotropic coefficient (parameter)
r_b	: Biaxial anisotropic coefficient
r_n	: Normal anisotropy
Δr	: Planer anisotropy
σ_y	: Uniaxial yield stress
σ_{ut}	: Ultimate tensile strength
σ_b	: Biaxial yield stress
σ_c	: Compressive yield stress
E	: Modulus of Elasticity
v	: Cross head speed
L_0	: Gauge length
ε_p	: Plastic strain
ε_w	: Width strain
ε_l	: Longitudinal strain
D_p	: Punch diameter
R_p	: Punch corner radius
R_d	: Die corner radius
D_d	: Die opening diameter
D_b	: Blank diameter
T	: Sheet thickness
F	: Size of the yield locus

$\bar{\sigma}$: Equivalent stress

S_i : Principal values of Cauchy deviator

$X'_{1,2}, X''_{1,2}$: Principal values of linearly transformed stress deviator

C : Fourth order transformation tensor

s : Softening ratio

T : Temperature

T_{ref} : Reference temperature

T^* : Homologous temperature

T_m : Melting point temperature

Q : Activation energy

R : Universal gas constant

Z : Zener-Hollomon parameter

σ_a : athermal component

σ_i : Intrinsic stress component

g_{oi}, g_{oe} : Normalized activation energies

K_b : Bolzmann constant

b : Burger vector

Q_0 : Strain hardening rate due to dislocation accumulation

Q_1 : Saturation hardening rate

R : Correlation coefficient

Δ : Average absolute error

S : Standard deviation

ε_1 : Major principal strain

ε_2 : Minor principal strain

h_0^A , h_0^B : Initial thickness of zone A and B respectively

f_0 : Inhomogeneity parameters

$d\overline{\varepsilon_A}, d\overline{\varepsilon_B}$: Equivalent strain

t_A, t_B : Instantaneous thickness of region A and B

ρ : Density

c : Specific heat capacity

α : Thermal coefficient of linear expansion

v : poisson's ratio

CHAPTER 1: INTRODUCTION

Sheet metal forming is a general term for a large group of metal working processes. These processes hold a key role in metal working industries because of its versatility and cost-effectiveness. It eradicates costly operations such as welding, machining and manufactures parts with reduced weight and good mechanical properties with high production rates. Specifically, in automotive and aerospace industries, sheet metal forming processes are extensively used as shown in Fig.1.1. (*Marciniak et al., 2002*). Therefore, sheet metal forming became a backbone of modern manufacturing industry (*Beddoes & Bibby, 1999*).

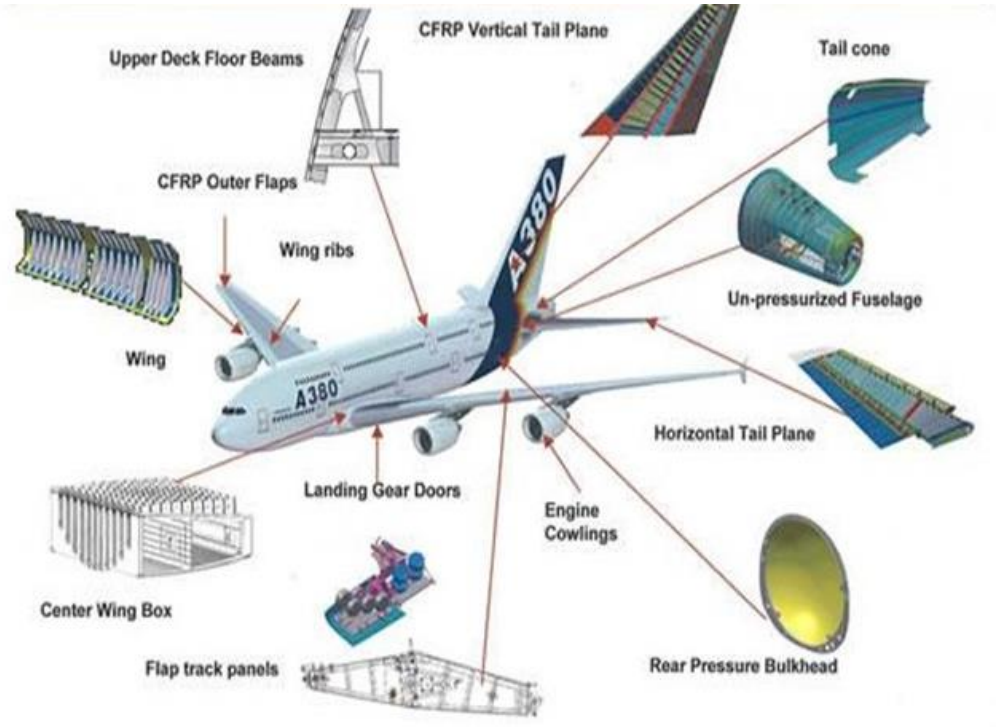

(a) Aerospace sector

(b) Automotive sector

Fig.1.1: Common applications of sheet metal forming processes (*Lange, 1985*).

In the sheet metal manufacturing industry, low carbon steels and austenitic stainless steels have been popularly used for a long time due to their exceptional formability at room temperature, strength, good surface finish, and low cost (*Brammar & Harris, 1975*). Nowadays, because of superior properties, demand of light weight alloys such as magnesium alloy, titanium alloy has increased significantly in automotive and aerospace industries (*Boyer et al., 1994).* However, despite having excellent properties, the light weight alloys have been ranked far behind than steels due to cost and formability issues at room temperature (*Bolt, 2001).* Formability of these alloys is a big challenge at room temperature (*Chen & Chiu, 2005).* Formability of these light weight alloys can be greatly improved at elevated temperatures (*Beal et al., 2006).*

1.1 Introduction to Ti-6Al-4V Alloy

Titanium and its alloys exhibit a unique combination of mechanical and physical properties and corrosion resistance which have made them desirable for critical,

demanding aerospace, industrial, chemical and energy industry service (*Cole & Sherman, 1995*). Among all the titanium alloys, Ti-6Al-4V alloy has been significantly used in many applications (*Lee & Lin, 1998*). The importance of Ti–6Al–4V alloy has been stated from the fact that presently it is most broadly used alloy, accounting for more than 50% of all titanium tonnage in the world (*Lütjering & Williams, 2003*). Ti–6Al–4V alloys exhibit a unique combination of mechanical and physical properties. Precisely, its high specific strength (strength/density) at low to moderate elevated temperature makes this alloy as a desirable candidate for selection of aerospace engines, airframe structures and components (*Cole & Sherman, 1995*). Its admirable corrosion/erosion resistance provides the prime motivation for chemical process, marine, energy and bio-medical industrial service (*Boyer et al., 1994*). Few important applications for Ti-6Al-4V alloy in aerospace and automotive sectors are shown in Fig.1.2.

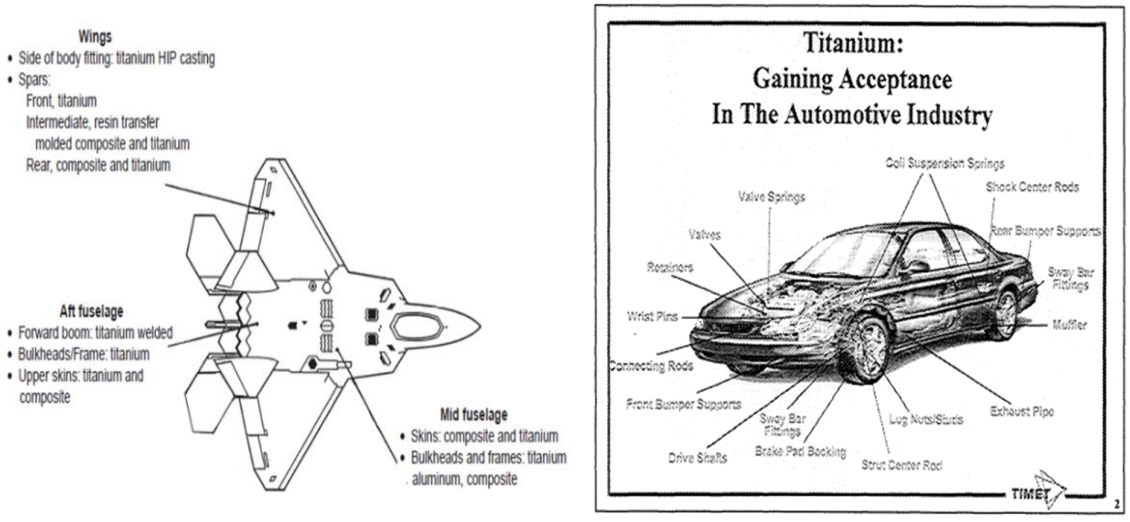

Fig.1.2:Sheet metal forming applications for Ti-6Al-4V alloy (*Beal et al., 2006*)

1.2 Fundamental of Sheet Metal Forming Process

Deep drawing is one of the widely used sheet metal working processes in the industries for producing cup shaped components at a very high rate. Cup drawing, besides its importance as forming process, also serves as a basic test for the sheet metal formability as shown in Fig. 1.3 (*Schuler, 1998*). The numerous process parameters influence the formability in deep drawing process as shown in Fig. 1.4 (*Banabic, 2010*). Therefore, assessing the formability using deep drawing process requires understanding interaction between these process parameters and its influence on the formability of sheet metal (*Keeler & Brazier, 1977*). Furthermore, the complexity involved in these process parameters is increased at elevated temperature (*Taylan et al.,1983*).

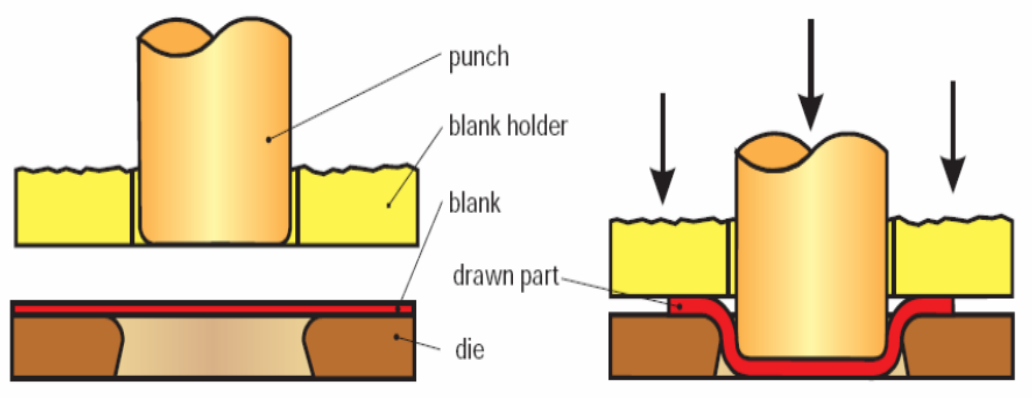

Fig.1.3: Schematic of circular deep drawing process (*Schuler, 1998*)

Formability is difficult to be defined and quantified accurately. It depends on the consequence of material properties and the complex tool sheet interactions (*Singh et al., 2008*). The quality of successful drawn cups has been commonly assessed using Limiting Draw Ratio (LDR), thickness distribution of cup, earing tendency of cup and Forming

Limit Diagram (FLD) (*Aly EI-Domiaty, 1992*). LDR is defined in a simple way as ratio of the diameter of the initial blank to the punch diameter (*Ramaekers, 1999*).

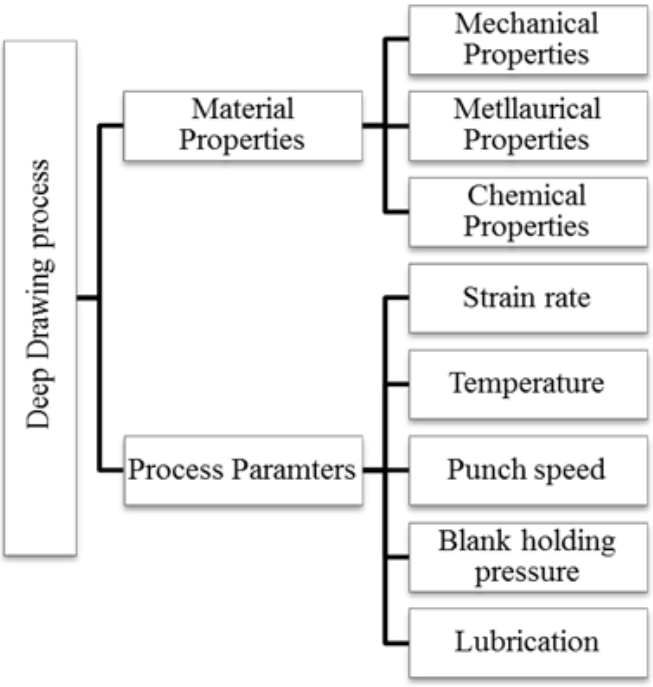

Fig.1.4: Parameters influencing sheet metal formability (*Banabic, 2010*)

Thickness is one of the main quality characteristics in deep drawn cups. Thickness is unevenly distributed in the part after deep drawing. Excessive variation of the thickness may cause stress concentration in the part, leading to the acceleration of damage (*Altan, 2003*). Additionally, earing tendency is one of the considerable parameter for assessing the quality of deep drawn cups. It is one kind of irregularity present in the deep drawn cups at the top periphery. More anisotropic properties lead to greater earing tendency in cup and then decrease efficiency of deep drawing process (*Hosford & Canddell, 2014*).

The Forming Limit Diagram (FLD) is a useful concept for characterizing the formability of sheet metal, which reflects the maximum principal strains that can be

sustained by sheet materials prior to the onset of localized necking (*Keeler SP, 1965*). Generally, there are three methods to establish FLD, i.e. experimental, theoretical and numerical methods (*Schuler, 1998*). The experimental methods based on the grid strain analysis technique for determining FLD are well established, where the principal strains (ε_1, ε_2) have been measured after specimen deformation (*Nakazima et al., 1971*). In experiment, the beginning of the necking depends on the judgment of the person who performed the experiments (*Ghosh, 1975).* Laboratory testing has shown that the FLDs are influenced by several factors (*Banabic, 2010*). However, determining FLDs experimentally can be time consuming and expensive, especially at elevated temperature, resulting in a great interest in employing numerical models to simulate FLDs.

1.3 Material Models for Numerical Analysis of Sheet Metal Forming Processes

The trustworthiness of these numerical models are largely dependent on accurate determination of input material properties and development of various appropriate material models (*Banabic, 2010*). Material properties play a significant role in assessing the formability of sheet metal. The material properties such as strain hardening exponent (n), strain rate sensitivity parameter (m), anisotropy parameter (r), yield stress (σ_y), ultimate tensile strength (σ_{ut}) and ductility play an important role to judge the formability of sheet metals (*Brammar & Harris, 1975*).

Many techniques are available to obtain the required material properties and flow stress behavior of a material (*Gutscher et al., 2004*). The flow stress curves determined using different tests and test conditions do not replicate each other due to effects of stress

state, yield criterion assumption, anisotropy effect, Bauschinger effect, experimental inaccuracies, temperature, and general weakness of the modeling (*Koç et al., 2001*). None of the test methods can be named as the best or optimal (*Koc et al., 2011*). Each has its own specific field of application due to certain straining paths. Among those test systems, the most widely used one is uniaxial tensile test (*Davis, 2004*).

Accuracy of the numerical models is significantly influenced by appropriate selection of material models. Material models are required to predict the plastic behavior of a material in a general stress state. The following two elements are needed to describe plastic behavior of a material.

(a) Yield criterion is a mathematical description for expressing a relationship between the stress components at the moment when plastic 'yielding' occurs

(b) Constitutive models (Hardening models) describe the relationship of the dynamic material properties and flow stress behavior with process parameters (strain, strain rate and temperature).

The yield point in uniaxial tension is established using the stress-strain curve of the material. However, in case of a multi-axial stress state it is more difficult to define a criterion for the transition from the elastic to the plastic state (*Hill, 1950*). A relationship between the principal stresses is needed specifying the conditions under which plastic flow occurs. Such a relationship is usually defined in the form of an implicit function known as the 'yield function (yield criterion)' (*Drucker, 1949*). The plastic flow rule is essential to relates plastic strain rates to stress rates. Associated and non-associated plastic flow rule is used to define relations between plastic strain and stress. The flow rule is said to be 'associated' to the yield function when the plastic strain rate vector, in the

strain space superposed to the stress space, is directed as the outward normal to the (smooth) 'yield surface' which forms the contour of the convex elastic domain. In most of the sheet metal applications associated flow rule are used (*Findley & Michno, 1976*).

The constitutive models are often used to describe the plastic flow properties of the metals and alloys in a form that can be used in computer code to model the forming response of mechanical part members under the prevailing loading conditions. Constitutive models are usually built by using uniaxial tensile test at low strain rates range for forming applications (*Lin & Chen, 2011*). Generally, an ideal constitutive model for metals and alloys should be able to accurately describe the material properties such as strain-rate dependence, forming temperature dependence, strain and strain-rate history dependence, work hardening or strain hardening behavior (both isotropic and anisotropic hardening) (*Liang & Khan, 1999*). However, a complete description of all of these phenomena in a single constitutive model is an extremely difficult task (*Lin et al., 2008*). Moreover, numerical models can be truly reliable only when an appropriate constitutive model is used (*Lin et al., 2009*). Therefore, it is necessary to test the suitability of yield criteria and constitutive models for particular metals and alloys (*Marciniak et al., 2002*).

1.4 Finite Element Analysis of Sheet Metal Forming Processes

Recently, advanced numerical Finite Element (FE) technology and CAE-tools makes a completely virtual process development. FE simulations are used extensively in the sheet metal industry where the technology has contributed to a better understanding of

chosen forming processes and where the prediction capabilities has significantly reduced the time consuming and costly die tryouts. Complex geometries in industrial applications with large deformations, nonlinear materials and contacts can be treated effectively and quickly (*Nielsen, 1997*). Numerous FE codes such as DYNAFORM/ LSDYNA/ ABAQUS/AUTOFORM are available for sheet metal forming simulations (*Tekkaya, 2000*). There are generally two types to methods available for FE analysis of sheet metal forming problems - (a) Implicit method and (b) Explicit method.

Implicit method is not suitable for highly nonlinear problems because of the convergence issue (*Van den Boogaard & Huétink, 2006*). Sheet metal forming is characterized by many nonlinearity not only due to structural and material nonlinearity, but also due to contact between the bodies makes the problem highly nonlinear. However, by using explicit method these nonlinearities can be treated without any problem (*Takuda et al., 2003*). Few advantages of the explicit formulation are:

- Few computations are required per time step.
- The algorithm is simple in logic and structure, so complex non-linarites are easily handled.
- It is reliable in accuracy and completion of computation.

Therefore, more than 60% of reported FE benchmarks are based on dynamic explicit time integration (*Nielsen, 1997*).

Although sheet metal forming has been subject to tremendous experimental and analytical work throughout the years, there are still many mechanisms, especially related to elevated temperature forming of Ti-6Al-4V alloy, influence of material models, finite

element (FE) analysis which are not described and understood in detail. Moreover, in last two decades due to tremendous demand of Ti-6Al-4V alloy in aerospace and automotive industries, elevated temperature forming of Ti-6Al-4V alloy has gained a special attention (*Cole & Sherman, 1995*).Therefore, it is crucial to investigate the possible forming behavior of Ti-6Al-4V alloy at elevated temperatures.

1.5 Methodology Adopted for the Study

The methodology adopted for the research work is shown in Fig. 1.5. The main objective of present work is to investigate the possible forming behavior of Ti-6Al-4V alloy from room temperature to 400^0C. The detailed investigations of various material properties and flow stress behavior are an essential prerequisite to analyze the forming behavior of a material. The material properties and flow stress behavior have been studied from room temperature to 400^0C at an interval of 50^0C with wide range of strain rates (10^{-5}, 10^{-4}, 10^{-3}, 10^{-2} s^{-1}) using uniaxial tensile tests. Microstructure and fractography investigations on failed tensile test specimens have been done at elevated temperatures.

The formability of Ti-6Al-4V alloy has been investigated from room temperature to 400^0C at interval of 50^0C using deep drawing process. The failures in the deep drawn cups have been identified namely; neck and wall failure and fractography study has been carried out. The various important qualitative aspects of deep drawn cups such as LDR, thickness distribution, earing profile have been studied at elevated temperatures. Furthermore, FLC has been investigated experimentally at 400^0C using Nakazima test. The various qualitative aspects of stretching process such as LDH, thickness distribution have been studied.

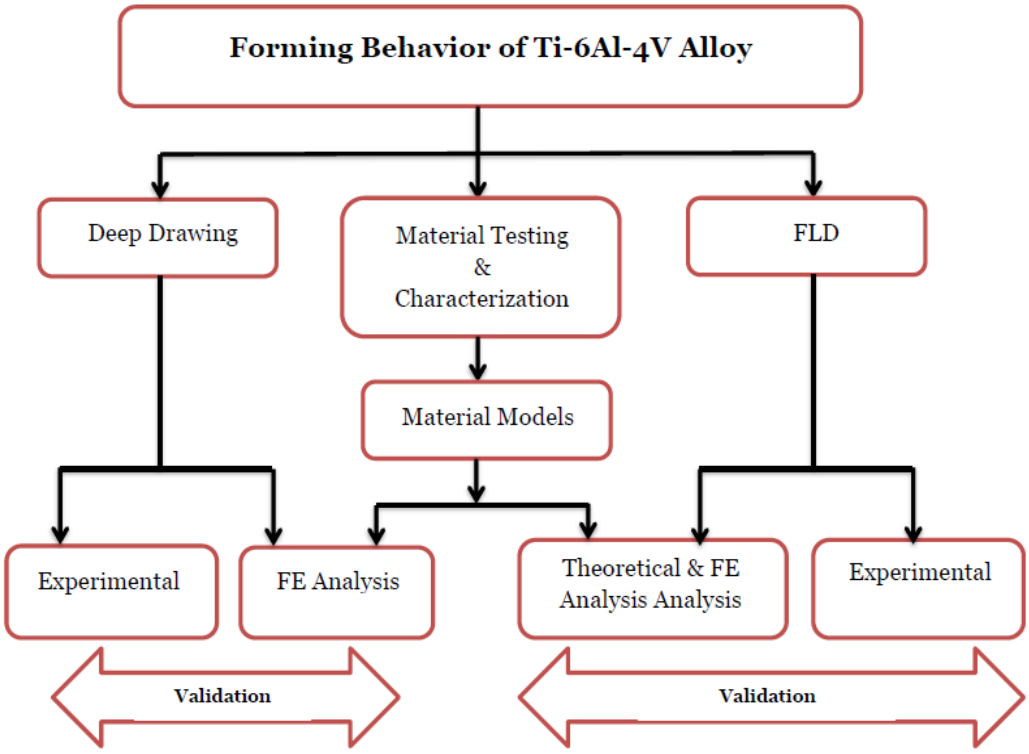

Fig.1.5: Methodology adopted for the present work

Based on the calculated material properties, various anisotropic yield criteria and constitutive models have been developed for Ti-6Al-4V alloy at elevated temperatures. The theoretical FLCs have been determined using Marciniak-Kuczynski (M-K) theory incorporating the developed yield criteria and constitutive models. FE analysis of deep drawing and stretching process has been carried out using DYNAFORM software with LS-Dyna solver. The important formability aspects such as thickness distribution, earing profile, LDH and FLC have been investigated. The results obtained from FE analysis is validated with experimental and theoretical analysis results.

1.6 Organization of the Thesis

The research work is presented in seven chapters as follows:

Chapter – 1: In this chapter, motivation and need of formability studies of Ti-6Al-4V alloy has been presented. The chapter also discusses about methodology adopted and organization of the thesis.

Chapter – 2: In this chapter, extensive literature review of various aspects of sheet metal forming process is presented. The various experimental, theoretical and numerical aspects of sheet metal forming at elevated temperature have been discussed. Based on extensive literature review, research gaps and objectives of the thesis have been identified.

Chapter – 3: This chapter presents experimental investigations of forming behavior of Ti-6Al-4V alloy from room temperature to 400^0C using deep drawing process. The required material properties and flow stress behavior have been studied from room temperature to 400^0C at an interval of 50^0Cwith wide range of strain rates (10^{-5}, 10^{-4}, 10^{-3}, 10^{-2} s^{-1}). The fractography study of failed tensile test specimens and failed deep drawn cups has been comprehensively studied. The various qualitative aspects of deep drawn cups have been investigated.

Chapter – 4: This chapter involves development of materials model for Ti-6Al-4V alloy at elevated temperature. The detailed analysis of various anisotropic yield criteria and its procedure to determine the material constants has been presented. Also, development of various constitutive models for Ti-6Al-4V alloy has been discussed.

Chapter – 5: This chapter discusses about experimental and theoretical investigations of FLCs at 400^0C. Experimental FLC has been determined at 400^0C using Nakazima test. The various qualitative aspects of stretching process such as LDH, thickness distribution and FLC have been studied. M-K theory has been used for theoretical FLCs prediction. . The theoretical FLCs results have been compared with experimental FLC at 400^0C.

Chapter – 6: This chapter involves FE analysis of deep drawing and stretching process at elevated temperatures. The detail procedure for FE analysis using DYNAFORM software has been discussed. The various qualitative aspects of deep drawing and stretching process have been investigated. The results obtained from FE analysis has been compared with experimental and theoretical results.

Chapter – 7: This chapter presents the conclusions and brief contribution towards the research. Further scope of work is also discussed.

The organization of thesis is shown in Fig.1.6. Next chapter presents literature review on major issues involved in sheet metal forming process.

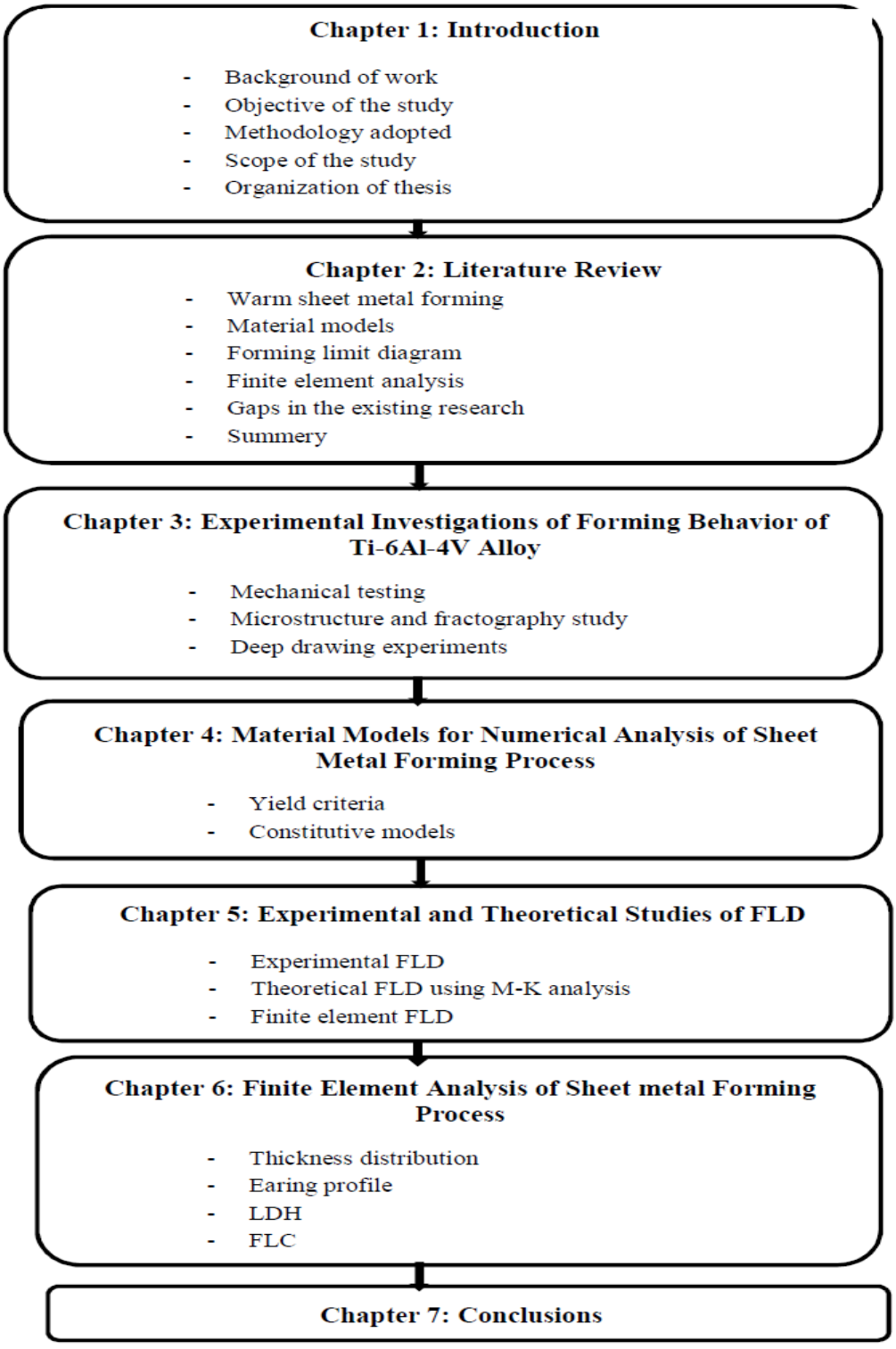

Fig.1.6: Organization of thesis

CHAPTER 2: LITERATURE REVIEW

In this chapter, extensive literature review on major issues involved for sheet metal forming analysis is presented. The various material properties and flow stress behavior essential for elevated temperature sheet metal forming are discussed in detail. Furthermore, various material models required for numerical analysis of sheet metal forming process have been investigated. Various qualitative aspects of deep drawing process and stretching process are presented. Additionally, various important aspects of FE analysis for sheet metal forming process have been discussed.

2.1 Introduction

Conventional deep drawing and stretching operations are the most popular operations in sheet metal forming. Especially, in the automotive and aircraft industries, these operations are widely utilized for forming a various shape and size components (*Brammar & Harris, 1975*). Sheet metal forming technologies are constantly challenged by the improvements in the automotive industry in the last several decades. Due to increasing customer expectations, safety requirements and market competitions, there is a strong need for products, which can be manufactured more successfully, more economically and rapidly to satisfy ever-increasing market needs (*Lange K., 1985*).

On the other hand, in recent years, environmental and safety concerns have forced the industry to choose lighter-yet-safer materials for aerospace and automotive production (*Cole & Sherman, 1995)*. Therefore, 'alternative' materials are being studied to replace conventional steel materials to reduce weight in many parts. For this purpose, various

light weight alloys such as titanium alloy, magnesium alloy, aluminum alloys sheet metal forming gain a special attentions (*Beal et al., 2006*).

Nowadays, titanium alloy are extensively used in aerospace and automotive sectors due to its attractive combination of characteristics in terms of high mechanical properties, elevated corrosion resistance and low density (*Seshacharyulu et al. 2000*). Among all the titanium alloy, Ti-6Al-4V alloy has been significantly used in many applications (*Lee & Lin, 1998).* The importance of Ti–6Al–4V alloy has been stated from the fact that presently it is most broadly used alloy, accounting for more than 50% of all titanium tonnage in the world (*Lütjering & Williams, 2003*). Presently, it has been extensively used in aerospace, automotive sectors for many sheet metal applications (*Beal et al., 2006*).

Despite the obvious advantages of the high strength to weight ratio and corrosion resistance of titanium alloys, they have a distinguishable downside in that their formability is considerably lower than traditional steel alloys at room temperature conditions (*Djavanroodi & Derogar, 2010*). Generally, titanium alloys are considered more difficult to form and often have less predictable forming characteristics than other metallic alloys such as steel and aluminum (*Boyer et al., 1994*). The literature states that titanium alloys can be formed in room temperature or at lower elevated temperatures to some extent. A high degree of spring back is common in cold and hot forming processes due to the high yield stress in combination with a low elastic modulus. Further, the Hexagonal Close Packing (HCP) crystal structure of the α-phase has anisotropic characteristics which implying consequences to the elastic properties (*Lütjering& Williams, 2003*).

Considering this, titanium components are commonly formed at elevated temperatures. Formability of titanium alloys can be greatly improved by warm forming. Since elevated temperature results in decreased flow stress and increased ductility in the sheet, it allows deeper drawing and more stretching to form products (*Odenberger et al., 2013*). Therefore, by increasing the forming temperature an increased formability is obtained in which the spring back and the scatter in yield stress can be reduced.

However, such techniques require heat resistant forming tools and the commonly slow forming velocities with subsequent holding times implying long exposure times at high temperatures and additional costs. As the temperature exposure increases a higher degree of contamination occurs (*Boyer et al.,1994*). Particularly for Ti-6Al-4V alloy, hot forming should generally not be performed at temperatures higher than ~400°C without a protective atmosphere to avoid deterioration of the mechanical properties. When oxygen enrichment of titanium occurs, the material becomes more brittle (*Odenberger, 2005*). Ti-6Al-4V alloy is sensitive to the strain rate and a higher formability is generally obtained when forming titanium alloys at lower strain rates (*Poondla et al., 2009*). Titanium alloys are also sensitive to the Bauschinger effect (stress asymmetry), which is reported to be most pronounced in room temperature (*Filip et al., 2003*).

2.2 Fundamental of Deep Drawing Process

Deep drawing is one of the basic and fundamental process in sheet metal forming (*Chen & Chiu, 2005*). The deep drawing process is defined in various ways. One of the popular definitions according to Schuler Metal Forming Handbook (1998) is: “Deep drawing is a method of forming under compressive and tensile conditions whereby a

sheet metal blank is transformed into a hollow cup, or a hollow cup is transformed into a similar part of smaller dimensions without any intention of altering the sheet thickness."

This is done by placing a blank of appropriate size over a shaped die and pressing the metal into the die with a punch. To prevent wrinkling of the sheet metal blank, the outer portion of the blank, which is called as the flange, is held by the blank holder. The outer portion of the die, which supports the blank holder, is also named as the flange.

The most popular shapes produce using deep drawing process is circular and rectangular shape. (*Hosford & Canddell, 2014*). The numerous process parameters are influencing the deep drawing process such as punch speed, blank holding pressure, lubrication, sheet thickness, clearance between die and punch, material properties and many more(*Banabic, 2010*). Moreover, these process parameters are become more predominant at elevated temperature condition which makes this process complicated (*Zhang et al., 2007*).

Formability is difficult to be defined and quantified accurately. It depends on the consequence of material properties and the complex tool sheet interactions (*Singh et al., 2008*). The quality of successful drawn cups has been commonly assessed using Limiting Draw Ratio (LDR), thickness distribution of cup, earing tendency of cup and forming limit diagram (FLD) (*Aly EI-Domiaty, 1992*). LDR is defined in simple way as ratio of the diameter of the initial blank to the punch diameter. On the other, it is the maximum value of the drawing ratio, which can be reached in a single drawing step (*Bolt, 2001*). The LDR is dependent on many factors like the tool geometry, lubrication conditions, and the amount of blank holding forces, sheet thickness and material properties (*Beddoes & Bibby, 1999*).

Furthermore, thickness is one of the major quality characteristics in deep drawn cups. The thickness is unevenly distributed in the part after deep drawing. Generally, the thickness is uniform at the bottom face of the punch, minimum at the punch nose radius and vertical surface, and thicker at the flange area (*Brammar & Harris, 1975*) Existence of thickness variation from the production stage may cause stress concentration in the part, leading to the acceleration of damage (*Altan, 2003*). Additionally, it is important to note that earing is one of the important characteristics in deep drawing since it is associated with the anisotropy in the sheet Earing in deep drawn cups occurs from different plastic strain ratio at different directions. After successful drawn cups, this irregularity is shown in the top of the cup. More anisotropic properties lead to greater earing tendency in cup and then decrease efficiency of deep drawing process (*Yoon & Barlat, 2006*).

During the deep drawing process, different stress zones have been observed which is shown in Fig. 2.1. Four different states can be defined as Force application zone, Force transmission zone, bending zone and forming zone (*Beddoes, 1999*). The punch force is applied onto the bottom of the drawn part, which is called the force application zone. Then it is transferred to the flange region. The force is transmitted along the wall of the cup. Bending happens over the die edge radius and forming takes places in the flange region (*Schuler, 1998*). It is clearly seen from Fig. 2.2, the stresses developed in the flange and wall regions are predominately in biaxial state of stress (*Marciniak et al., 2002*)

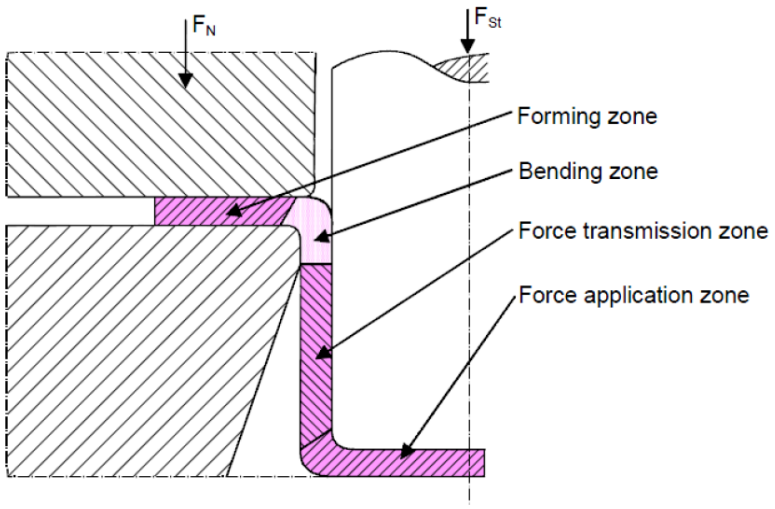

Fig.2.1: Four different zones in deep drawing (*Schuler, 1998*)

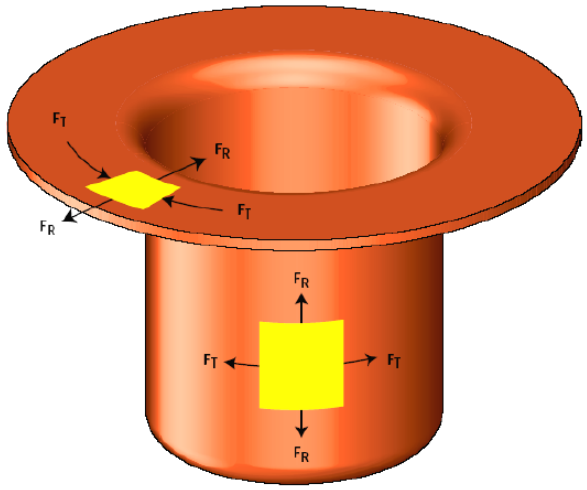

Fig.2.2: Forces in deep drawing of a cylindrical cup (*Schuler, 1998*)

2.3 Mechanical Properties

Determination of mechanical properties accurately is one of the key issues in analyzing the deformation behavior of the materials. The mechanical properties of sheet metals vary considerably, depending on the base metal, alloying elements present,

processing, heat treatment (*Davis, 2004*). The Lankford anisotropy coefficient (r), strain rate coefficient (n), strain rate sensitivity (m) and the yield stress (σ_y), ultimate tensile strength (σ_{ut}), ductility have the strongest influences on formability (*Bong, 2013*).

Anisotropy (r) is defined as the directionality of properties and it is associated with the variance of atomic or ionic spacing within crystallographic directions (*Drucker, 1949*). In sheet metal forming point of view, the sheet texture affects crystal anisotropy and crystal anisotropy is the dependence of flow characteristics of a material with respect to direction (*Beddoes, 1999*). Lankford coefficient (parameter) (*Lankford et al., 1950*) is a measure of anisotropy. It can be called as the 'resistance to thickness change'. The Lankford anisotropy coefficient depends on the in-plane direction. In orthogonal anisotropy three *r*-values are determined: Along the, along 45° to rolling direction and perpendicular to rolling direction (transverse direction,). These values are denoted as r_0, r_{45}, and r_{90} respectively. In sheet metal working, anisotropy is subdivided into normal and planar anisotropy. Normal anisotropy (r_n) influences the maximum drawability of sheet, whereas planar anisotropy leads to earing. A material with a high r_n value cab be experience less thinning during a deep drawing operation than a material having a smaller r_n value, provided that their flow characteristics are identical (*Banabic et al. 2000*). It is mathematically expressed as Equation (2.1).

$$r_n = \frac{r_0 + 2 \times r_{45} + r_{90}}{4} \tag{2.1}$$

In the study of *Weilong and Wang* (*2002*) it is shown that although materials having greater *r*-values are more suitable for deep drawing, their deformation resistance is also increased with increasing *r*-values. It was stated by *Marciniak, Duncan & Hu* (*2002*) that

for materials having larger value r_n than unity, width strain is greater than the thickness strain in the tensile test; which is associated with a greater strength in the through-thickness direction, and generally a resistance to thinning. A high r_n value allows deeper parts to be drawn and in shallow, smoothly contoured parts (like automobile panels) a high value may reduce the chance of wrinkling or ripples in the part. Therefore for a deep drawing operation, a suitable material must have an r_n-value, which is larger than unity (*Weilong & Wang, 2002*).

Planer anisotropy (Δr) can be expressed by difference strain ratio values in various directions of the sheet plane. It is responsible for the formation of ears in the drawn cups as well as uneven thinning. Mathematically, it is expressed as Equation (2.2).

$$\Delta r = \frac{r_0 - 2 \times r_{45} + r_{90}}{2} \tag{2.2}$$

It was stated by *Marciniak, Duncan & Hu (2002)* that if the magnitude of the planar anisotropy parameter is large, the orientation of the sheet with respect to the die or the part to be formed will be important. In such cases, asymmetric forming and earing will be observed. As the magnitude of the value increases, the ear heights increase. Therefore for deep drawing operations, suitable materials must have smaller Δr value.

Strain-hardening coefficient (n) is determined by the dependence of the flow (yield) stress on the level of strain (*Hollomon, 1945*). In materials with a high n value, the flow stress increases rapidly with strain. This tends to distribute further strain to regions of lower strain and flow stress. A high n value leads to a large difference between yield strength and ultimate tensile strength which is an indication of good formability. The strain hardening characteristics of a material is usually dependent on strain, strain rate

and temperature (*Davis, 2004*). The detail test procedure for determining *n* value is as per *ASTM E -646 –07* standard.

The strain rate sensitivity (*m*) is calculated based on the strain rate dependency of flow curves (*Davis, 2004*). There are two commonly used methods of determining *m* value. One is to obtain continuous stress-strain curves at several different strain rates and compare the levels of stress at a fixed strain. The other is to make abrupt changes of strain rate during a tension test and use corresponding level of $\Delta\sigma$. This method is popularly known as rate-change test or jump test (*Zyczkowski et al., 1981*). Generally, use of continuous stress-strain curves yields larger value of *m* than jump test. The jump test has an advantage that several strain rate changes can be made on a single specimen, whereas continuous stress-strain curves require a specimen for each strain rate (*Marciniak et al. 2002*).

In addition to this; few other mechanical priorities are required for formability analysis such as yield strength (σ_y), elastic modulus (E), ultimate tensile strength (σ_{ut}), percentage ductility (*Marciniak et al., 1992*). Yield strength and ultimate tensile strength is related to the strength of the formed part. Although for lightweight materials, higher yield strengths are preferable, such materials are harder to form and combined with low elastic moduli, it induces increased spring back problems (*Brammar & Harris, 1975*).

Numerous techniques are available to obtain the required material properties and flow stress behavior of a material (*Gutscher et al., 2004*). The various established techniques are tensile, compression, torsion, shear, biaxial tensile and hydraulic bulge test (*Makinde et al., 1992*). The flow stress curves determined using different tests and test conditions do not replicate each other due to effects of stress state, yield criterion assumption,

anisotropy effect, Bauschinger effect, experimental inaccuracies, temperature, and general weakness of the modeling (*Koç et al., 2001$_a$*). Hence, none of the test methods can be named as the best or optimal. Each has its specific field of application due to definite straining paths. None of the test methods can be named as the best or optimal (*Koc et al., 2011*). Among those test system, the most widely used one is uniaxial tensile test (*Davis, 2004*).

In tensile tests, the maximum achievable strain is reported to be limited (~30%) and this leads to interpolations of the test data that are necessary beyond the fracture point. However, limitations of uniaxial tensile test have been described by several researchers (*Davis, 2004*). On the other hand, biaxial stress state tests provides flow curves for the materials with extended range of plastic strain levels up to ~70% before bursting occurs (*Banabic et al., 2005*). Another benefit of using biaxial state of stress test is that it is more appropriate for sheet metal forming operations in which the deformation mode is biaxial rather than uniaxial (*Jones, 2001*). Therefore, by the use of more realistic loading during the test such as the introduction of biaxial loading conditions leads to a more accurate representation of the expected behavior of the structure in-service (*Naumenko & Atkins, 2006*).

In recent years, various tests have been designed in an attempt to produce forces that are closely related to those that the material is subjected to during normal service conditions (*Li & Ghosh, 2004*). Biaxial tensile tests can be used to produce forces that occur in more than one direction simultaneously. From this test, stress–strain curves can be obtained for different directions of the test specimen (*Boehler et al., 1994*). However, relatively few experimental investigations have been carried out to characterize sheet

metals under biaxial tension (*Green et al., 2004*). There are numerous methods of producing biaxial stresses in material for different types of specimens. These include the bulge test (*Altan, 2003*), combined tension–torsion test (*Keefe et al., 1998*), combined bending and in-plane test (*Banabic et al., 2005*) and biaxial tensile testing of sheet metal (*Hannon & Tiernan, 2008*).

Among these all the biaxial state of tests, biaxial tensile testing with various types of cruciform specimens and bulge test has been used extensively for biaxial stress state test (*Geiger et al., 2005*). One of the most challenging aspects of a biaxial testing system is test specimen design (*Xiang-Dong et al., 2005*). Although specimens of the cruciform type have been investigated quite extensively, no standard geometry exists for the specimen design. Commonly, cross-shaped specimen is typically used (*Lin and Ding, 1995*). The lack of standard specimen geometry makes it difficult to compare test results from different laboratories (*Makinde et al., 1992*). Different biaxial tests have been performed in parallel to finite element simulation in an attempt to achieve an optimum specimen design. The design of the cruciform specimen is the main difficulty that restricts application for the cruciform biaxial tensile test (*Yong et al., 2002*).

On the other hand, bulge test has been known as a convenient method for judging the ductility of sheet metal and is an appropriate method for ascertaining biaxial stress–strain relationships (*Atkinson, 1996*). A major advantage of the bulge test over the cruciform biaxial tensile test is that simplicity of specimen preparation (*Gutscher et al., 2004*). Since the bulge test has not been standardized yet, the ‘bulge test’ term in literature refers to variety of test systems including both testing of sheet and tube-formed samples with several differences in practice (*Koç et al., 2011*). Tube bulge test is preferred mainly for

determining the hydro-formability of the tubular materials as developed and explained in various previously published studies (*Koc et al., 2001$_a$; Koc et al., 2001$_b$*). On the other hand, sheet bulge test systems can be categorized in terms of the pressure source for the bulging, the die shape or die dimensions used. Bulging is mostly achieved via pumping hydraulic fluid into the cavity (*Dziallach et al., 2007*). However, in some cases, in order to prevent leakage, viscous material was used as described in, or pneumatic (gas) pressurization was utilized as well at elevated temperature levels (*Rees et al., 1995*). Die shapes in bulge tests are mainly spherical or elliptical. Elliptical dies were preferred to determine anisotropic constants of the materials (*Banabic et al., 2005*).

Based on the above discussion, it can be observed that high temperature formability of sheet metal is dependent on strain rate and temperature. Therefore, detailed analysis of material properties and flow stress behavior at elevated temperatures are essential to analyze the sheet metal formability. These material properties are useful for development of various material models which is required for numerical analysis of sheet metal forming.

2.4 Material Models for Numerical Analysis of Sheet Metal Forming Processes

From the beginning of the 1990s there was an explosive increase of the practical utilization of numerical analysis of sheet forming processes in the industry (*Lange, 1985*). The advanced numerical finite element (FE) technology and CAE-tools in combination with existing computer capacity makes a completely virtual process development possible (*Crisfield, 1997*).

FE simulations are used extensively in the sheet metal industry where the technology has contributed to a better understanding of chosen forming processes and where the prediction capabilities has significantly reduced the time consuming and costly die tryouts (*Crisfield, 1997*). Complex geometries in industrial applications with large deformations, nonlinear materials and contacts can be treated effectively and quickly (*Nielsen, 1997*). However, the reliability of the numerical simulations depends not only on the models and methods used but also on the accuracy and applicability of the input data. The material model and related property data must be consistent with the conditions of the material in the process of interest (*Hol, 2009*).

Nowadays, dynamic, explicit codes were dominating the software market General purpose codes like DYNAFORM, LS-DYNA and ABAQUS/Explicit, and specialized codes such as PAM-STAMP and OPTRIS are examples of codes in use. Currently, more attentions are given for finite element analysis at warm conditions due to experimental complexity (*Bong et al., 2013*). The influence of yield criterion and hardening model are predominating in FE analysis of sheet metal forming (*Nielsen, 1997*).

2.4.1 Yield Criteria

Yield criterion is mathematical description for expressing a relationship between the stress components at the moment when plastic 'yielding' occurs (*Banabic, 2010*). The yield point in uniaxial tension is established using the stress-strain curve of the material (*Davis, 2004*). However, in case of a multi-axial stress state, it is more difficult to define a criterion for the transition from the elastic to the plastic state. It is usually defined in the form of an implicit function which is popularly known as the 'yield function' (*Banabic, 2010*).

$$F(\sigma_1, \sigma_2, \sigma_3, \sigma_y) = 0 \tag{2.3}$$

where, σ_1, σ_2, σ_3 are the principal stresses and σ_y is the yield stress obtained from a simple test (tension, compression or shearing). Equation (2.3) can be interpreted as the mathematical description of a surface in the three dimensional space of the principal stresses usually called the 'yield surface'. It must be closed, smooth and convex. All the points located in the inside of the surface ($F < 0$) are related to an elastic state of the material. The points belonging to the surface ($F = 0$) are related to a plastic state. The points located outside the surface ($F > 0$) have no physical meaning (*Banabic, 2010*).

The sheet metal analysis is considers as a plane stress problem. Therefore, In the case of plane stress (e.g. $\sigma_3 = 0$) the yield surface reduces to a curve in the plane of the principal stresses σ_1 and σ_2. (*Findley & Michno, 1976*). The expression of the yield function is established on the basis of some phenomenological considerations concerning the transition from the elastic to the plastic state. The most widely used yield criteria for isotropic materials have been proposed by Tresca ('maximum shear stress criterion') and Huber–Von Mises ('strain energy criterion') (*Zyczkowski, 1981*). However, these two popular yield criteria do not take into account of anisotropic of sheet metal. Therefore, these criteria are not very well suited for sheet metal forming analysis (*Pöhlandt etal., 2002*).

In the last few years, several efforts have been made for the development of anisotropic yield criteria which consider plastic anisotropy (*Drucker, 1949 & Hill, 1950*). For example, Hill proposed an extension of the Von Mises isotropic criterion which considers plastic anisotropy. This model considered orthotropic symmetry and four

anisotropy coefficients in the plane stress condition (*Hill, 1952*). Moreover, Barlat proposed independently another anisotropic yield criterion which also required four parameters to describe a yield locus (*Barlat & Lian, 1989*).

This early stage development of Hill 1948 and Barlat 1989 model consider sheet metal anisotropy. This model requires only the uniaxial tensile test material properties. Specifically, the material properties required are r_0, r_{45}, r_{90} and σ_Y (*Banabic, 2010*). Therefore, these yield criteria are popularly used in sheet metal forming industries because of ease way of determining the material properties using uniaxial tensile test only (*Hosford, 1972*). As discussed previously, biaxial material properties are vital to capture accurate deformation in sheet metal forming (*Rees, 1995*). Therefore, further development in the yield criteria have been done based on the consideration of biaxial data (*Yu, 2002*).

Experimental studies showed that HCP crystal structure alloy is very difficult to model with the above yield criteria. At the beginning of 1990, several researchers have focused their interest on this problem (*Barlat et al., 1997*$_a$). Barlat and co-workers proposed a more general expression of the yield function. However, finite element simulations based on this criterion revealed some inaccuracies in predicting blank earing in deep-drawing (*Bababic, 2010*). In order to improve the performance of his criterion, Barlat and co-workers modified the generalization made in 1994 criterion (*Barlat et al., 1997*$_b$). This yield criterion is popularly known as Baralt 1996 yield criterion. This yield criterion requires 8 material parameters to determine the yield function. The great number of parameters ensures a good flexibility of the criterion but implies a large number of mechanical tests (*Banabic, 2010*). Simulations of deep-drawing of cylindrical cups using

the new criterion revealed a very good agreement of the predicted earing with experimental data (*Yoon, et al. 1999*). However, Barlat 1996 yield criterion found some major drawback such as the convexity of the yield functions is not guaranteed and the derivatives of the equivalent stress are difficult to obtain analytically. This leads to larger CPU time for FE analysis of sheet metal forming (*Chung & Shah, 1992*).

In order to remove the disadvantages of the Barlat 1996 yield criteria, but aiming to preserve their flexibility, Barlat proposed in 2000 a new model particularized for plane stress (2D) (*Barlat et al., 2003*). This is popularly known as *8* parameters Barlat 2000 yield model. In addition to uniaxial tensile test, biaxial yield stress and biaxial anisotropic coefficient are required for Bralat 2000 yield criterion. As discussed previously, popular way to determine biaxial yield stress is bulge test and biaxial anisotropic coefficient is determined using coin or compression test (*Banabic, 2010*). The yield function has been tested for different aluminum alloys exhibiting a pronounced anisotropy. The model has proved its capability to provide an accurate prediction of the planar variations of the uniaxial yield stress and coefficient of plastic anisotropy (*Barlat, 2007*). However, one of the major drawback of Barlat 2000 yield model is complexity of the formulation (*Banabic, 2010*).

Above discussed yield criteria considered symmetry in yielding between tension and compression. However, the stress asymmetry in the case of HCP crystal structure is considerable (*Liu et al., 1997*). Considering the effect of asymmetry in yielding further development in the yield criterion is done by Cazacu et al. The most important advantage of this yield criterion consists in its capability to provide an accurate description of the tension/compression behavior specific to the magnesium and aluminum alloys (*Cazacu et*

al., 2006). However, limited study has been reported for the development of these anisotropic yield criteria for Ti-6Al-4V alloys at elevated temperatures.

The present state-of-the-art is somewhat confusing since most of the above-described yield criteria are still being used. The most important factors that must be taken into account when choosing the yield criterion are as follows (*Banabic, 2010 & Yoon, 2006*):

- Accuracy of the prediction both of the yield locus and the uniaxial yield stress and uniaxial coefficient of plastic anisotropy
- Computational efficiency and ease of implementation in numerical simulation codes
- Number of mechanical parameters needed by the identification procedure
- Robustness of the identification procedure
- Experimental difficulties caused by the determination of the mechanical parameters involved in the identification procedure
- Acceptance of the yield criterion in the scientific/industrial community.

2.4.2 Constitutive Models

The constitutive models are often used to describe the plastic flow properties of the metals and alloys that can be used in numerical analysis of sheet metal forming processes (*Liang & Khan, 1999*). Constitutive models are usually built by using uniaxial tensile test at low strain rates for forming applications (*Lin & Chen, 2011*).

Generally, an ideal plasticity model for metals and alloys should be able to accurately describe the material properties such as forming temperature, strain and strain-rate history dependence, strain hardening behavior (*Lin & Chen, 2011*). However, a complete description of all of these phenomena in a single constitutive model is an extremely difficult task. Therefore, some assumptions have been made before plastic flow stress models are proposed (*Liang & Khan, 1999*). In recent years, a number of constitutive models have been proposed or modified to describe the strain-rate, stain and temperature-dependent flow behavior of metals and alloys (*Lin et al., 2008*).

The constitutive models are mainly divided into the two categories - (a) Phenomenological based model (b) Physical based model

(a) Phenomenological constitutive model

It provides a definition of the flow stress based on empirical observations, and consists of some mathematical functions. However, the phenomenological constitutive model is lack of physical background that just fits experimental observations. Additionally, the notable feature is that they reduce number of material constants and can be easily calibrated. However, due to their empirical characteristics, they are usually used

in limited application fields (covering limited ranges of strain-rate and temperature) (*Shin & Kim, 2010*).

(b) Physical-based constitutive model

These models considers various physical aspects such as theory of thermodynamics, thermally activated dislocation movement, and kinetics of slips. Compared to the phenomenological descriptions, they allow for an accurate definition of material behavior under wide ranges of loading conditions by some physical assumptions and a larger number of material constants (*Khan et al., 2004*).

Significant amount of the work has been done on austenitic stainless steel, alloy steels, ferritic steel, aluminum alloys and magnesium alloys at elevated temperature in past few decades to link the flow stress with the process parameters through the empirical, semi-empirical and physically based constitutive models (*Lee & Lin, 1998*). As of now, studies in the field of constitutive modeling have been mostly focused on FCC and BCC metals due to their simple crystalline structures (*Lin & Chen, 2011*). Slight attention has been given on the hexagonal close-packed (HCP) metals, particularly alloys of a more complicated crystalline structure, such as two phase ($\alpha + \beta$) Ti–6Al–4V alloy (*Khan et al., 2004; Khan et al., 2007*).

Zerilli and Armstrong (*ZA* model) proposed a constitutive model for HCP metals based on an argument that HCP metals have partial structural characteristics of BCC and FCC metals (*Zerilli & Armstrong, 1995*). A new constitutive model for Ti6A14V alloy was proposed by generalizing their FCC model (*Nemat-Nasser et al., 2001*). A physical based constitutive model was developed for Ti6A14V alloy which contains thermal and

athermal component dependent on internal state variable theory (*Picu & Majorell, 2002*). Quasi-static and dynamic loading response under compressive loading for Ti–6Al–4V alloy investigated over wide range of temperature (*Khan et al., 2007*). Furthermore, a new constitutive model based on thermally activated dislocation motion in crystal structure for high strain rate and temperature has been developed for Ti-6Al-4V alloy (*Gao et al., 2011*). Therefore, very spare efforts have been made on the development of constitutive models for Ti-6Al-4V alloy.

2.5 Forming Limit Diagram (FLD)

FLD represents the maximum extent of the deformation of sheet metal until plastic instability occurs in a material. It is a significant performance index and used to describe quantitatively the formability of sheet metal (*Narayanasamy & Narayanan, 2007*). FLD must cover as much as possible the strain domain which occurs in industrial sheet metal forming processes. The diagrams are established by experiments that provide pairs of values of the limit strains ε_1 and ε_2 obtained for various loading patterns (equibiaxial, biaxial, uniaxial etc.) (*Ghosh et al., 1985*). The concept of FLD was first introduced by Keeler and Goodwin (*Keeler, 1965, Goodwin, 1968*). This test consists in the use of punches having different radii in order to vary the stress state. Disadvantages of the test are the large amount of experimental work; only the positive section of the forming limit diagram(right hand side) is obtained, and the shape and position of the forming limit is influenced by the punch radii (*Keeler, 1965*). Later, Goodwin plotted the curve for the tension/compression domain (left hand side) by using different mechanical tests (*Goodwin, 1968*). The diagrams of Keeler (right side) and Goodwin (left side) are

currently called the Forming Limit Diagram (FLD). Connecting all of the points corresponding to limit strains leads to a Forming Limit Curve (FLC).

Further development in experimental FLD is Nakazima Test. The test consists of drawing rectangular specimens having different widths using a hemispherical punch and a circular die (*Nakazima et al., 1971*). By varying the width of the specimen and the lubricant one may obtain both the positive and the negative domain of the FLD. Advantages of the test are the simplicity of the tools, the simple shape of the specimens and the possibility of covering the entire domain of the FLDs (*Banabic, 2010*). Disadvantages are the possibility of wrinkling and errors of measurement caused by the curvature of the punch. This method is standardized by the *ISO 12004* standard ('Metallic materials. Determination of the forming limit curves').

Laboratory testing has shown that the FLDs are influenced by several factors including as shown in Fig. 2.3 (*Banabic, 2010*). However, determining FLDs experimentally can be time consuming and expensive, especially at elevated temperature, resulting in a great interest in employing numerical models to simulate FLDs.

Various theoretical models have been developed for the calculation of FLDs as shown in Fig. 2.4. The first theoretical model has been proposed by Swift and Hill assuming homogeneous sheet metals (*Swift, 1952; Hill, 1952*). Marciniak proposed a model taking into account that sheet metals are non-homogeneous from both the geometrical and the structural point of view (*Marciniak & Kuckzynski, 1967*). The Swift model has been developed later by Hora (so-called Modified Maximum Force Criterion-MMFC) (*Hora & Tong, 1994*).

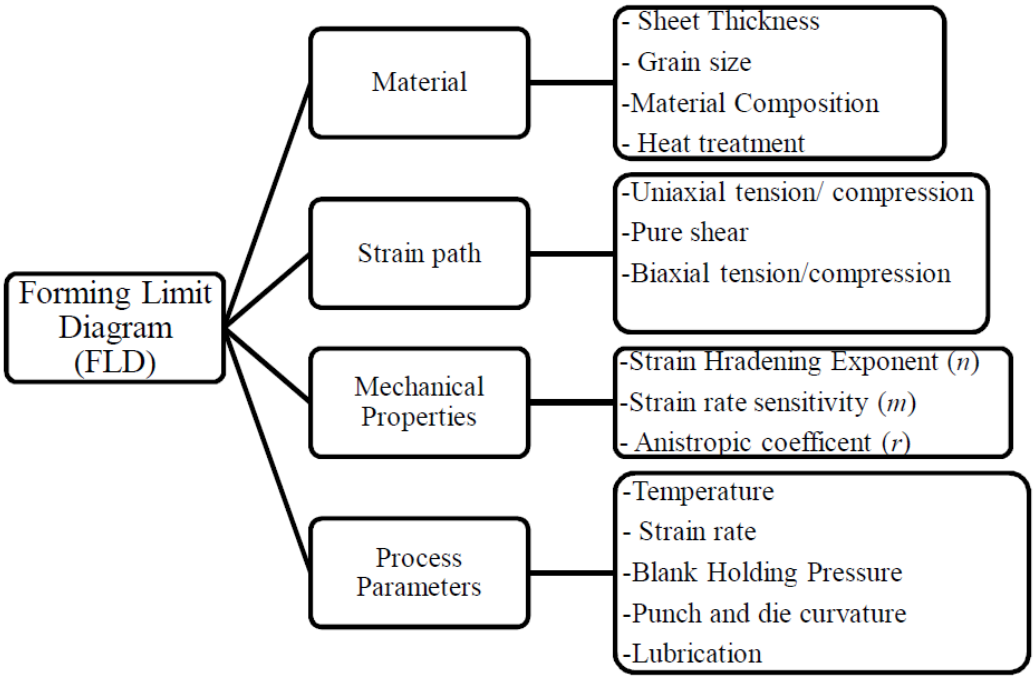

Fig.2.3: Important influencing factors affecting the experimental FLD (*Banabic, 2010*)

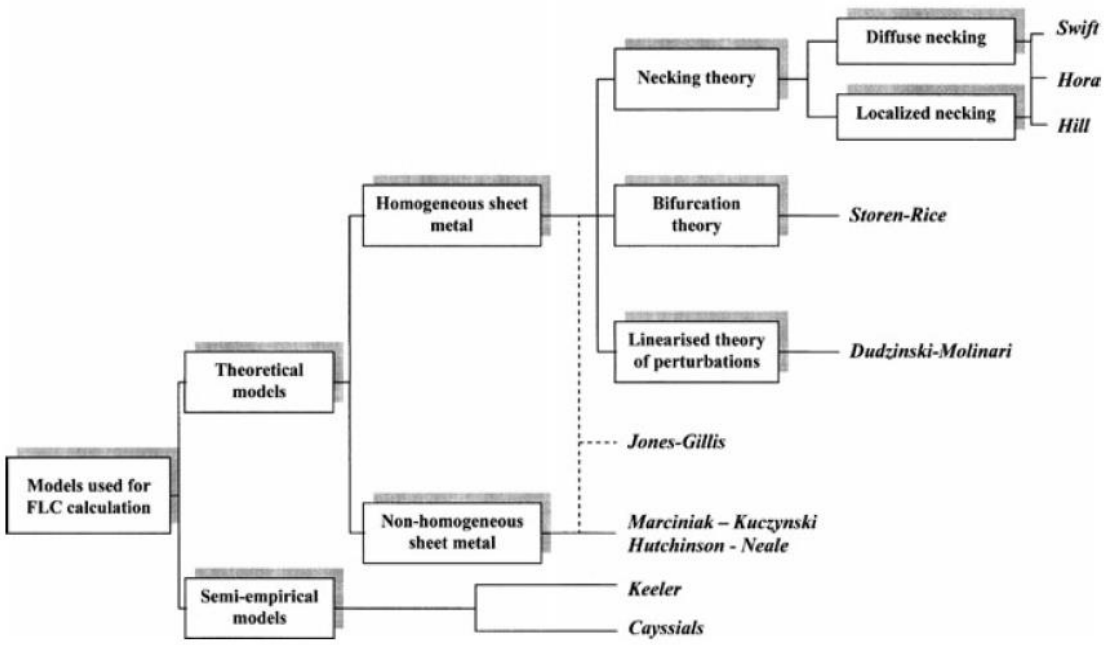

Fig.2.4: Various theoretical models available for FLD prediction (*Banabic, 2010*)

The first realistic mathematical model has been developed by Marciniak-Kuczynski (M-K) (*Marciniak & Kuckzynski, 1967*). It is supposed that an infinite sheet metal contains a region of local imperfection where heterogeneous plastic flow develops and localizes. Generally, theoretical FLDs can be significantly influenced by the yield criterion and constitutive model (*Sansot Panich et al., 2013*). The influence of different yield functions namely; Von Mises, Hill 1948 and Hill 1979 and Barlat 1996 with Swift and Voce constitutive model on forming limit diagram for AA6016-T4 alloy was investigated. The study revealed that FLD using Barlat 1996 criterion with Voce model was in good agreement with experimental data points (*Butuc, 2003*). Subsequently, many efforts have been made to construct reliable forming limit prediction models from the perspective of theoretical calculation for steel and aluminum alloy (*Fang Gang et al., 2012; Moshksar & Mansorzadeh, 2003; Butuca et al., 2002*). In addition to that, recently few studies have been reported for prediction of theoretical FLD at elevated temperature (*Van den Boogaard, 2006*)

However, titanium alloy, very limited literature have been reported for FLDs at elevated temperatures (*Toussaint, 2008; Djavanroodi & Derogar, 2010*). FLDs were determined experimentally using a special process of hydroforming deep drawing assisted by floating disc for Ti6Al4V titanium and Al6061-T6 aluminum alloys sheets The results were compared with finite element analysis using Hill-swift and NADDRG models (*Djavanroodi & Derogar, 2010*). Recently, FLDs prediction of Ti-6Al-4V alloy using Marciniak and Kuczynski (M–K) theory along with Von Mises yield criterion at elevated temperature were investigated at elevated temperature (*Xiaoqiang Li et al., 2014*). However, much research needs to be done on the theoretical FLDs prediction

using various anisotropic yield criteria in combination with different hardening models at warm conditions for Ti-6Al-4V alloy.

2.6 Finite Element Analysis of Sheet Metal Forming Process

In sheet metal forming, modelling and simulation can be used for many purposes, for example to predict material flow, to analyze stress-, strain- and temperature-distribution, to determine forming forces, to forecast potential sources of defects and failures, to improve part quality and complexity and to reduce manufacturing costs (*Thomas & Altan T, 1998*). Today, several commercial codes are already available for forming simulation. Besides general purpose codes such as MARC, COSMOS or ABAQUS, recently special codes dedicated for sheet metal forming are more widely and more often applied. Among them, the PAM-STAMP, Auto-FORM, DYNAFORM, ITS-3D, OPTRIS, FAST FORM3D are the leading tools (*Makinouchi, 1996*).

Sheet metal forming is characterized by many nonlinearity not only due to geometrical and material nonlinearity, but also due to contact between the bodies makes the problem highly nonlinear (*Nielsen, 1997*). However, by using explicit method these nonlinearities can be treated without any problem (*Takuda et al., 2003*). Concerning the geometrical complexity, sheet metal forming processes in some cases can be simulated as two-dimensional, axi-symmetric problems, but in most cases three-dimensional solutions are required (*El-Khaldy, et al., 1992*). Since in forming processes, the component is usually subjected to large plastic deformation, as the simulation proceeds, the distortion of the mesh is also significant, hence, it is necessary to perform re-meshing and

interpolate the data from the old mesh to the new one to obtain accurate results. This feature makes indispensable an automatic and adaptive re-meshing capability of the simulation code as a built-in technique (*El-Khaldi & Lambriks, 2002*). The reliability of the FE simulations largely depends on the material models used and accuracy of the input material data (*Nielsen, 1997*). Mainly, selection of a suitable yield criterion is vital because it provides an accurate prediction of the observed initial and subsequent yield behaviors of a material (*Odenberger EL & Oldenburg M, 2013*).

Very limited efforts have been reported on material model development for Ti-6Al-4V alloy at elevated temperatures and its implementation in FE analysis of sheet metal forming processes. Spring back analysis of warm deep drawing of TC1 alloy (Ti-2Al-1.5Mn) was extensively studied (*Zhang et al., 2007*). Spring back of cylindrical cup was greatly suppressed by warm forming. FE model to simulate and optimize the bending forming process of a commercially pure (CP) titanium part and found that a good prediction of spring back was due to the adoption of the Hill criterion which can describe the anisotropic plastic behavior of the material with notable precision (*Toussaint et al., 2011*). Ti-6242 is suitable to be formed by hot sheet metal forming. The minimum spring back is achieved with suitable subsequent holding time (*Odenberger E-L et al., 2005*). Numerical simulation on the bending of a Ti-6Al-4V bar and suggested that the spring back was dependent on the size of the middle material zone, which remained in an elastic state during bending process (*Adamus & Lacki, 2011*).

The FLC of Ti–6Al–4V alloy at 973 K was measured experimentally by conducting the hemispherical dome test with specimens of different widths. The experimental results were validated with Marciniak and Kuczynski (M-K) theory along with Von Mises yield

criterion (*Xiaoqiang Li, et al., 2014*). Formability, fracture mode and strain distribution during forming of Ti6Al4V titanium alloy and Al6061-T6 aluminum alloy sheets has been investigated experimentally using a special process of hydroforming deep drawing assisted by floating disc. The experimental FLD was compared with Hill-swift and NADDRG theoretical forming limit diagram and simulated FLD using ABAQUS/Standard (Djavanroodi & Derogar, 2010). However, much research needs to be done on effect of various material models development and its implementation in FE analysis of Ti-6Al-4V alloy at elevated temperatures.

2.7 Objectives of the Study

The main objectives of this research work on Ti-6Al-4V alloy are:

(I) Study of mechanical properties and flow stress behavior up to 400^0C.

(II) Microstructure and fractography study at elevated temperatures.

(III) Formability study up to 400^0C using deep drawing process.

(IV) Investigation of various yield criteria at elevated temperatures.

(V) Study of different constitutive models at elevated temperatures.

(VI) Experimental and theoretical analysis of forming limit curve at 400^0C.

(VII) Validation of experimental and theoretical formability results with finite element (FE) analysis.

2.8 Summary of Literature Review

The extensive literature review has been done on various aspects of formability for Ti-6Al-4V alloy at elevated temperatures. Based on the literature extensive literature review, research gaps and objectives of the study has been identified

The next chapter discusses about experimental formability investigations of Ti-6Al-4V alloy at elevated temperatures using deep drawing process.

CHAPTER 3: EXPERIMENTAL INVESTIGATIONS OF FORMING BEHAVIOR FOR TI-6AL-4V ALLOY

This chapter covers experimental investigations on sheet metal forming of Ti-6Al-4V alloy using deep drawing process at elevated temperatures. The detailed understanding of material properties and flow stress behavior is an essential prerequisite to assess the forming behavior of a material. Tensile test experiments are performed to establish required material properties and flow stress behavior of Ti-6Al-4V alloy at elevated temperatures. Furthermore, the microstructure and fractography study of Ti-6Al-4V alloy with variation of temperature have been studied. Formability of Ti-6Al-4V alloy from room temperature to 400^0C at an interval of 50^0C has been investigated using deep drawing process and the various qualitative aspects such as Limiting Drawing Ratio (LDR), thickness distribution, earing profile have been studied.

3.1 Material Properties

In this study, Ti–6Al–4V alloy sheet of 0.9 mm thickness is used. The chemical composition of as-received Ti-6Al-4V alloy is presented in Table 3.1.

Table 3.1: Chemical composition of as received Ti–6Al–4V alloy

Element	Al	V	Fe	C	Ti
Comp (wt. %).	5.560	4.070	0.185	0.022	89.997

For tensile tests, the dimensions of the specimen are as per *ASTM E8/E8M-11* sub-size standard specimen, as shown in Fig. 3.1. The specimens are machined by wire-

cutting electro-discharge machining process for high accuracy and finish. Isothermal tensile tests are carried out on a computer controlled universal testing machine (UTM), as shown in Fig. 3.2, which has a maximum load capacity of 100 kN.

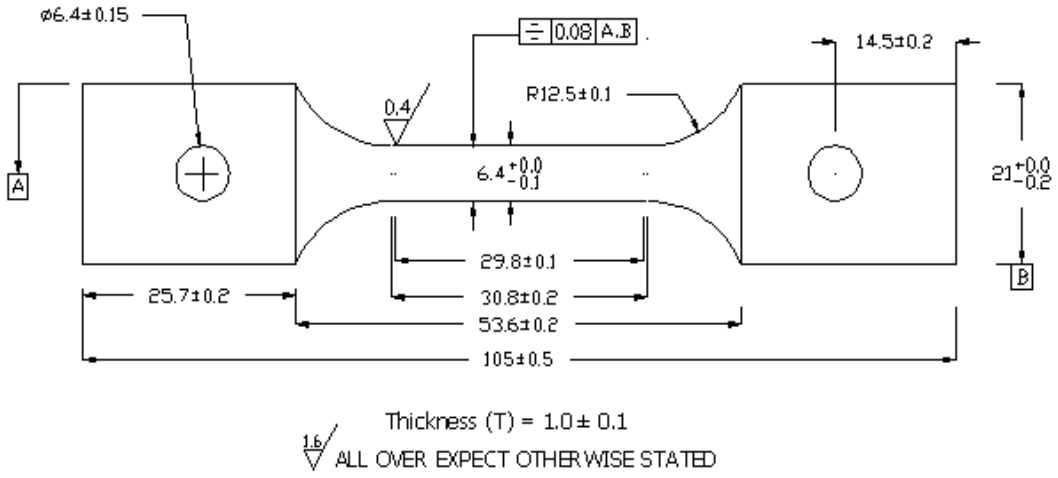

(All dimensions are in *mm*)

Fig.3.1: Dimension of tensile test specimen as per ASTM E8/E8M-11 sub-sized standard

UTM is equipped with a feedback control system to impose exponential increase of the actuator speed to obtain constant true strain rates. The cross head speed is varied with respect to time as per Equation (3.1).

$$v = \dot{\varepsilon} L_0 \exp(\dot{\varepsilon} t) \tag{3.1}$$

where, v is the cross head speed, $\dot{\varepsilon}$ is the constant strain rate, L_0 is the gauge length of the specimen (30 *mm*) and t is time. Software modifications have been ingeniously done to have exponentially increasing crosshead speed for constant strain rate.

A high temperature contact type extensometer is used to measure the extension of the specimen which is shown in the magnified view of Fig. 3.2. The pull rods for the high temperature testing are made of nickel base super alloy CM-247. Machine is attached

with a 3-zone split furnace for high temperature testing as shown in Fig. 3.3. It has uniform distribution of heating coils, which are arranged in three zones to achieve temperature up to 1000°C with ± 3°C accuracy.

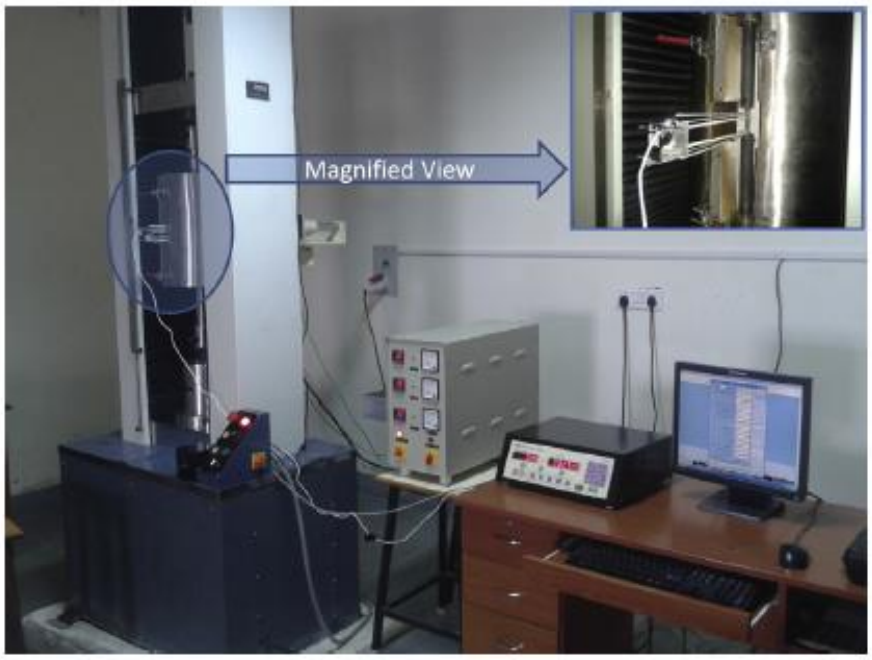

Fig.3.2: Computerized UTM with magnified view of high temperature contact type extensometer

Generally, the lower strain rate range is considered for forming applications (*Dieter, 2000*). Hence, experiments have been performed at 10^{-5}, 10^{-4}, 10^{-3} and 10^{-2} s^{-1} strain rates. Regarding temperature range, forming at temperatures higher than 400^0C increases the oxygen contamination in Ti-6Al-4V alloy and with oxygen the material becomes more brittle due to formation of α-scale. Therefore it is preferred to perform tensile testing of Ti–6Al–4V alloy at higher than 400^0C in an inert or protective atmosphere (*Odenberger et al., 2013*). Due to lack of facility for inert or protective atmosphere, experiments have been conducted from room temperature to 400^0C at an interval of 50^0C.

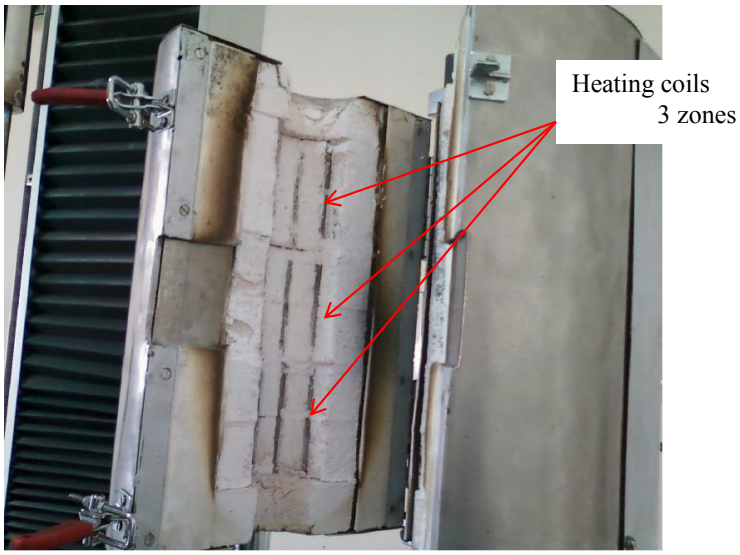

Fig.3.3: 3-zone split furnace attached to UTM for high temperature tensile testing

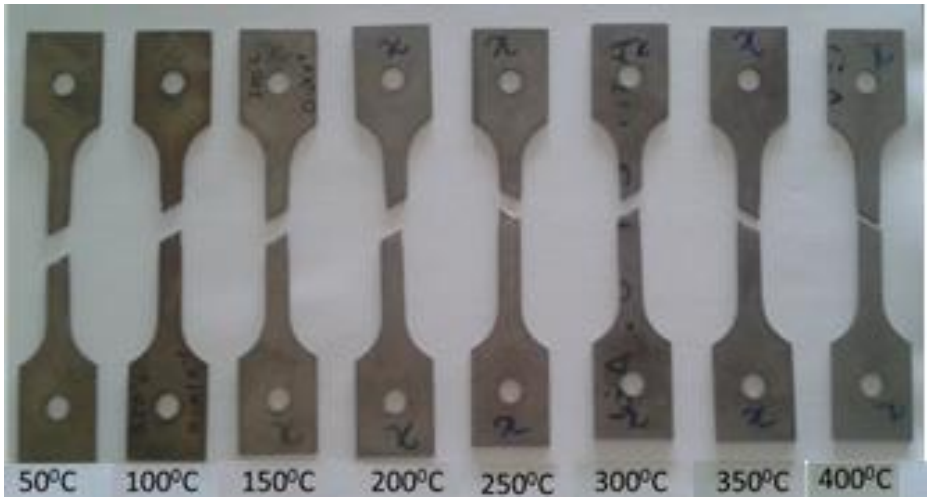

Fig.3.4: Representative broken tensile test specimen after tests at various temperatures

Fig. 3.4 shows the representative broken tensile tests specimen at various temperatures. A computer control system is used to record the load versus displacement curve which is converted into true stress versus true strain curve. The elastic region is subtracted from the true stress–true strain curve to get true stress - true plastic strain data.

The representative true stress vs. true strain curves are shown in Fig. 3.5 (a, b) and Fig. 3.6 (a, b).

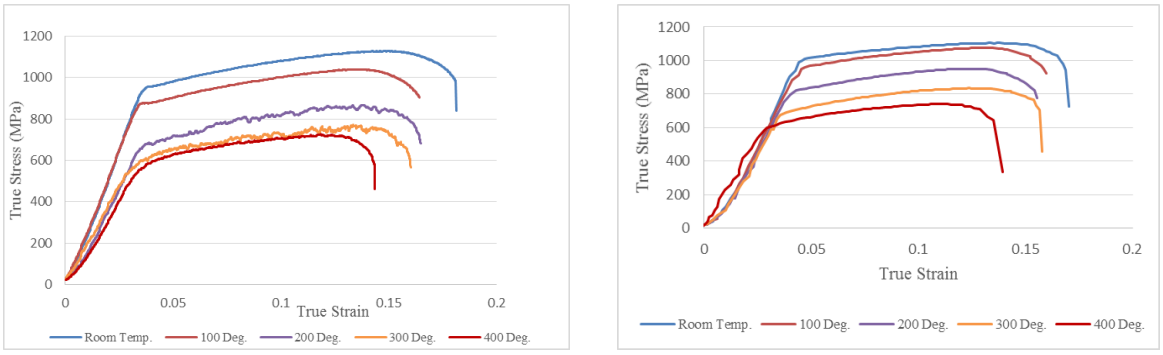

(a) (b)

Fig. 3.5: Representative true stress-strain curves at various temperatures (a) 10^{-5} s^{-1} strain rate (b) 10^{-2} s^{-1} strain rate

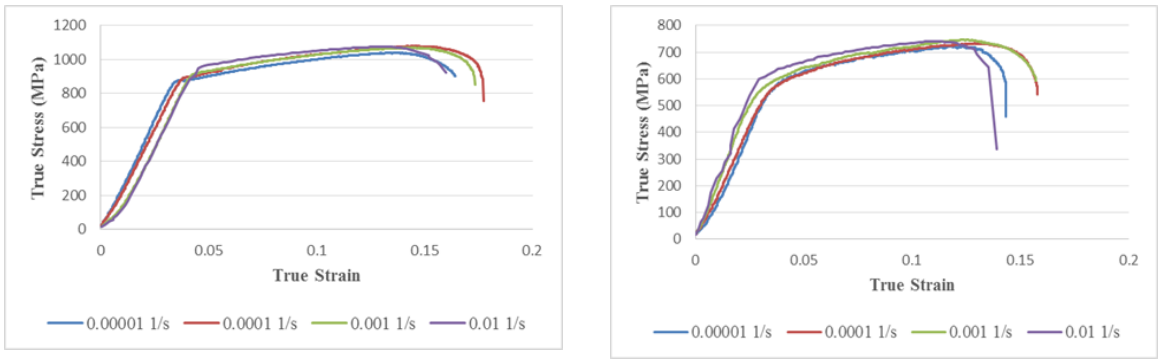

(a) (b)

Fig. 3.6: Representative true stress vs true strain curves at various strain rates (a) 100^0C (b) 400^0C

The flow stress behavior of Ti-6Al-4V alloy is significantly dependent on temperature as show in Fig 3.5 (a & b). However, there is slight variation in flow stress behavior due to strain rate change as shown in Fig. 3.6 (a & b). It indicates that strain rate dependency of Ti-6Al-4V alloy is negligible up to 400^0C.

Based on the true stress-strain data obtained from tensile tests, various important material properties such as strain hardening exponent (n), strain rate sensitivity (m), Lankford parameters (r), yield strength (σ_y), ultimate tensile strength (σ_u) and percentage ductility have been determined. The detailed procedure to determine the important material properties is discussed below.

3.1.1 Strain Hardening Exponent (n)

Strain-hardening exponent (n) is determined by the dependence of the flow stress on the level of strain. In materials with a high n value, the flow stress increases rapidly with strain. A high n value leads to a large difference between yield strength and ultimate tensile strength which is an indication of good formability. The strain hardening characteristics of a material is usually dependent on strain, strain rate and temperature (*Mishra et al., 1989*).

If strain rate and temperatures are assumed constant, the plastic-state Equation can be approximated by the constitutive Equation (3.2) (*Hollomon et al., 1945*).

$$\sigma = K\varepsilon^n \tag{3.2}$$

Taking natural log on both sides the above Equation becomes (3.3)

$$\log\sigma = \log K + n\log\varepsilon \tag{3.3}$$

Equation (3.3) is a straight line Equation with x-axis as a log of true strain and y-axis as log of true stress. The slope of this line gives the strain hardening exponent (n) and y-intercept of the line gives the log of strength coefficient (K). The detail test procedure for determining n value is as per *ASTM E 646 – 07e1* standard.

3.1.2 Strain Rate Sensitivity (*m*)

The logarithmic strain rate sensitivity *m* is originally defined from the extended Hollomon Equation (3.4).

$$\sigma = K.\varepsilon^{n}.\dot{\varepsilon}^{m} \tag{3.4}$$

For determining strain rate sensitivity (*m*) value, there are two commonly used methods. One is to obtain continuous stress-strain curves at several different strain rates and compare the levels of stress at a fixed strain using Equation (3.4). The other is to make abrupt changes in strain rate during a tension test and use corresponding level of $\Delta\sigma$. This method is popularly known as strain rate change test or jump test. For the present study, continuous stress- strain curves at several different strain rates approach has been considered. Table 3.2 shows values of strain hardening exponent (*n*) and strain rate sensitivity (*m*) at various temperatures.

Table 3.2: Strain hardening exponent (*n*) and strain rate sensitivity (*m*) at various temperatures

Temp. (^{0}C)	n_0	n_{45}	n_{90}	n_{avg}	m
RT.	0.033	0.033	0.040	0.035	0.001
50	0.033	0.040	0.041	0.038	0.003
100	0.041	0.041	0.041	0.041	0.006
150	0.046	0.046	0.046	0.046	0.009
200	0.057	0.056	0.057	0.057	0.010
250	0.059	0.059	0.061	0.059	0.010
300	0.063	0.064	0.065	0.064	0.011
350	0.067	0.070	0.071	0.069	0.012
400	0.067	0.071	0.071	0.070	0.012

3.1.3 Anisotropy Coefficient (*r*)

The anisotropy coefficient (*r*) value is dependent on orientation of sheet The anisotropy coefficient is also called as a 'Lankford parameter' Fig. 3.7 shows the specimen directions with respect to sheet rolling direction.

The anisotropy coefficient *r* is defined by Equation (3.5).

$$r = \frac{\varepsilon_{width}}{\varepsilon_{Thickness}} \tag{3.5}$$

The above Equation can be rewritten as Equation (3.6)

$$r = \frac{ln\frac{w}{w_0}}{ln\frac{t}{t_0}} \tag{3.6}$$

where, *w* and *t* is the final width and thickness and w_0 and t_0 is the initial width and thickness of the specimen. As the thickness of the specimen is very small compared to its width, the relative errors of measurement of the two strains will be quite different. Therefore the above relationships are replaced by considering the length of the specimen. Equation (3.6) is rearranged as Equation (3.7)

$$r = \frac{ln\frac{w}{w_0}}{ln\frac{l_0 \,.\, w_0}{l.w}} \tag{3.7}$$

Generally, anisotropy is expressed in two ways (Normal anisotropy and Planer anisotropy). Normal anisotropy (r_n) is the average of *r* values obtained for different directions in the plane of the sheet It is mathematically expressed as Equation (2.1). It indicates the drawability of sheet

Planer anisotropy (Δr) can be expressed by difference strain ratio values in various directions of the sheet plane. It is responsible for the formation of ears in the drawn cups as well as uneven thinning. Mathematically, it is expressed as Equation (2.2).

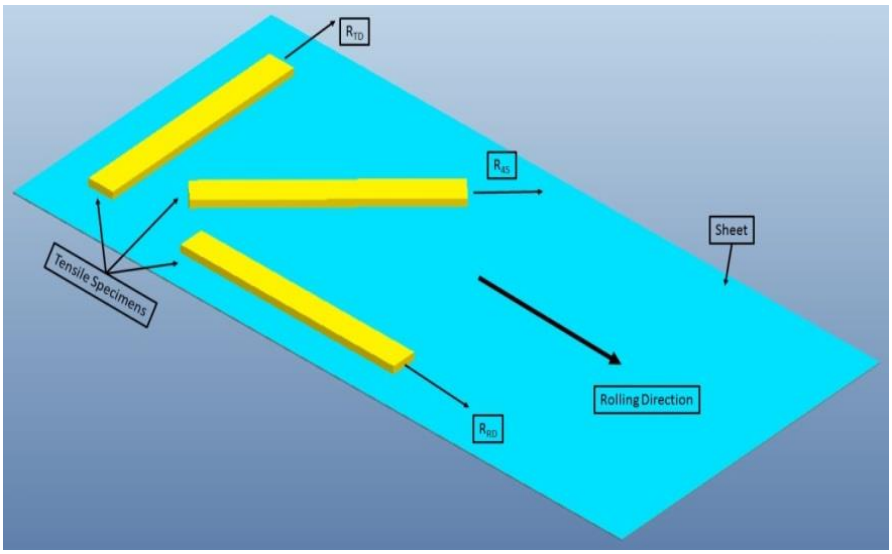

Fig. 3.7: Specimen orientations with respect to the sheet rolling direction

r-value is evaluated as per *ASTM E517 – 00(2006)* using uniaxial tensile tests. The dimensions of specimens prepared for *r* value determination is shown in Fig. 3.8. The gauge length of specimen is considered as *25 mm* and divided in to *5* equal segments along the gauge length. Width and length of these segments are measured before test. These divisions are made in order to increase the accuracy of measurement. Generally, specimen is elongated up to 10% of strain after yielding. Final length and width of the specimen after elongation have been measured.

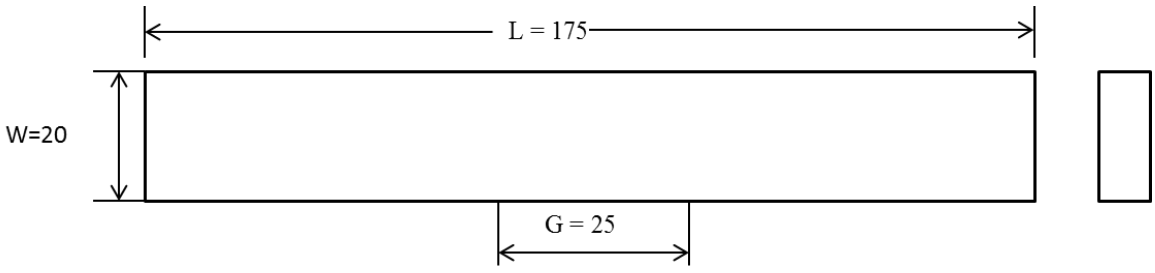

(*All dimensions are in mm*)

Fig. 3.8: Dimensions of specimen used for anisotropic coefficient (*r*) calculation

Width strain (ε_w) and longitudinal strain (ε_l) are measured and used in Equation 3.7 to find '*r*'. Table 3.3 shows *r* values with 0^0, 45^0 and 90^0 rolling direction of sheet

Table 3.3: Anisotropic coefficient (*r*) for Ti-6Al-4V alloy at various temperatures

Temp. (^{0}C)	r_0	r_{45}	r_{90}
RT	0.4698	1.4325	0.2939
50	0.4832	1.4235	0.3025
100	0.5278	1.3925	0.3489
150	0.5625	1.3711	0.3694
200	0.6036	1.6144	0.5605
250	0.7964	1.1854	0.7093
300	0.7594	1.1523	0.4896
350	0.7139	1.0727	0.5329
400	0.6010	1.2632	0.5124

3.1.4 Other Uniaxial Material Properties

Table 3.4 indicates variation of yield strength, ultimate tensile strength and % ductility for Ti-6Al-4V alloy at various temperatures. As expected, yield stress and ultimate tensile strength decrease with the increase in the temperature. Moreover, ductility also increases with the increase in temperature. From Table 3.4, it can be observed that Ti-6Al-4V alloy becomes more flowable and easy to draw at higher temperatures.

Table 3.4: Variation of yield strength (σ_y), ultimate tensile strength (σ_{ut}) and % ductility at various temperatures

Temp. (^{0}C)	σ_0 (MPa)	σ_{45} (MPa)	σ_{90} (MPa)	$\sigma_{yavg.}$ (MPa)	σ_{ut0} (MPa)	σ_{ut45} (MPa)	σ_{ut90} (MPa)	$\sigma_{utavg.}$ (MPa)	Ductility (Avg.) (%)
RT	879	824	875	860	945	922	937	935	8.45
50	876	806	882	855	941	905	926	924	8.50
100	845	780	842	823	913	882	908	901	9.45
150	795	740	784	773	842	819	832	831	12.21
200	728	642	757	709	811	789	803	801	12.78
250	707	617	727	684	761	721	749	744	14.56
300	687	598	702	663	751	733	739	741	15.21
350	683	595	693	657	742	702	732	726	16.45
400	681	591	691	655	737	697	729	721	16.89

3.1.5 Biaxial Material Properties

Uniaxial test material properties are inadequate to predict material behavior for forming analysis because the state of stress for forming analysis is predominately in biaxial mode (*Rees DW, 1995*). Therefore, it is necessary to capture biaxial data for accurate prediction for forming analysis. Specifically, biaxial yield stress is crucial for accurate prediction of yielding in sheet metal forming analysis (*Xiang-Dong W, et al., 2005*). In the present study due to the lack of available biaxial test facility, the required biaxial yield stress and compressive yield stress values have been taken from the literature (*Odenberger, 2013*).

Biaxial anisotropic coefficient is essential to take in to account non-symmetric behavior in the material model. This fact is also a consequence of the biaxial plastic anisotropy (*Barlat et al., 2003; Poehlandt et al., 2002*). One of the easy ways to determine r_b is compression test /coin test (*Banebic, 2010*). A set of circular specimens are subjected to a normal pressure. Due to the plastic anisotropy, the discs become elliptic during the compression. By measuring the major and minor axes of the elliptic specimen, the corresponding principal strains can be evaluated. The ratio of the principal strains will define the coefficient of biaxial anisotropy. It can be observed that variation in biaxial anisotropic coefficient is very negligible over the range of temperature. Table 3.5 shows biaxial material properties and compressive yield stress for Ti-6Al-4V alloy at various temperatures.

Table 3.5: Biaxial material properties and compressive yield stress for Ti-6Al-4V alloy

Temp. (^{0}C)	σ_b (MPa)	r_b	σ_c (MPa)
RT	1070.5	1.02	1106.2
50	1070.5	1.02	1106.2
100	1023.4	1.02	1055.8
150	977.0	1.02	1005.4
200	930.6	1.02	955.0
250	884.2	1.02	904.6
300	837.8	1.02	854.2
350	791.4	1.02	803.7
400	745.0	1.02	753.3

3.2 Microstructure and Fractography Study

The as-received sample has been cold mounted by using commercially available cold setting compound (resin powder + liquid) and then wet ground on progressively finer grades of silicon carbide impregnated emery paper using copious amounts of water both as a lubricant and as a coolant. Subsequently, the ground samples have been mechanically polished using five-micron diamond solution. Fine polishing to a perfect mirror-like finish of the surface has been achieved using one-micron diamond solution as the lubricant. The polished samples have been etched using with Kroll solution (H_2O: 92 ml, HF: 5 ml, HNO_3: 10 ml). The polished and etched surface of the sample has been observed under an optical microscope and photographed using standard bright field illumination technique.

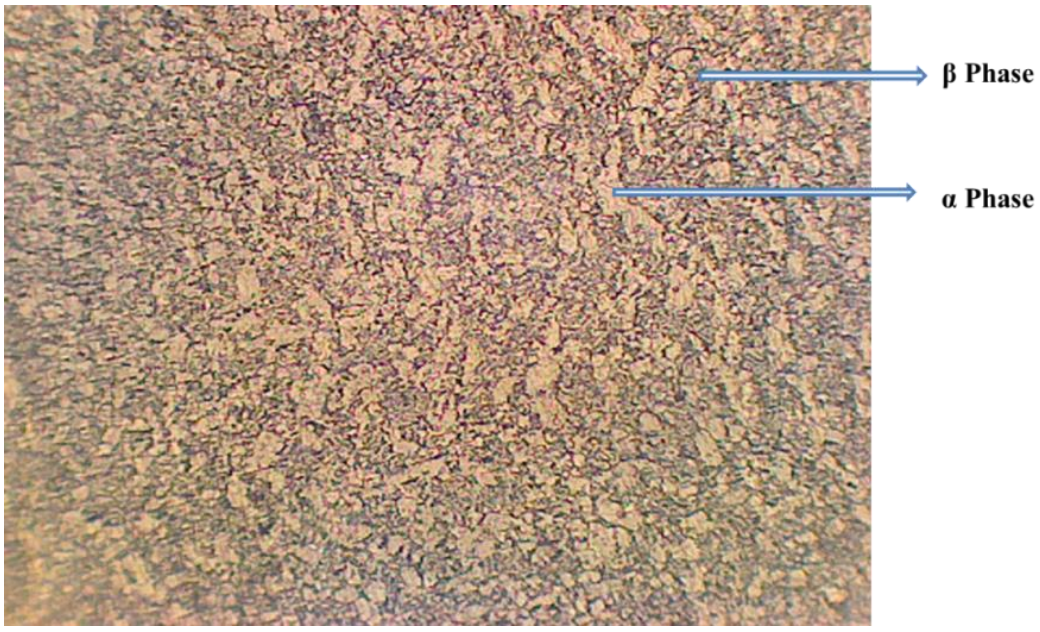

Fig.3.9: Optical micrographs showing the key micro-constituents in Ti-6Al-4V alloy at 200X magnification

The as-received initial microstructure is equiaxed in which broad α and fine β alternate to form packets, as shown in Fig.3.9. Observations over a range of magnifications revealed the two distinctly different micro constituents, α (hexagonal closed packed – HCP) and β (body centered cubic – BCC) phases. The grains of the alpha (α) phase (light) are well dispersed in the matrix of the transformed beta (β) (dark phase). The average grain size of both α phase and the transformed β phase are *3-4* μm.

The fracture surface of the fully deformed tensile test samples are comprehensively examined using a scanning electron microscope (SEM) of make *Hitachi, S-3400N accelerating voltage* $15kV$. The samples for observation are sectioned parallel to the fracture surface. The fracture surfaces are observed at different magnifications to determine the macroscopic fracture mode and to concurrently characterize the intrinsic features on the tensile fracture surface during uniaxial tensile deformation.

Representative fractographs of the tensile fracture surface of Ti–6Al–4V sheet at various temperatures are shown in Fig. 3.10. Overall morphology of the tensile fracture surface at 150X and 500X magnification appeared to be rough and uneven as shown in Fig. 3.10 (a, c, e) over the range of temperature. Observation of fracture surface at higher magnification of 2000X over the range of temperature revealed a healthy population of shallow type dimples of varying size and shapes as shown in Fig. 3.10 (b, d, f).

When overload is the principal cause of fracture, Ti–6Al–4V alloys fail by a process known as microvoid coalescence. The microvoids nucleate at regions of localized strain discontinuity, such as that associated with second phase particles, inclusions, grain boundaries, and dislocation pile-ups. As the strain in the material increases, the microvoids grow, coalesce, and eventually form a continuous fracture surface. The

cuplike depressions are referred to as dimples, and the fracture mode is known as dimple rupture.

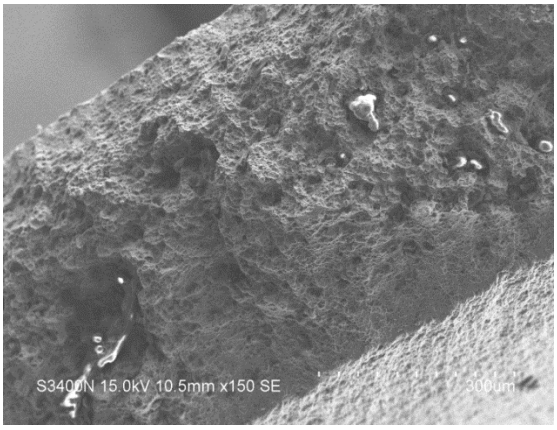

(a) 150 X Magnification at RT

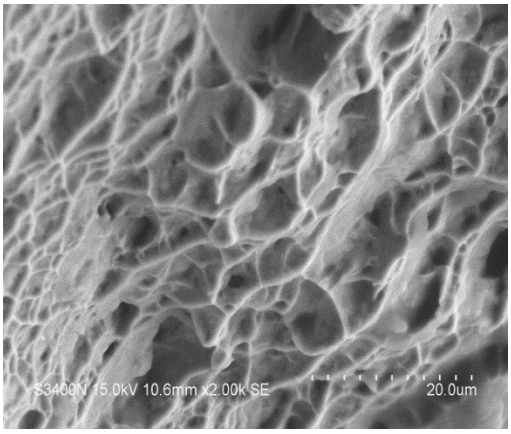

(b) 2000X Magnification at RT

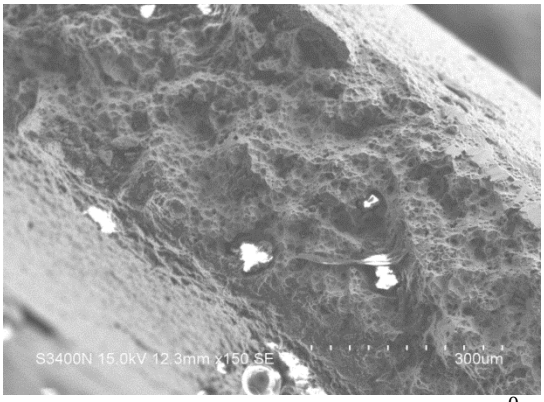

(c) 150 X Magnification at 300^0C

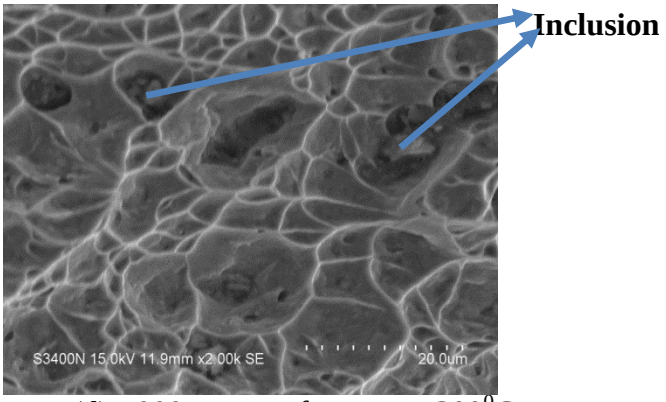

(d) 2000X Magnification at 300^0C

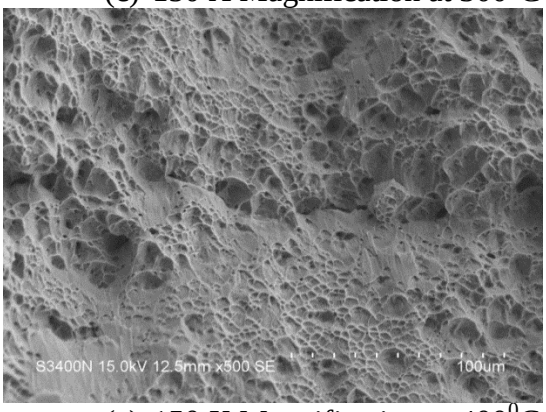

(e) 150 X Magnification at 400^0C

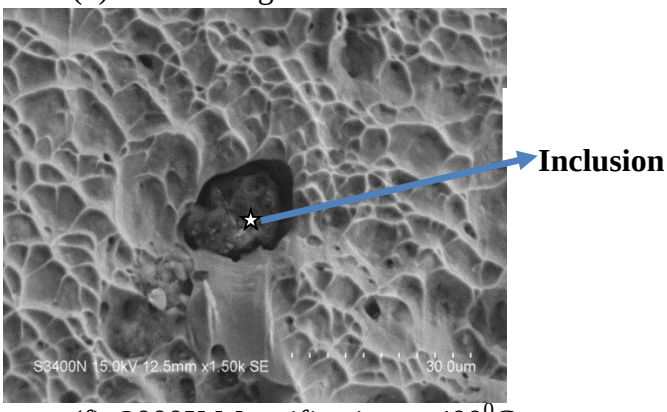

(f) 2000X Magnification at 400^0C

Fig.3.10: Representative fractography images of fracture tensile specimens over the range of magnification

Small dimples with varying size and shapes are formed when numerous nucleating sites are activated and adjacent microvoids join (coalesce) before they have an opportunity to grow to a larger size as shown in Fig. 3.10 (b, d, f). The formation of shallow type dimples might involve the joining of microvoids by shear along slip bands. Formation of large amounts of small shape and size dimples and microvoids are observed in the fracture surface which indicates ductile fracture. Few inclusions are also reported in the high magnification fracture surface morphology as shown in Fig. 3.10 (d & e). Fig. 3.11 shows Energy-Dispersive X-ray Spectroscopy (EDS) analysis of inclusion present at 400^0C. Based on EDS analysis, it clearly indicates that inclusion is present in the fracture surface. It could be a complex silicate containing major portion of silica and oxygen.

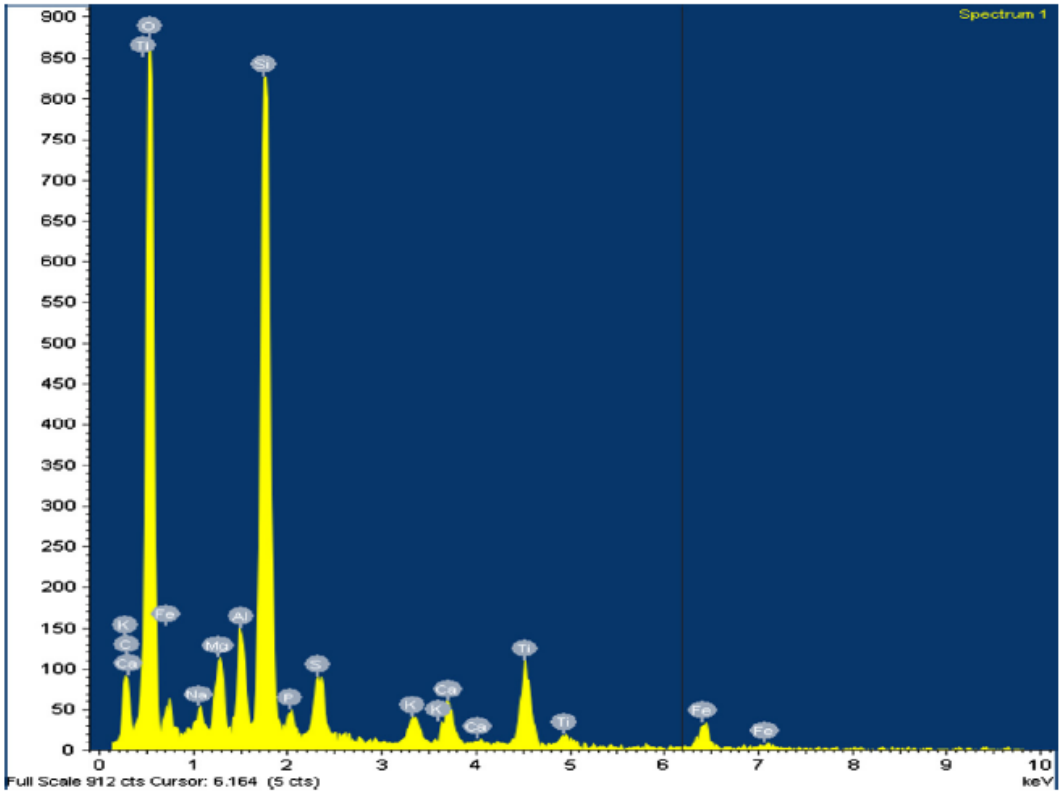

Fig.3.11: EDS analysis of inclusion portion show in Fig. 3.10 (f)

3.3 Experimental Investigation on Deep Drawing of Ti-6Al-4V Alloy

3.3.1 Experimental Set up for Deep Drawing Process

Circular deep drawing process has been used to study the forming behavior of Ti-6Al-4V alloy sheet at elevated temperatures. The basic geometry in a simple cup drawing operation is shown in Fig. 3.12. Punch size (D_p), punch corner radius (R_p), die opening (D_d), die corner radius (R_d) and blank size (D_b) are the important physical parameters which affect the deep drawing process. The clearance between die opening and punch is another important parameter. Small clearance may lead to ironing, which is simply the intentional thinning of the blank at the die cavity. Normally, to avoid ironing, the clearance must be larger than the blank thickness (t). Usually, the clearance is 20% larger than the initial blank thickness (*Beddoes & Bibby, 1999*). The other parameters which affect the deep drawing operations are blank holder force, punch speed, lubrication, properties of blank material (*Ghosh et al. 1985*). In a typical deep drawing process, a circular blank of radius R_0 and thickness t_0 is drawn by a flat-bottomed punch through a die opening of radius r_d with a constant blank-holding force.

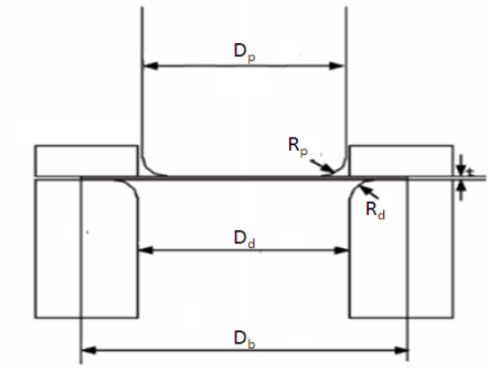

Fig. 3.12: Basic geometry in a simple cup drawing process

The experiments have been carried out on the test rig which is shown in Fig. 3.13. This test rig is specifically designed so that deep drawing operations can be performed at elevated temperatures. The technical specification of experimental set up is mentioned in Table 3.6. Inconel die and punch have been manufactured on CNC lathes and tested for geometrical features such as cylindricity, ovality, and taper. Nickel based super alloy has been used for manufacturing die, blank holder and punch. Two sets of furnaces have been utilized for 20 ton hydraulic press. One heater is employed to heat the blank. Another heater is used to heat lower die in order to prevent the blank from becoming cold before the actual drawing starts. Fig. 3.14 shows induction heating coil arrangement for deep drawing process.

Fig. 3.13: Experimental test rig for deep drawing process

Table 3.6: Technical specifications of experimental test rig

Capacity of the press	20 tons
Electrical motor HP	5 HP
No of main cylinders	1 no
Blank holder ram bore diameter	40 mm
Blank holder ram rod diameter	25 mm
Blank Holder ram stroke	300 mm
No of blank holder cylinders	2 no's
Pressing speed	30~ 500 mm/min
Max operating pressure	140 Kg/cm^2
Furnace	2 nos

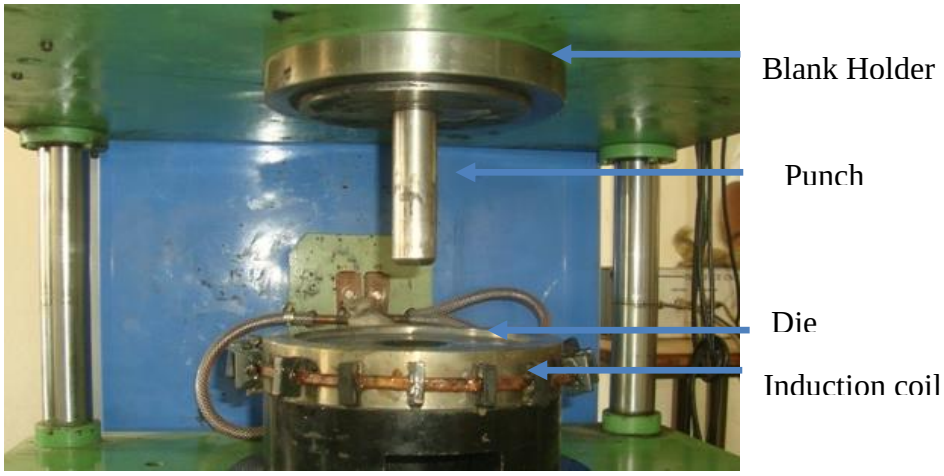

Fig. 3.14: Induction heating coil arrangement for deep drawing process up to 400^{0}C

The setup temperature has been controlled and prevented from overheating by means of water circulation from cooling tower. A noncontact type pyrometer is used to measure the operating temperature. Circular blanks have been machined by using wire-cut electro-discharge machining process for high accuracy and finish.

One major factor in deep drawing is the die corner radius and punch corner radius. Sharp corners on the punch and die cause it to cut the sheet A radius of curvature on the edge is necessary to change the force distribution and cause the metal to flow over the curvature into the die cavity. Considering this, the radius of curvature to the punch corner is kept 4 to 5 times of the sheet thickness; while the radius of curvature to the die corner is given as 8 to 10 times of the sheet thickness (*Hosford & Canddell, 2014*).

Thinning in drawn cup is unavoidable, but it should be as minimum as possible for a good quality cup. Maximum thinning occurs most likely on the punch corner region. A correctly drawn cup may have up to 25% reduction in the thickness in this area (*Singh SK, 2008*). Considering above factors, the appropriate dimension of tooling geometry used for deep drawing process is shown in Fig. 3.15.

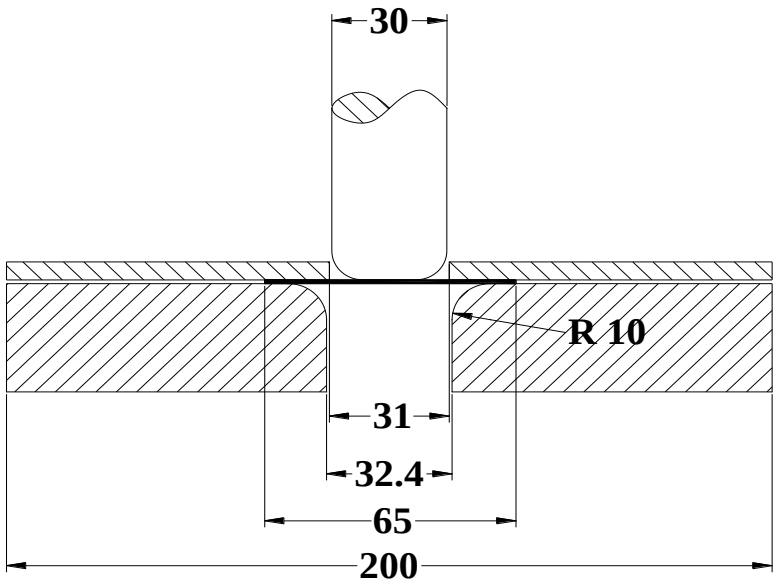

(*All dimensions are in mm*)

Fig. 3.15: Dimensions of tooling geometry used for deep drawing process

The possible forming behavior of Ti-6Al-4V alloy has been found by performing deep drawing experiments from room temperature to 400^0C at an interval of 50^0C. The circular blanks have been made form 48 mm diameter at interval of 2 mm. Molykote has been used as an effective lubricant during the deep drawing process at elevated temperatures (*Singh SK, 2008*).

Circular blanks have been kept at particular temperature for certain duration (approximately 3-5 minutes) for uniform heating of sheet Deep drawing operation has been performed when the blank reaches required temperature. The experiments have been performed at punch speed of 20 mm/min and approximately 2% of yield strength as a blank holding pressure. Data acquisition system is used to capture punch load and the punch displacement data during the deep drawing process.

3.3.2 Failure Study in Deep Drawing Cups

The failure in the deep drawn cups has been studied. The fracture can be distinguished in two ways; initial fracture and final fracture as shown in Fig. 3.16. Similar fractures have been reported for HCP crystal structure alloy in the previous literature (*Djavanroodi & Derogar, 2010; Zhang S.H, et al., 2007*). Initial fracture appears in the punch corner region since the material possesses very low *n* value at room temperature. For larger diameter blanks, due to more punch load requirement the extent of thinning is more hence failure will be appeared in the neck region. The similar failure is seen up to 100^0C and is shown in Fig. 3.16 (a & b).

(a) (b) (c)

Fig.3.16: Type of failures occurred during experimentation (a) neck failure at 50^0 C (b) neck failure at 100^0 C (c) fracture at upper wall at 400^0C

Another type of fracture observed is final fracture, i.e., chipping of wall materials from upper region. This type of fracture is seen at the temperature of 400^0C with larger blank diameter (above 56 *mm*). The main reason might be a Bauschinger effect which is more pronounced in Ti-6Al-4V alloy up to lower elevated temperature (*Odenberger Eva-Lis, 2005*). Heavy compressive hoop stresses and radial tensile stresses are developed in the flange region. Since the material losses its compressive strength due to Bauschinger effect, even slight tendency of wrinkling will lead to fracture. On the other hand, it might be possible of increasing a friction at die corner region due to ineffectiveness of Molykote lubricant at high temperature. Therefore, excessive shear stresses are developed on the outer surface of material in the bend region of die. In addition to this, compressive stresses are developed on inner curvature of blank. Since the material is weak in compression due to Bauschinger effect, the inner curvature of blank may become the site for initiation of failure. As discussed before, this material does not exhibit much strain hardening even at higher temperatures, hence drawing may lead to shear fracture in the

upper region of the wall. One of the possible solutions to overcome this problem is to increase the die curvature, which decreases the intensity of the compressive stresses on the inner surface of the sheet metal. When large diameter blank is being drawn, due to the excessive shear stresses on the bend region of die, the initiated crack has sufficient time to grow and fracture the material. However, for smaller diameter blanks, the initiated crack does not have sufficient time to propagate and the cups can be successfully drawn before failure takes place.

Furthermore, the fracture surfaces of the failed cups have been comprehensively examined using SEM of make *ZEISS, SUPRA 55 VP* accelerating voltage *20 kV*. The samples for observation have been sectioned parallel to the fracture surface using wire cut EDM. Representative fractographs of the fracture surface in neck region at 50^0C and 100^0C are shown in Fig. 3.17 and Fig. 3.18 respectively.

Overall morphology of fracture surface appears rough and uneven when seen in lower magnification fractography images. Observations of the fracture surface from Fig. 3.17 (b & c) and Fig. 3.18 (b & c) at higher magnification reveals a healthy population of shallow type equiaxed dimples of varying size and shapes. Equiaxed dimple indicates that failure occurred due to excessive tensile stresses. Ti–6Al–4V alloy is failed by a process known as microvoid coalescence. The microvoids nucleate at regions of localized strain discontinuity, such as that associated with second phase particles, inclusions, grain boundaries and dislocation pile-ups.

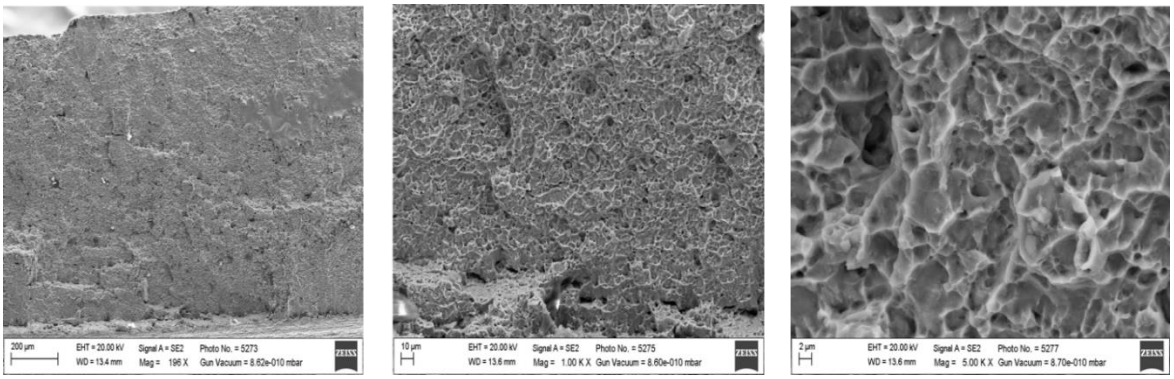

(a) 200X (b) 1000X (c) 5000X

Fig.3.17: SEM fractography images of neck region at room temperature

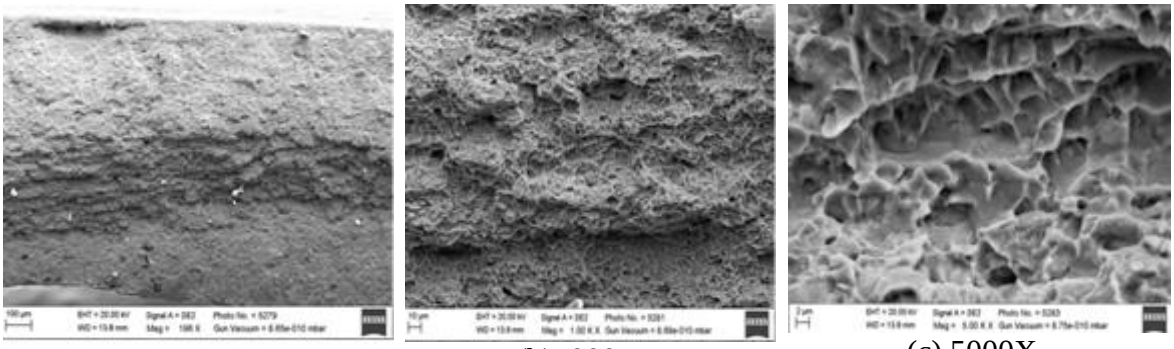

(a) 200X (b)1000 X (c) 5000X

Fig.3.18: SEM fractography images of neck region at 100^0C

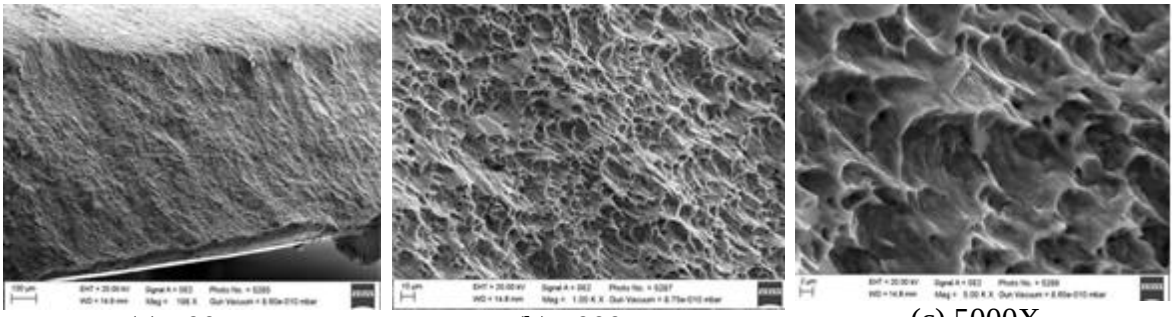

(a) 200X (b) 1000X (c) 5000X

Fig.3.19: SEM fractography images of wall region at 400^0C

As the strain in the material increases, the microvoids grow, coalesce and eventually form a continuous fracture surface. Small dimples with varying size and shapes observed at higher magnification fractographs are formed when numerous nucleating sites are

activated and adjacent microvoids join (coalesce) before they have an opportunity to grow to a larger size as shown in Figure 3.17 (c) and Fig. 3.18 (c). This is a clear indication of ductile failure in the neck region. The fractograph of wall region also shows irregular and rough surface morphology and it is shown in Fig. 3.19 (a). Unidirectional dimples are observed at wall region which is a clear evidence of shear failure. This failure can be seen at higher magnification fractographs shown in Fig. 3.19 (b & c). This is an evidence of chipping of materials due to excessive shear stress in the top of the wall region.

3.3.3 Formability Study

Formability in the deep drawing process has been studied using LDR, thickness distribution and earing profile.

Limiting Drawing Ratio (LDR)

Formability is difficult to be defined and quantified accurately. It depends on the consequence of material properties and the complex tool blank interactions. LDR is a quantifiable measure to calculate formability of sheet metal (*Singh & Ravi Kumar, 2008*). Ti-6Al-4V alloy is difficult to draw up to 150^0C. This can be also be seen from Table 3.2 that *n* value is very low at room temperature. Similar range of *n* values is reported in the previous literature (*Aly EI-Domiaty, 1992*). There is a gradual increase in *n* value as the temperature increases which implies the material has more scope for elongation before necking. This could be the main reason of Ti-6Al-4V alloy being drawn only above 150^0C. LDR at various temperatures is presented in Table 3.7. The maximum LDR of 1.86 is obtained which is substantially lesser than other metallic structural materials such

as austenitic stainless steels (*Singh et al., 2010*). Fig. 3.20 shows representative successfully drawn cup at various temperatures.

Table 3.7: LDR at various temperatures

Temp. (^{0}C)	200^{0}C	300^{0}C	400^{0}C
LDR	1.7	1.8	1.86

(a) (b) (c)

Fig. 3.20: Successfully drawn cups at various temperatures (a) 200^{0}C (b) 300^{0}C (c) 400^{0}C

Thickness Distribution

The cups have been cut using wire cut EDM and thickness is measured from base of the cup to the top of the wall. For every setting, three experiments have been performed and average values of thickness values are considered. Thickness distribution of 52 mm blank diameter with variation of temperature from 150^{0}C to 400^{0}C at interval of 50^{0}C is shown in Fig. 3.21 (a). As expected, neck formation appeared near the punch corner radius and increase in thickness has been observed in wall region. As temperature increases, reduced necking tendency has been observed due to consistent increase of *n* value.

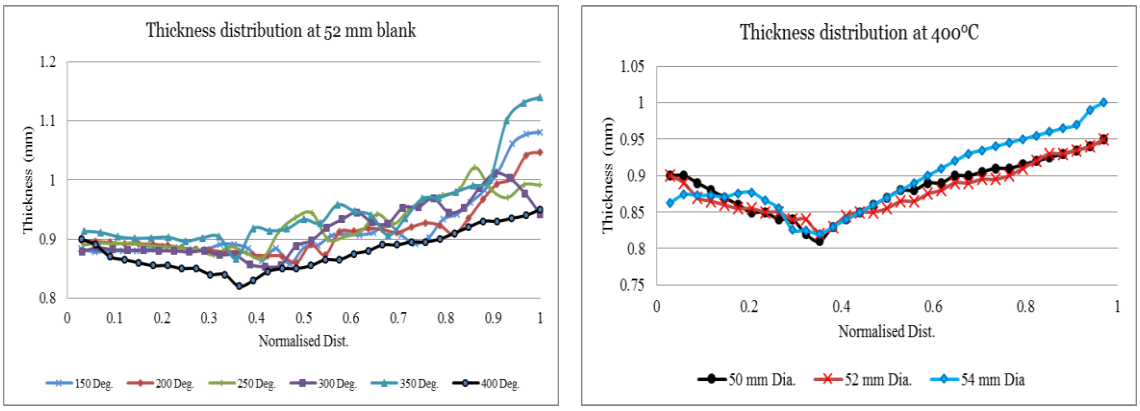

(a) (b)

Fig. 3.21: Representative thickness distribution with variation of (a) temperature (b) blank diameter

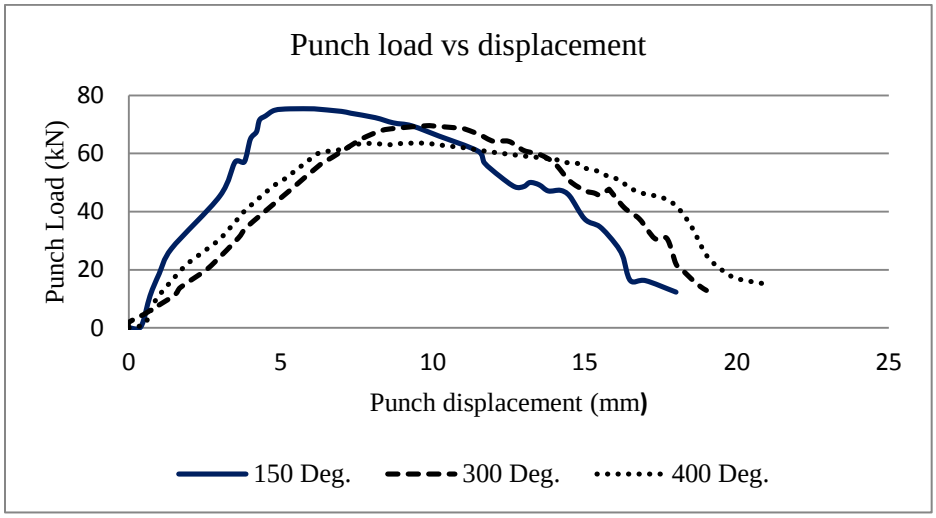

Fig. 3.22: Representative punch vs. load displacement for 52 mm blank diameter with variation of temperature

Additionally, as the temperature of blank is increased, there is a consistent decrease in ultimate tensile strength and yield strength of material as shown in Table 3.4. This decreases the mean flow stress at which the material is being drawn. Hence, lesser amount of forces is appeared on the punch (Fig. 3.22); this further decrease the variation

of the thickness in drawn cup. As expected, the representative punch displacement of 54 mm blank diameter with variation of temperature is shown in Fig. 3.22. Therefore, at higher temperature more uniform thickness can be observed due to lower mean flow stress and slightly larger *n* value. Alternatively, for larger blank diameter increased tendency of thinning is observed at the punch corner as shown in Fig. 3.21 (b). Based on this observation, it can be concluded that as temperature is increased, thickness is more uniform which means better quality of cup will be obtained with optimum blank diameter.

Earing Profile

It is important to note that earing is one of the important characteristics in deep drawing since it is associated with the anisotropy in the sheet Earing in deep drawn cups occurs from different plastic strain ratio at different directions (*Yoon & Barlat, 2006*). Fig. 3.23 shows the representative earing profile of 54 mm blank diameter at 400^0C. The significant earing tendency (four ears) has been observed in all the deep drawn cups.

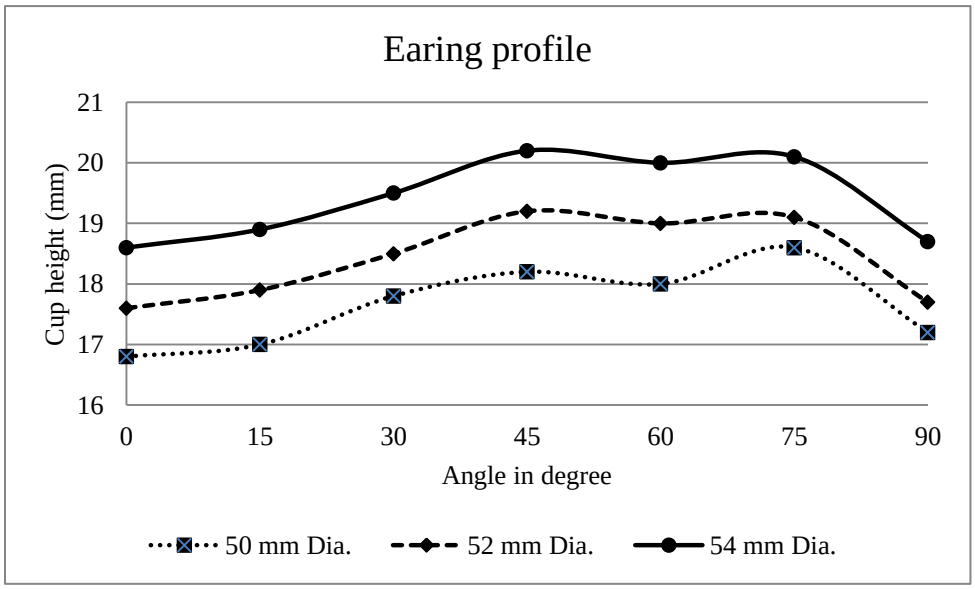

Fig. 3.23: Representative earing profile of 54 mm blank diameter at 400^0C

3.4 Summary

This chapter discussed the experimental investigations about the forming behavior of Ti-6Al-4V alloy at elevated temperatures using deep drawing process. The uniaxial and biaxial material properties have been studied at various temperatures. The microstructure and fractography study of failed tensile specimens have been investigated over the range of temperature. The various qualitative aspects of deep drawn cups such as LDR, thickness distribution and earing profile have been studied. Ti-6Al-4V alloy is difficult to draw up to 150^0C. The maximum LDR is found to be 1.86 at 400^0C which is substantially lower than the other structural alloys. The thickness distribution is significantly dependent on temperature and blank diameter. The substantial earing tendency has been observed in deep drawn cups.

These experimental findings need to be supported by the numerical analysis. The reliability of the numerical techniques is largely dependent on the input material properties and the appropriate selection of material models. Therefore, appropriate material models need to be developed for Ti-6Al-4V alloy. The next chapter will discuss about the development of various anisotropic yield criteria and constitutive models for Ti-6Al-4V alloy at elevated temperatures.

CHAPTER 4: MATERIAL MODELS FOR NUMERICAL ANALYSIS OF SHEET METAL FORMING PROCESS

Numerical analysis is an essential tool for understanding the complex deformation mechanisms that occur during sheet metal forming processes. Accuracy of these techniques is largely dependent on the use of appropriate material models that describes the complex behavior of the material. Material models involve the concepts of yield criteria and constitutive models.

4.1. Yield Criteria

A yield surface is defined as the hyper surface which encloses the elastic region. Usually for sheet metal forming, yield locus is defined in the plane stress space. Many yield criteria have been developed over the years. For isotropic metallic materials, the well-known Von Mises or Tresca yield functions are often sufficient to describe the plastic behavior of metals. However, in sheet metal forming the sheet materials are usually anisotropic with respect to their plastic properties. In order to take into account this plastic anisotropy, the yield function can be considered by introducing additional parameters to describe the plastic anisotropic behavior (*Beddoes et al., 1999*). In the present study, various advanced anisotropic yield criteria namely; Hill 1948, Barlat 1989, Barlat 1996, Barlat 2000 and Cazacu Barlat have been developed for the Ti-6Al-4V alloy at elevated temperatures.

4.1.1 Hill 1948 Yield Criterion

In 1948, Hill proposed an anisotropic yield criterion as a generalization of the Huber-Mises-Hencky criterion. The material is supposed to have an anisotropic with three orthogonal symmetry planes. In case that the principal directions of the stress tensor are coincident with the anisotropic axes, Hill 1948 yield criterion can be written as a dependence of the principal stress as per Equation (4.1).

$$\sigma_1^2 - \frac{2r_0}{1+r_0}\sigma_1\sigma_2 + \frac{r_0(1+r_{90})}{r_{90}(1+r_0)}\sigma_2^2 = \sigma_0^2 \tag{4.1}$$

Therefore, in order to define the yield under plane stress condition, three mechanical parameters, namely the coefficients r_0, r_{90}, and one of the uniaxial yield stresses σ_0 and σ_{90} are required.

4.1.2 Barlat 1989 Yield Criterion

Further popular development in the anisotropic yield criterion is Barlat 1989 yield model. This model is the extension of Hosford theory to incorporate effects in materials exhibiting normal anisotropy has been proposed by Barlat and Richmond (*Banbic, 2010*). For transversely isotropic material, the Barlat 1989 criteria is mathematically a variation of Hill 1948 in which the yield function exponent *m* takes the value 2. The exponent is dependent on crystallography and it is considered as 6 for BCC structure and 8 for FCC structure (*Keum, et al., 2001*). Barlat 1989 yield criterion is expressed as per Equation (4.2)

$$f \equiv a|k_1 + k_2|^M + a|k_1 - k_2|^M + c|2k_2|^M = 2\sigma^a \tag{4.2}$$

where, k_1 and k_2 are invariants of the stress tensor, as per Equation (4.3 and 4.4)

$$k_1 = \frac{\sigma_{11} + h\sigma_{22}}{2}; \tag{4.3}$$

$$k_2 = \sqrt{\left[\left(\frac{\sigma_{11} - h\sigma_{22}}{2}\right)^2 + p^2\sigma_{12}^2\right]} \tag{4.4}$$

a, *c* and *h* are material parameters determined by:

$$a = 2 - c = 2 - 2\sqrt{\frac{r_0 r_{90}}{(1 + r_{90})(1 + r_0)}} \tag{4.5}$$

$$h = \sqrt{\frac{r_0(1 + r_{90})}{r_{90}(1 + r_0)}} \tag{4.6}$$

The detailed procedure for determination of material constants have been mentioned in previous literature (*Barlat & Lian,1989*). The calculated material constants of Barlat 1989 yield criterion for Ti-6Al-4V alloy at various temperatures is shown in Table 4.1.

Table 4.1: The material constants of Barlat 1989 yield criterion for Ti-6Al-4V alloy

Temp. (^{0}C)	*a*	*c*	*h*	*p*
RT	1.73	0.26	1.18	1.18
50	1.72	0.27	1.18	1.20
100	1.70	0.29	1.15	1.24
150	1.68	0.31	1.15	1.32
200	1.63	0.36	1.09	1.47
250	1.62	0.42	1.09	1.52
300	1.57	0.44	1.07	1.62
350	1.54	0.47	1.07	1.66
400	1.50	0.50	1.05	1.70

4.1.3 Baralt 1996 Yield Criterion

The yield criterion proposed by *Barlat.et al.,* is expressed as per Equation (4.7)

$$\phi = \propto_1 |S_2 - S_3|^a + \propto_2 |S_3 - S_1|^a + \propto_3 |S_1 - S_2|^a = 2\bar{\sigma}^a \tag{4.7}$$

where, $\bar{\sigma}$ is equivalent stress and *a* is a material parameter which is the same as Barlat 1989 yield criterion. S_i corresponds to principal values of Cauchy stress deviator.

The equivalent stress deviator is defined as

$$[s] = [L][\sigma]$$

$$\text{where,} \quad L = \begin{bmatrix} (c_2 + c_3)/3 & -c_3/3 & -c_2/3 & 0 \\ -c_3/3 & (c_3 + c_1)/3 & -c_1/3 & 0 \\ -c_2/3 & -c_1/3 & (c_1 + c_2)/3 & 0 \\ 0 & 0 & 0 & c_4 \end{bmatrix} \tag{4.8}$$

c_1, c_2, c_3, c_4 are material constants and $\propto_{i=1,2,3}$ depends upon the orientation of frame of the principal value of *S* and anisotropy axis (*Barlat & Lian, 1989*).

$$\propto_i = \propto_x P_{1i}{}^2 + \propto_y P_{2i}{}^2 + \propto_z P_{3i}{}^2 \tag{4.9}$$

For a plane stress condition when shear stress is zero the yield function becomes

$$\phi = \propto_x |S_y - S_z|^a + \propto_y |S_z - S_x|^a + \propto_{z0} |S_x - S_y|^a = 2\bar{\sigma}^a \tag{4.10}$$

where,

$$S_x = \frac{c_3 + c_2}{3}\sigma_x - \frac{c_3}{3}\sigma_y$$

$$S_y = \frac{-c_3}{3}\sigma_x + \frac{c_{11} + c_3}{3}\sigma_y$$

$$S_z = \frac{-c_2}{3}\sigma_x - \frac{c_1}{3}\sigma_y$$

For instance, consider $\propto_{z0}= 1$. Therefore, seven material constants are calculated by solving above seven non-linear equations. The detailed procedure for material constants determination has been mentioned in the previous literature (*Barlat et al., 1997a*). The calculated material constant for Barlat 1996 yield criteria is presented in Table 4.2.

Table 4.2: The material constants of Barlat 1996 yield criterion for Ti-6Al-4V alloy

Temp. (^{0}C)	c_1	c_2	c_3	c_4	α_x	α_y	α_{z0}	α_{z1}
RT	1.08	1.35	1.87	1.90	1.83	0.84	1	0.95
50	1.06	1.30	1.85	1.88	1.80	0.82	1	0.93
100	1.04	1.20	1.79	1.84	1.75	0.78	1	0.89
150	1.02	1.10	1.75	1.80	1.71	0.74	1	0.85
200	1.01	1.09	1.71	1.76	1.65	0.67	1	0.81
250	0.91	0.94	1.61	1.70	1.54	0.64	1	0.77
300	0.87	0.90	1.41	1.61	1.43	0.60	1	0.58
350	0.81	0.84	1.35	1.59	1.30	0.58	1	0.67
400	0.75	0.80	1.22	1.43	1.25	0.55	1	0.65

4.1.4 Barlat 2000 Yield Criterion

Barlat 2000 yield function represents as two complex functions as per Equation (4.11) (*Banabic, 2010*).

$$\phi' = |{X_1}' - {X_2}'|^a;\ \phi'' = |2{X_2}'' + {X_1}''|^a + |2{X_1}'' + {X_2}''|^a$$
$$\phi = |{X_1}' - {X_2}'|^a + |2{X_2}'' + {X_1}''|^a + |2{X_1}'' + {X_2}''|^a = 2{\sigma_y}^a \quad (4.11)$$

$$\{X'\} = [C']\{s\} = [C'][T][\sigma] = [L'][\sigma]$$

$$\{X''\} = [C'']\{s\} = [C''][T][\sigma] = [L''][\sigma] \qquad (4.12)$$

$$where, \quad [T] = \begin{bmatrix} 2/3 & -1/3 & 0 \\ -1/3 & 2/3 & 0 \\ 0 & 0 & 1 \end{bmatrix}$$

$X'_{1,2}$ and $X''_{1,2}$ are the principal values of the linearly transformed stress deviator matrices {s},

When the matrices C' and C'' are taken as identity matrix the above criteria reduces to isotropic case. For the simplicity of calculation, anisotropy parameters and the coefficients of L' and L'' are related as

$$\begin{bmatrix} L'_{11} \\ L'_{12} \\ L'_{21} \\ L'_{22} \\ L'_{66} \end{bmatrix} = \begin{bmatrix} 2/3 & 0 & 0 \\ -1/3 & 0 & 0 \\ 0 & -1/3 & 0 \\ 0 & 2/3 & 0 \\ 0 & 0 & 1 \end{bmatrix} \begin{bmatrix} \alpha_1 \\ \alpha_2 \\ \alpha_7 \end{bmatrix} \qquad (4.13)$$

$$\begin{bmatrix} L''_{11} \\ L''_{12} \\ L''_{21} \\ L''_{22} \\ L''_{66} \end{bmatrix} = \begin{bmatrix} -2 & 2 & 8 & -2 & 0 \\ 1 & -2 & -4 & -4 & 0 \\ 4 & -4 & -4 & 1 & 0 \\ -2 & 8 & 2 & -2 & 0 \\ 0 & 0 & 0 & 0 & 9 \end{bmatrix} \begin{bmatrix} \alpha_3 \\ \alpha_4 \\ \alpha_5 \\ \alpha_6 \\ \alpha_8 \end{bmatrix} \qquad (4.14)$$

Exponent a is the same parameter as in the three parameter Barlat's criterion. Matrices C' and C'' are expressed in terms of eight anisotropy coefficients $\propto_i$, for isotropic case $\propto_i$ is unity. For determination of material parameters $\propto_1$ to $\propto_8$, eight mechanical parameters are required. Yield stress (σ_y) and Lankford parameters (r) in 0^0,

45^0 and 90^0 orientation have been taken from uniaxial tensile tests. Additionally, biaxial yield stress (σ_b) and biaxial anisotropy coefficient (r_b) have been considered for constant determination (*Banabic, 2010*). The detailed parameter descriptions were mentioned in previous literature (*Barlat F et al., 1997*). The calculated material constants for Barlat 2000 yield criterion is presented in Table 4.3.

Table 4.3: The material constants of Barlat 2000 yield criterion for Ti-6Al-4V alloy

Temp. (^{0}C)	a_1	a_2	a_3	a_4	a_5	a_6	a_7	a_8
RT.	1.43	0.20	0.50	0.90	0.91	0.62	1.05	1.29
50	1.40	0.32	0.53	0.91	0.91	0.62	1.05	1.33
100	1.37	0.40	0.54	0.93	0.92	0.63	1.06	1.38
150	1.33	0.58	0.56	0.95	0.92	0.63	1.06	1.44
200	1.20	0.68	0.58	0.95	0.93	0.64	1.08	1.52
250	1.14	0.74	0.60	0.96	0.93	0.64	1.10	1.55
300	1.09	0.80	0.62	0.97	0.94	0.66	1.10	1.58
350	1.03	0.83	0.67	0.98	0.94	0.69	1.11	1.62
400	0.97	0.87	0.69	0.98	0.96	0.74	1.13	1.66

4.1.5 Cazacu Barlat Yield Criterion

Stress asymmetry (Bauchinger effect) is more predominate in HCP crystal structure alloy. Anisotropic yield criterion which consists of both tension and compression asymmetry is proposed by Cazacu et al. (*2006*). For extending this criterion, stress deviators is linearly transformed and the principle values of Cauchy stress deviator in the yield function are replaced by transformed tensor. The proposed anisotropic yield function is given as Equation (4.15)

$$[|\Sigma_1| - k\Sigma_1]^a + [|\Sigma_2| - k\Sigma_2]^a + [|\Sigma_3| - k\Sigma_3]^a = F \tag{4.15}$$

$$\text{where, } \Sigma = C[s] \text{ and } \mathrm{C} = \begin{bmatrix} C_{11} & C_{12} & C_{13} & & & \\ C_{12} & C_{22} & C_{23} & & & \\ C_{13} & C_{23} & C_{33} & & & \\ & & & C_{44} & & \\ & & & & C_{55} & \\ & & & & & C_{66} \end{bmatrix} \tag{4.16}$$

where, C is a fourth order transformation tensor with reference to orthotropic (x, y, z) axes and F is the size of yield locus, k is based on yield stress in tension/compression and material parameter a in the yield function. The detailed procedure for constant determination has been mentioned in the previous literature (*Cazacu et al., 2006*).

In the present study, linear approximation has been considered for determination of biaxial yield stress and compressive stress value at intermediate temperature range (*Odenberger etal., 2013*). However, Cazacu Barlat yield criterion considers stress asymmetry (Bauschinger effect). It means the yield locus is not symmetric. Hence, the calculation of material constants at intermediate temperature is not possible due to convergence issue. Therefore, Cazacu Barlat yield criteria constants are determined only at 400^0C, as presented in Table 4.4.

Table 4.4: The material constants of Cazacu-Barlat yield criterion for Ti-6Al-4V alloy

Temp. (^{0}C)	C_{11}	C_{22}	C_{33}	C_{12}	C_{13}	C_{23}	C_{44}	a	k
400	1.95	1.83	1.95	0.68	0.48	0.45	1.88	8	-0.08

4.1.6 Comparison of Yield Criteria

The performance of the yield criteria must be evaluated by thorough comparison with the experimental data. These comparisons should not be limited to the analysis of the yield locus shape. They should also envisage the planer distribution of the uniaxial yield stress and uniaxial coefficient of plastic anisotropy. The selection of yield criteria is also dependent on number of material parameters required and complexity involved for parameter determination (*Banabic, 2010*).

Fig. 4.1 (a & b) shows representative yield loci using Hill 1948 and Barlat 1989 yield criteria respectively. It can be observed that the prediction capability of both these yield criteria is very poor in biaxial state of stress and compressive state stress. Moreover, yield stress and anisotropic coefficient variation is poorly predicted by Hill 1948 and Barlat 1989 yield criteria as shown in Fig. 4.2 (a & b). But, these two models are popularly used in sheet metal industry because parameters required for determination of constants are less and determination procedure is easy. The similar observations were observed in previous literature for highly anisotropic materials (*Banabic, 2010*).

Fig. 4.1 (c & d) shows representative yield locus using Barlat 1996 and Barlat 2000 yield criteria. It can be seen that the prediction capability of these two yield criteria is far superior to Hill 1948 and Barlat 1989 yield criteria. However, still the prediction capability is poor in case of compressive state of stress. The main reason for poor prediction is that these yield criteria do not consider stress asymmetry in account. However, in Ti-6Al-4V alloy, Bauschinger effect is more noticeable at elevated

temperatures. Additionally, yield stress and anisotropic coefficient variation is more accurately predicted by using Barlat 1996 and Barlat 2000 yield criteria.

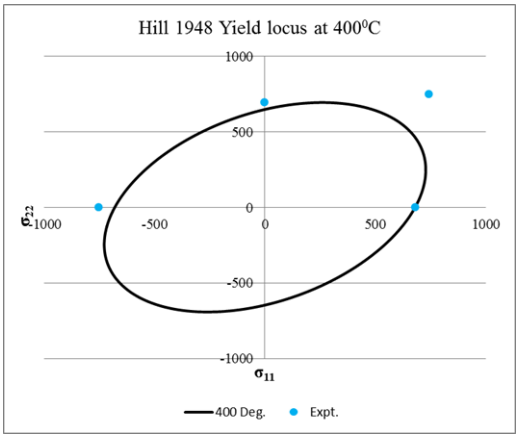

(a) Hill 1948

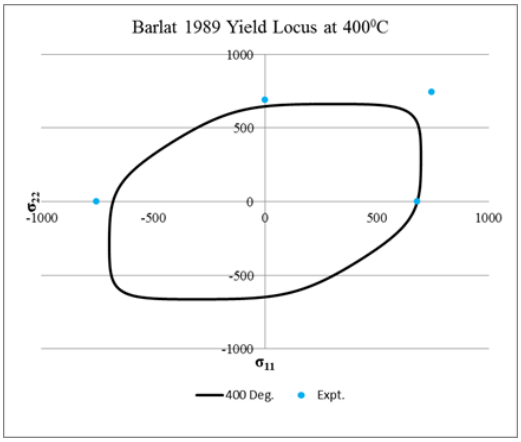

(b) Barlat 1989

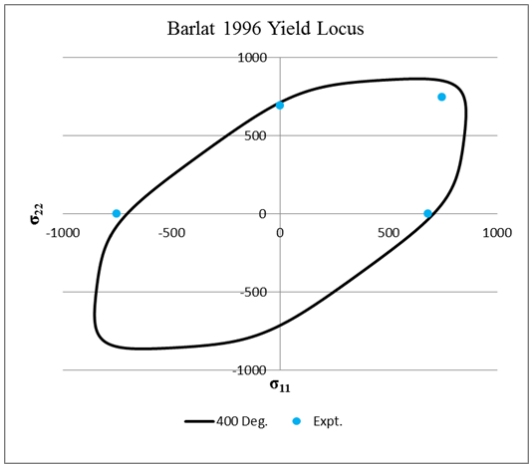

(c) Barlat 1996

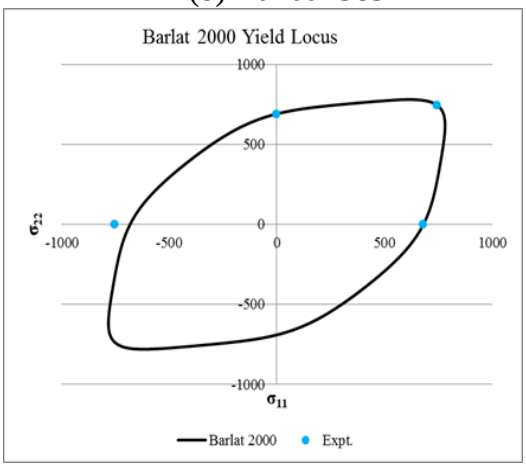

(d) Barlat 2000

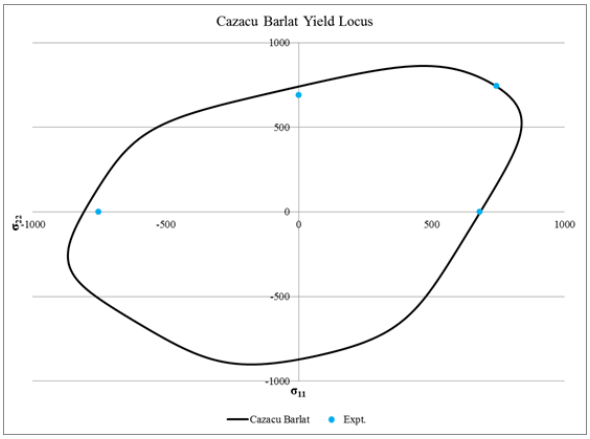

(e) Cazacu Barlat

Fig.4.1:Representative yield loci for Ti-6Al-4V alloy at 400^0C

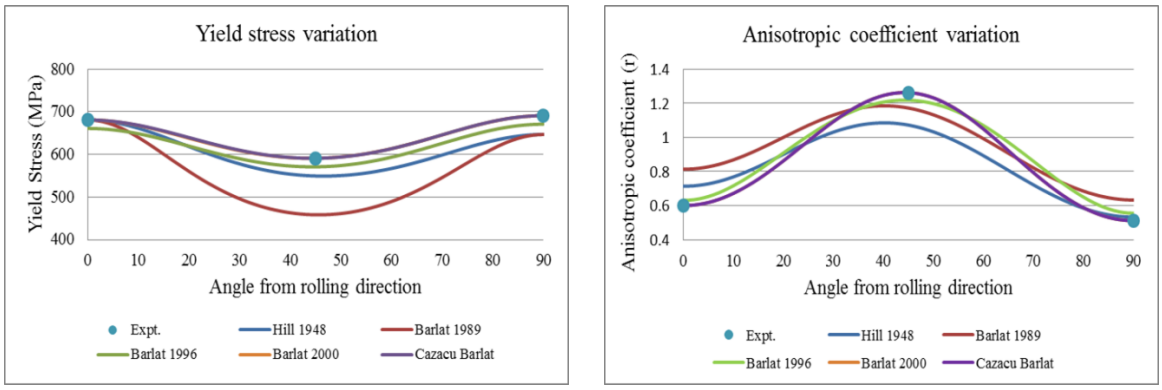

(a) (b)

Fig.4.2: Representative planer distribution of variation (a) yield stress (b) anisotropy coefficient

Table 4. 5: Mechanical tests required for various considered yield criteria

Yield Model	Parameters	Tests Required								
		σ_0	σ_{45}	σ_{90}	σ_b	r_0	r_{45}	r_{90}	r_b	σ_c
Hill 1948	4	*		*		*		*		
Barlat 1989	4	*				*	*	*		
Barlat 1996	8	*	*	*	#	*	*	*	#	
Barlat 2000	8	*	*	*	#	*	*	*	#	
Cazacu Barlat	8	*	*	*	#	*	*	*	#	×

* Uniaxial Tensile test

Biaxial Tensile test

× Compression test

However, these yield criteria involves more number of material parameters which require more number of mechanical tests need to be done for determination of material constants. Table 4.5 shows mechanical tests required for determination of material constants using various yield criteria.

Further accuracy in yielding prediction can be achieved by considering stress asymmetry. Cazacu Barlat yield criterion is very well suited for stress asymmetry or

Bauschinger effect. Fig. 4.1 (e) shows representative yield locus using Cazacu Barlat yield criteria at 400^0C. It can be observed that all the state of stress is accurately predicted using Cazacu Baralt yield criteria. Also, yield stress and anisotropic coefficient variation (Fig. 4.2) prediction is accurate with experimental data points. Therefore based on the above observations, it can be concluded that Cazacu Barlat yield criterion is very well suited for Ti-6Al-4V alloy at elevated temperatures.

4.2 Constitutive models

In the present study, three phenomenological based constitutive models namely; modified Fields-Backofen (*m-FB*), Johnson Cook (*JC*), modified Arrhenius (*m-Arr.)* and two physical based constitutive models viz.; modified Zerilli and Armstrong (*m-ZA*) and Mechanical Threshold Stress (MTS) model have been developed for Ti-6Al-4V alloy at elevated temperatures.

4.2.1 Modified Fields-Backofen Model

Fields and Bachofen (*FB*) proposed the constitutive model which is an extension of modified Hollomon power law (*Fields & Bachofen, 1957*). *FB* model is mathematically represented by Equation (4.17).

$$\sigma = K.\varepsilon^{n}.\dot{\varepsilon}^{m} \tag{4.17}$$

where, *K* is the strength coefficient, *n* is the strain-hardening exponent, and *m* is the strain-rate sensitivity exponent. This equation is widely used to describe the stress–strain relationship and it can well express the work-hardening phenomenon by the strain-

hardening exponent (*n*-value) and the strain-rate sensitivity exponent (*m*-value), which are the important parameters influencing the workability of metals or alloys.

Generally, the flow deformation behavior exhibited softening character at higher temperature under lower strain-rate. *FB* model is inaccurate to describe the softening behavior (*Cheng et al., 2008*). Therefore, in modified Fields Bachofen (*m-FB*) introduced a softening items into *FB* model to describe the softening behaviors (*Zhang, 2003*). The modified proposed Equation is mentioned below.

$$\sigma = K\varepsilon^{n}\dot{\varepsilon}^{m}(bT + s\varepsilon) \tag{4.18}$$

where,
$$s = \frac{dln\sigma}{d\varepsilon} = 0.92656 \tag{4.19}$$

b is the material constant and *s* is softening ratio of Ti-6Al-4V due to increase of strain, *s* is mathematically represented by Equation (4.19). The material constants are calculated using unconstrained nonlinear optimization procedure for minimization of error. Parameters *K* and *n* vary with respect to both temperature and strain rate whereas *m* varies with respect to temperature only. The variation of the parameters with respect to temperature and strain rate is empirically represented by Equations (4.20 - 4.22).

$$K = \alpha + \beta \ln \dot{\varepsilon} + \frac{\gamma}{T} \tag{4.20}$$

$$n = A + B \ln \dot{\varepsilon} + \frac{C}{T} \tag{4.21}$$

$$m = D - \frac{E}{T} \tag{4.22}$$

The material constant for *m-FB* model is presented in Table 4.6.

Table 4.6: Material constants for modified Fields–Backofen (*m-FB*) constitutive model

α	β	γ	A	B
1677.50	-3.6383	-415.99	0.0416	-0.0032
C	D	E	b	s
0.5561	0.1743	-42.62	0.0004	0.9265

4.2.2 Johnson Cook Model

The Johnson Cook (*JC*) constitutive model is a most widely known as a temperature, strain and strain-rate-dependent phenomenological flow stress model, and is successfully used for a variety of materials with different ranges of deformation temperature and strain-rate (*Johnson & Cook, 1983*). The original Johnson–Cook model can be expressed as per Equation (4.23)

$$\sigma = (A + B\varepsilon^{n})\,(1 + C\ ln\ \dot{\varepsilon}^{*})(1\ -\ T^{*m}) \tag{4.23}$$

where, σ stands for flow stress, A stands for yield stress at reference strain rate ($\dot{\varepsilon_0}$) and reference temperature (T_{ref}), B for coefficient of strain hardening, ε for plastic strain, $\dot{\varepsilon}^{*}$ for dimensionless strain rate (where $\dot{\varepsilon}^{*} = {\dot{\varepsilon}}/{\dot{\varepsilon_0}}$ with $\dot{\varepsilon}$ is strain rate) and T^{*} for homologous temperature.

$$\text{where, } T^{*} = \frac{T - T_{ref}}{T_m - T_{ref}} \tag{4.24}$$

T is current absolute temperature and T_m is the melting temperature; for Ti-6Al-4V alloy, the melting temperature is $1923K$. It should be noted that the original *JC* model considered the effect of the strain rate and temperature individually. The detailed procedure for constant determination has been mentioned in previous literature (*Gupta et al., 2013*).The material constants for *JC* model is mentioned in Table 4.7.

Table 4.7: Material constants for Johnson Cook (*JC*) constitutive model

Parameter	*A* (GPa)	*B* (GPa)	*n*	*C*	*m*
Value	0.8694	0.6495	0.3867	0.0093	0.7579

4.2.3 Modified Arrhenius Model

The Arrhenius equation is most widely used to describe the relationship between the strain-rate, flow stress and temperature, especially at high temperatures. The effects of the temperatures and strain-rate on the deformation behavior can be represented by Zener–Hollomon parameter in an exponent-type Equation (4.25).

$$Z = \dot{\varepsilon} \exp(\frac{Q}{RT}) \tag{4.25}$$

where, *Q* is the activation energy (*KJ mol*$^{-1}$), *R* is the universal gas constant (*8.314 J mol*$^{-1}$*K*$^{-1}$), *T* is the temperature in Kelvin and $\dot{\varepsilon}$ = strain rate and can also be expressed by the function in Equation (4.26)

$$\dot{\varepsilon} = A[\sinh(\alpha\sigma)]^n \exp(-\frac{Q}{RT}) \tag{4.26}$$

Therefore, final flow stress Equation (4.27) is:

$$\sigma = \frac{1}{\alpha}\ln\left\{\left(\frac{Z}{A}\right)^{1/n} + \left[\left(\frac{Z}{A}\right)^{2/n} + 1\right]^{1/2}\right\} \tag{4.27}$$

The effect of strain is not taken into account by this constitutive Equation (4.35). Modification in the constitutive equation has been proposed by Equation (4.28) (*Xiao and Guo, 2011*).

$$\sigma = \beta_0 \varepsilon^{\beta_1} \exp(-\beta_2 \varepsilon) \tag{4.28}$$

where, β_0, β_1 and β_2 are constants.

Now, final constitutive Equation which satisfactorily describe the effect of strain rate, temperature and strain on steady state flow stresses, is developed by combining (4.27) and (4.28) as follows:

$$\sigma = \frac{\beta_0}{\alpha}\varepsilon^{\beta_1} \exp(-\beta_2 \varepsilon) \ln\left\{\left(\frac{Z}{A}\right)^{1/n} + \left[\left(\frac{Z}{A}\right)^{2/n} + 1\right]^{1/2}\right\} \tag{4.29}$$

The material constants A,α, n, Q, β_0, β_1 and β_2 are determined by using the stress strain data from the experiments done under different deformation temperatures and strain rates. β_0, β_1 and β_2 are calculated for each strain rate and temperature. The detailed

procedure for constant determination has been mentioned in previous literature (*Xiao and Guo, 2011*). The constants determined for the *m-Arr* model are listed in the Table 4.8 and Table 4.9.

Table 4.8: Material constants for modified Arrhenius (*m-Arr*.) model

Parameter	α(MPa^{-1})	n	Q (kJ/mol)	A (s^{-1})
Value	1.35	65.17	202.40	2.56e9

Table 4.9: Coefficients of Equation β with Zener-Hollomon parameter (*Z*)

Parameter	β_0		β_1		β_2	
Value	*A*	*B*	*A*	*B*	*A*	*B*
	-0.0061	1.4907	-0.0013	0.1189	-0.0154	0.4106

4.2.4 Modified Zerilli Armstrong Model

The modified Zerilli Armstrong (*m-ZA*) model is derived based on dislocation mechanisms, which in fact play a main role in determining the inelastic behavior of a metal and its flow stress under different load conditions (*Zerilli & Armstrong, 1987*). *m-ZA* model represents flow stress mathematically as per Equation (4.30).

$$\sigma = (C_1 + C_2\varepsilon^n)\ \exp\{-(C_3 + C_4\varepsilon)T^* + (C_5 + C_6T^*)\ln\dot{\varepsilon}^*\} \quad (4.30)$$

where, σ stands for flow stress, ε for equivalent plastic strain, ἐ for strain rate, $T^* = T - Tref$, where T is current temperature, T_{ref} is reference temperature ($T_{ref} = 323\ K$) and $C_1, C_2, C_3, C_4, C_5, C_6$ and n are the material constants.

m-ZA equation considers the phenomena of isotropic strain hardening, temperature softening, strain rate hardening, and the coupled effects of temperature, strain and of strain rate while predicting the flow stress at elevated temperatures. The reference strain rate is taken as 0.1 s^{-1} and reference temperature is *323 K*. The detailed procedure for constants determination has been used from previous literature (*Gupta et al., 2013*). The calculated material constants for *m-ZA* model are mentioned in Table 4.10.

Table 4.10: Material constants for modified Zerilli Armstrong (*m-ZA*) model

C_1	C_2	C_3	C_4	C_5	C_6	n
869.40	640.50	0.0013	-9.57e-4	0.0095	6.94e-6	0.3867

4.2.5 Mechanical Threshold Stress model

Mechanical Threshold Stress model is a physical based model. The flow stress behavior is expressed as Equation (4.31)

$$\sigma_y\left(\varepsilon_p, \dot{\varepsilon}, T\right) = \sigma_a + (s_i\sigma_i + s_e\sigma_e)\frac{\mu(p,T)}{\mu_o} \tag{4.31}$$

where, σ_y is flow stress as a function of equivalent plastic strain ε_p, and strain rate $\dot{\varepsilon}$ and temperature T. σ_a is the athermal component of mechanical threshold stress, σ_i is the intrinsic component of the flow stress due to barriers to thermally activated dislocation motion, σ_e is the component of the flow stress which depends upon strain hardening of material.

S_i and S_i temperature and strain rate dependent scaling factors which takes Arrhenius form expressed as Equation (4.32 and 4.33)

$$S_i = \left\{1 - \left[\frac{kT}{E(T)b^3 g_{oi}}\right] ln \left[\frac{\dot{\varepsilon}_{oi}}{\epsilon}\right]^{\frac{1}{qi}}\right\}^{\frac{1}{pi}} \tag{4.32}$$

$$S_e = \left\{1 - \left[\frac{k_b T}{E(T)b^3 g_{oe}}\right] ln \left[\frac{\dot{\varepsilon}_{oe}}{\epsilon}\right]^{\frac{1}{qe}}\right\}^{\frac{1}{pe}} \tag{4.33}$$

where, g_{oi}, g_{oe} are normalized activation energies and $\dot{\varepsilon}_{oi}, \dot{\varepsilon}_{oe}$ are constant reference strain rates. p_i, q_i, p_e, q_e are constants generally vary from 1 to 2. K_b is the Boltzmann constant and *b* is magnitude of Burger's vector (*Holmedal, 2007*).

σ_e represents the strain hardening component of mechanical threshold stress model. It is represented by modified Voce model as per Equation (4.34)

$$\frac{d\sigma_e}{d\epsilon_p} = \theta(\sigma_e) \tag{4.34}$$

$$\theta(\sigma_e) = \theta_0 [1 - F(\sigma_e)] + \theta_1 [F(\sigma_e)] \tag{4.35}$$

$\theta(\sigma_e)$ is expressed as mentioned in Equation (4.50) where θ_0 is the strain hardening rate due to dislocation accumulation, θ_1 is a saturation hardening rate usually taken as zero.θ_0 is empirically related with strain rate and temperature as Equation (4.36)

$$\theta_0 = a_0 + a_1 ln\dot{\varepsilon} + a_2 ln\sqrt{\dot{\varepsilon}} + a_3 T \tag{4.36}$$

$$F(\sigma_e) = \frac{tanh\left(\alpha \frac{\sigma_e}{\sigma_{es}}\right)}{\tanh(\alpha)} \tag{4.37}$$

$$\ln(\sigma_{es}/(\sigma_{oes}) = \left(\frac{k_b T}{E(p,T)b^3 g_{oes}}\right) ln\left[\frac{\dot{\epsilon}}{\dot{\epsilon}_{oes}}\right] \quad (4.38)$$

where, a_0, a_1, a_2, a_3 constants and α is best fit constants that implies the rate at which saturation is achieved.$\dot{\epsilon}$ strain rate, T is temperature and σ_{es} is the saturation stress at zero strain hardening rate, σ_{oes}, g_{oes}, and $\dot{\epsilon}_{oes}$ is saturation threshold stress for deformation at *0K*, associated normalized activation energy and is the maximum strain rate respectively. The detailed procedure for constant determination has been mentioned in the previous literature (*Banerjee, 2007*). The material constant values for mechanical threshold stress model are listed in Table 4.11.

Table 4.11: Material constants for Mechanical Threshold Stress (*MTS*) constitutive model

σ_a^0	n	σ_i (MPa)	g_{oi}	σ_{oes} (MPa)	g_{oes}
900	0.075	412.6894	0.0242	1740.0062	0.0429

4.2.6 Comparison of constitutive models

Graphical comparison between the experimental and the predicted values of flow stress for all the models at four representative settings is shown in Fig. 4.3 (a, b, c & d). Two settings are at low temperature with low and high strain rates (a & b) and the other settings is at high temperature with low and high strain rates (c & d).

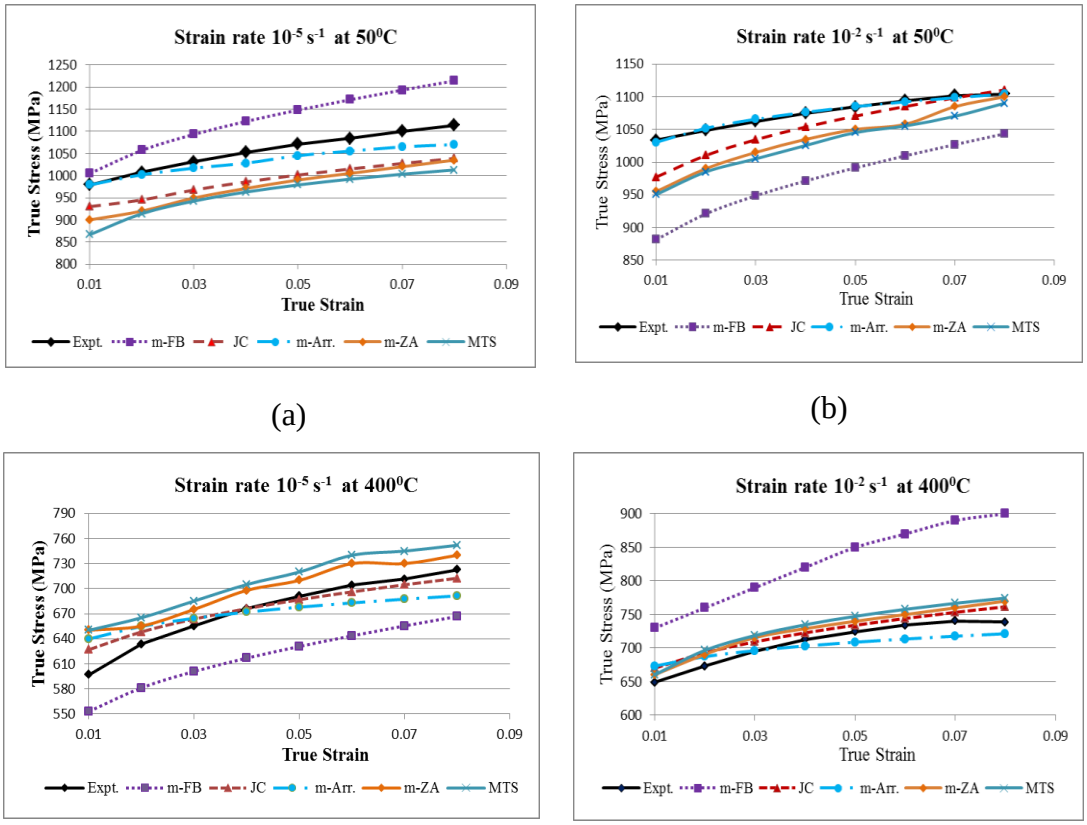

Fig.4.3: Representative flow stress prediction using various constitutive model prediction

Correlation coefficient (R) is a commonly used statistical tool which provides information on the strength of linear relationship between the experimental and predicted values. Although the value of R might be high, it is not necessary that the performance of the model is high, as the model might have a tendency to be biased towards higher values or lower values of the data. Hence, average absolute error (Δ), which is computed through a term by term comparison of the relative error, is an unbiased statistics for measuring the predictability of the model. Therefore, the prediction capability of constitutive models has been assessed by correlation coefficient (R), average absolute error (Δ) and its standard deviation (S). Also, the suitability of these models is compared based on the number of material constants to be evaluated and the procedure of their evaluation. Table

4.12 shows comparison of various constitutive models based on statistical measures and number of material constants. Fig. 4.4 shows the *R* graphs for all the considered constitutive models.

Table 4.12: Comparison of various constitutive models based on statistical measures and number of material constants

	m-FB	*JC*	*m-Arr.*	*m-ZA*	*MTS*
R	0.8702	0.9777	0.9757	0.9787	0.9614
$\Delta_{avg}(\%)$	6.65	3.17	2.85	3.95	3.21
S (%)	5.98	2.21	1.67	3.01	2.96
Number of material constants	10	5	10	7	6

As it can be seen from Fig.4.3 and Table 4.12 that the predictions of *m-FB* model have more deviation from the experimental values, whereas the predictions of all other models (*JC*, *m-Arr*.,*m-ZA* and *MTS*) are very close to the experimental values. This is also evident from Fig. 4.4 (a) and Table 4.12, as the *R* (0.8702) value for *m-FB* model is lesser than that of other four models and higher value of error (*Δ*= 6.65%) and its standard deviation (*S* = 5.98%) proves *m-FB* model to be least suitable for prediction of flow stress.

Considering the correlation coefficient, all the models show very high degree of goodness of fit as the R value is above 0.96. This R value may be biased towards higher or lower values. Therefore, average absolute error and its standard deviation are used to check the accuracy of the predictions. The m-Arr. model gives the least error of 2.85 % and standard deviation of 1.67 %.However, the drawback of m-Arr. model as compared to other models is it requires 10 material constants to be evaluated, which increases the

computational time and complexity. The *JC* model requires only 5 material constants and the error value (Δ = 2.21%) is also close to that of *m-Arr*. model.

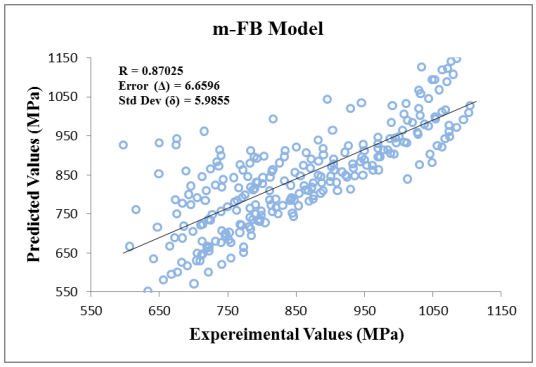

(a) m-FB

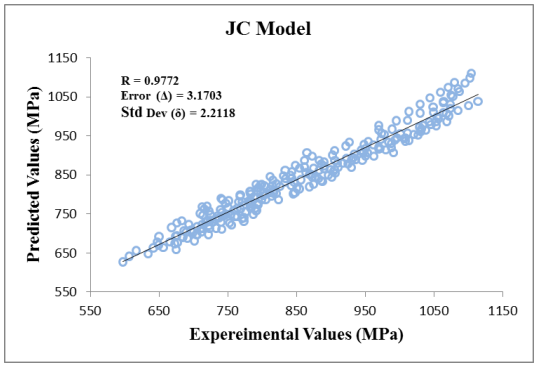

(b) JC

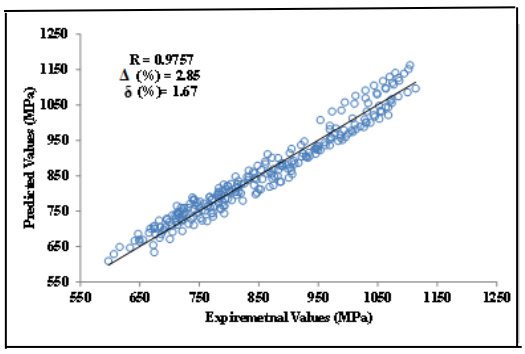

(c) m-Arr.

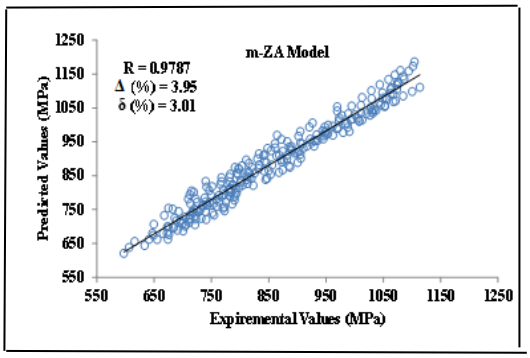

(d) *m-ZA*

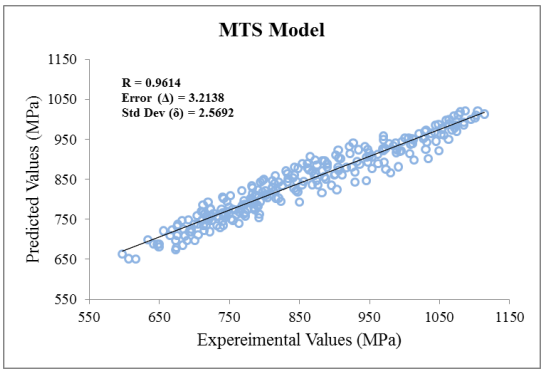

(d) MTS

Fig.4.4: Correlation coefficient for various constitutive models

JC and *m-Arr*. models are phenomenological models, i.e., these do not consider the physical aspects while predicting the flow stress, whereas both *m-ZA* and *MTS* models are physical based models and consider the physical aspects of materials like theory of thermodynamics, thermally activated dislocation movement, and kinetics of slips. Hence, considering all these points, i.e., statistical measures, physical aspects for flow stress predictions, number of material constants and the complexity involved in the computation of the material constants, *MTS* model is a preferred model over the other models considered in this study.

4.3 Summary

This chapter discussed about development of various anisotropic yield criteria and constitutive model for Ti-6Al-4V alloy at elevated temperatures. The detailed procedures for determining the material constants have been discussed. Based on the various evaluation parameters, The Cazcau Barlat yield criterion and MTS constitutive model is best suited for Ti-6Al-4V alloy at elevated temperatures.

These material models (yield criteria + constitutive models) are essentially required as an input for theoretical and numerical analysis of Forming Limit Diagram (FLD). The next chapter discuss about experimental and theoretical investigations of FLD using various material models.

CHAPTER 5: EXPERIMENTAL AND THEORETICAL STUDIES OF FORMING LIMIT DIAGRAM

Forming Limit Diagram (FLD) offers a convenient and useful tool to predict the forming limit in sheet metal forming processes. FLD attempts to provide a graphical description of material failure during sheet metal forming processes such as deep drawing, stretching, bending, etc. It shows the critical combinations of major strain and minor strain in the sheet surface at the onset of necking failure.

In this chapter, experimental and therotical analysis of FLD have been investigated. The experimental FLD has been determined using Nakazima test method. The detailed fractography analysis of failed stretched specimen has been examined using SEM. Additionaly, therotical FLDs are determined using Marciniak-Kuczynski (M-K) theory. The developed anisotropic yield criteria and hardening models are incorporated in M-K theory. The therotical FLD results are compared with the experimental FLD.

5.1 Introduction to Forming Limit Diagram

The most useful tool to assess formability is the forming limit diagram (FLD). The research in this area is initiated by *Keeler* (*1965*). During forming, the initial circles of the grid become ellipses. Keeler plotted the major strains against the minor strains obtained from such ellipses at fracture of parts after biaxial stretching as shown in right side of Fig. 5.1. Later, *Goodwin* (*1968*) plotted the curve for the tension/compression domain by using different mechanical tests, which is shown in left side of Fig. 5.1. The combined diagram of Keeler (right side) and Goodwin (left side) is popularly called as

the FLD. Connecting all of the points corresponding to limit strains leads to a Forming Limit Curve (FLC). The FLC splits the 'fail' (i.e. above the FLC) and 'save' (i.e. below the FLC) regions. The intersection of the limit curve with the vertical axis (which represents the plane strain deformation ($\varepsilon_2 = 0$) is an important point of the FLC. The position of this point depends mainly on the strain hardening coefficient (n) and also on thickness of sheet (*Banabic, 2010*).

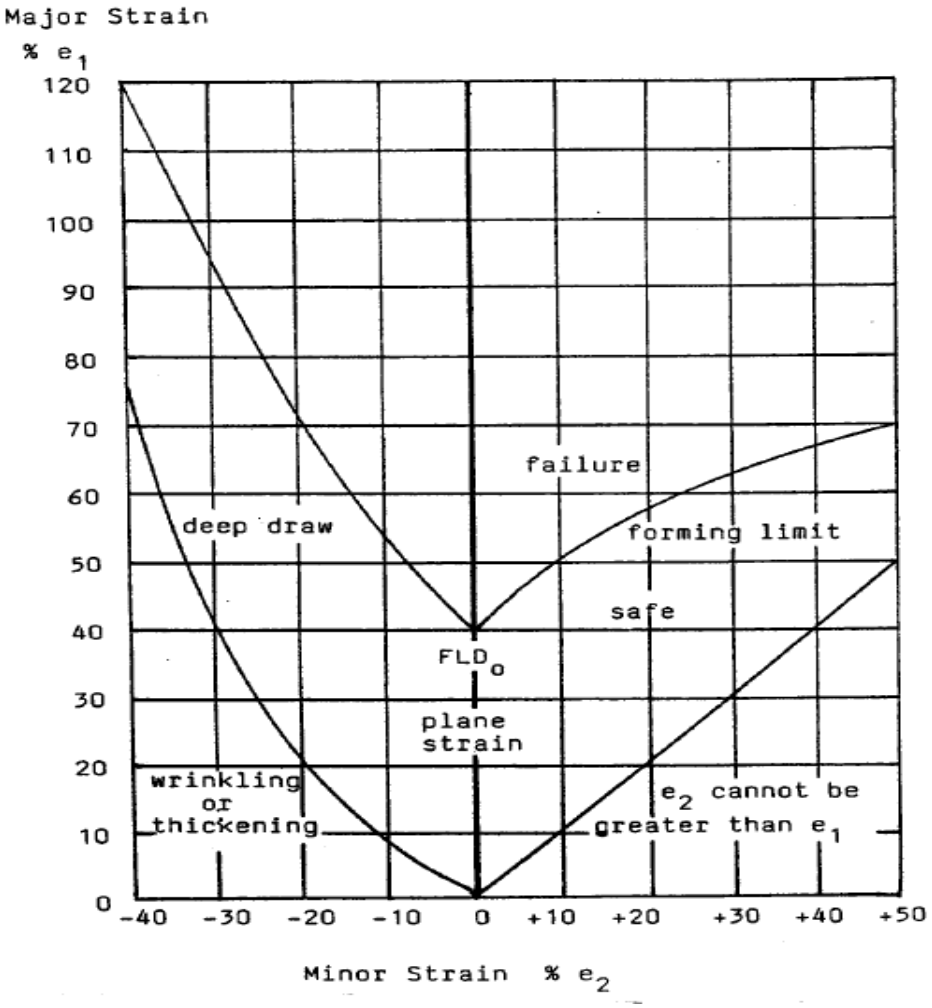

Fig.5.1: Forming limit diagram as defined by Keeler and Goodwin (*Banabic, 2010*)

Currently, depending on the kind of limit strains, different types of FLD's are determined: for necking and for fracture as shown in Fig. 5.2. FLDs must cover as much

as possible the strain domain which occurs in industrial sheet metal forming processes. The diagrams are established by experiments that provide pairs of values of the limit strains, ε_1 and ε_2, obtained for various loading patterns (uniaxial, biaxial, plane strain, etc.).

There are various tests such as simple tension test, hydraulic bulge test, Keeler test, Nakazima test and their combinations are used to determine various strain paths in FLD. Generally, a popular test method used for FLD determination is Nakazima test (*Banabic, 2010*).

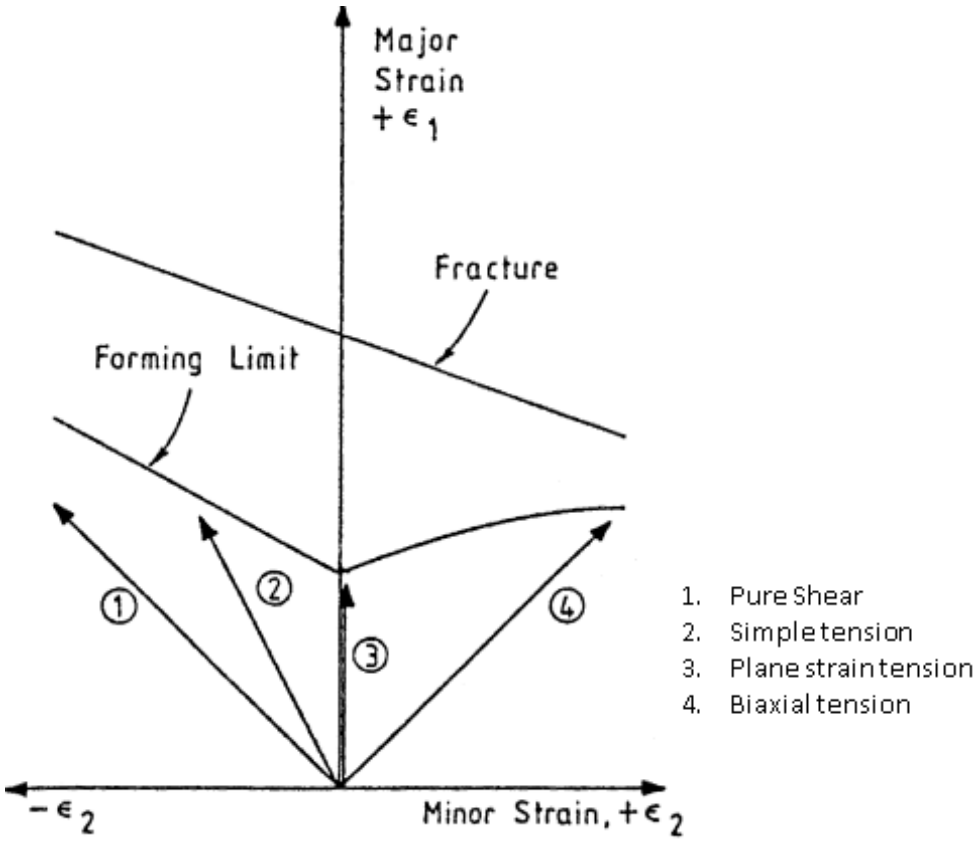

Fig.5.2: Forming limit diagram for necking and fracture (*Banabic, 2010)*

5.2 Experimental Forming Limit Curve

Experimental FLC has been plotted by conducting Nakazima test as per *ASTM E2218* standards. It has been observed that stretching capability i.e. LDR of Ti-6Al-4V is substantially lower than the other structure alloy at elevated temperatures. However, the maximum LDR (better stretching capability) is found at 400^0C. Therefore in the present study, FLC has been determined at 400^0C. The test set up is made of a hemispherical punch, die, blank-holder and draw-bead to prevent any sliding motion as shown in Figure 5.3. The experimental procedure mainly involves three stages - grid marking on sheet specimens, punch-stretching the grid-marked samples (up to safe, neck and failure) and measurement of strains. The specimen dimensions have been considered from *120 mm* × *120 mm* and subsequently reducing one side by *10 mm* for every specimen up to *30 mm*. This is done to subject the sheet samples for different states of strain, i.e. the uniaxial tension-compression zone, plane strain and the biaxial tension zone. Fig. 5.4 shows dimensions of specimens used for FLC study.

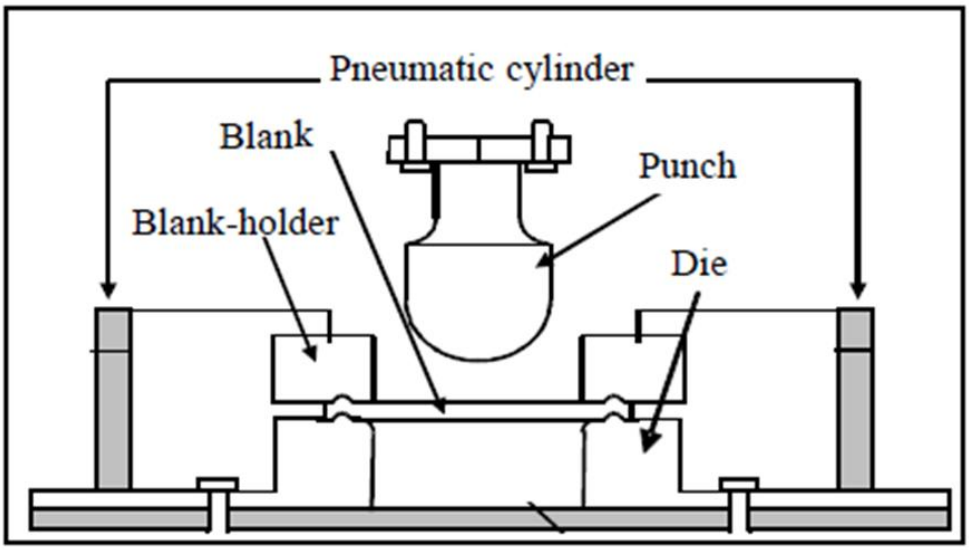

Fig.5.3: FLD test setup as per *ASTM E2218* standard

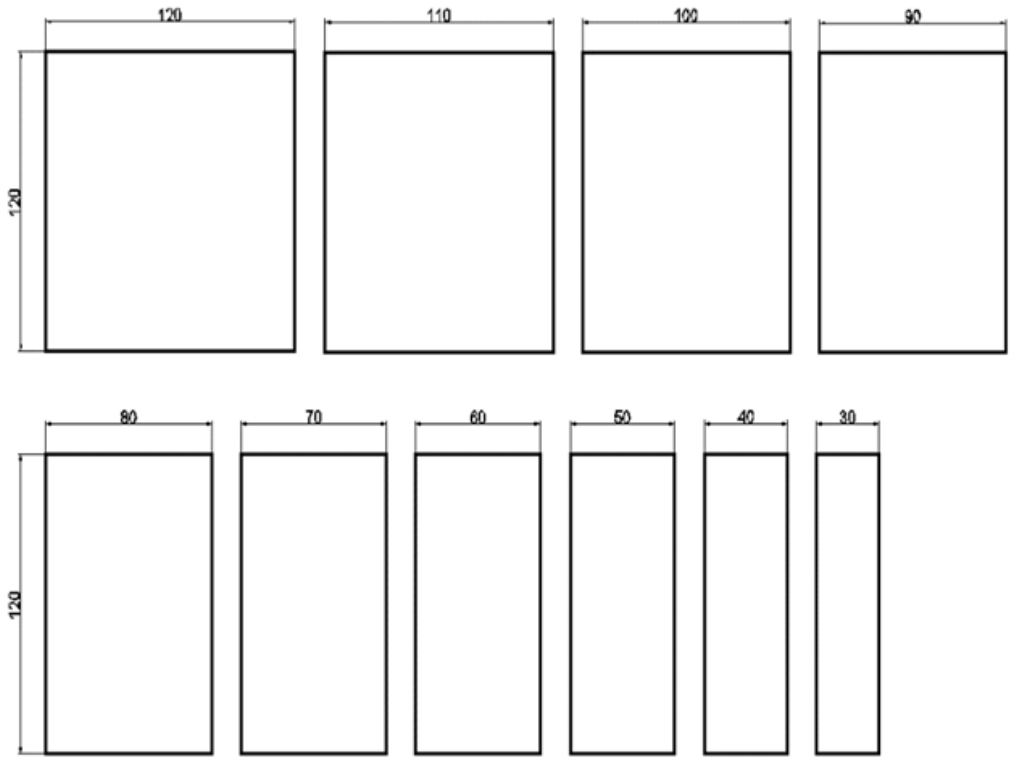

(All dimensions are in *mm*)

Fig.5.4: Dimension of specimens used for experimental FLC

Circular grid pattern on Ti-6Al-4V alloy sheet has been etched using electro-chemical etching process (grid circle diameter = 5 *mm*). Then, specimens have been stretched using hemispherical punch. The strains have been estimated by measuring the deformation of the grid as near as possible to the fracture zone, neck zone and safe zone using a traveling microscope. FLC has been drawn by plotting the minor strain (ε_2) in abscissa and corresponding major strain (ε_1) in ordinate. The experimental FLC is shown in Fig. 5.5. The strains of the specimen corresponding to plane strain is a characteristic of the material. It has been noted that the strains at plane strain condition is approximately equal to the *n* value at 400^0C (*n=0.067*).

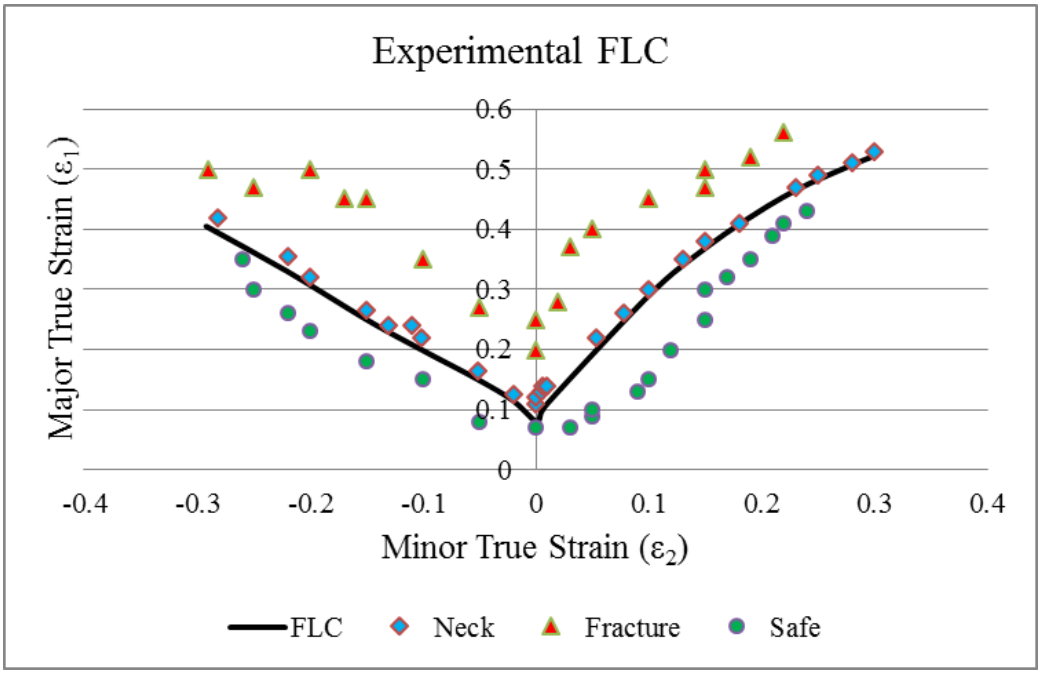

Fig.5.5: Experimental FLC for Ti-6Al-4V alloy at 400^0C

Dome height of the specimens have been measured with variation of width of the specimens as shown in Fig. 5.6. It is observed that, the dome height is minimum at plane strain condition and it increases in the region of uniaxial and biaxial state of stress region. This curve is popularly called as a Limiting Dome Height (LDH) diagram (*Ghosh, 1975*). In spite of its advantages of easy calculation of dome height, the method has been little used in industry (*Banabic, 2010*).

The thickness distribution of successfully drawn stretched specimens have been measured from one end to another end. The representative thickness distribution of various width specimens which cover biaxial, plane strain and uniaxial state of stress is shown in Fig. 5.7. As expected, the maximum deformation zone is observed at the centre portion of stretched specimen. Therefore, minimum thickness is obtained at the centre portion as shown in Fig. 5.7. The thickness reduction is more in case of biaxial state of

stress region (*120 mm ×120 mm*) than the plane strain (*120 mm ×80 mm*) and uniaxial state of stress region (*120 mm × 30 mm*). It indicates that the material has possibly more deformation in biaxial and plane strain region than the uniaxial state region.

Fig.5.6: LDH diagram for Ti-6Al-4V alloy at 400^0C

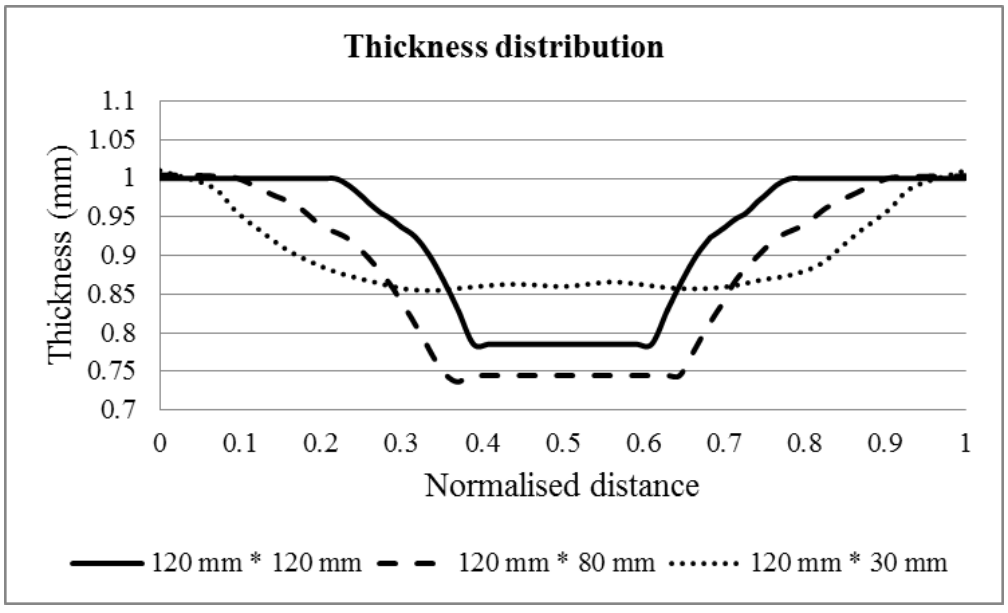

Fig.5.7: Representative thickness distribution at various widths of specimen

5.3 Fractography Study

The fracture surfaces of the representative failed specimens have been comprehensively examined using SEM of make *ZEISS, SUPRA 55 VP* accelerating voltage *20 kV*. The samples for observation have been sectioned parallel to the fracture surface using wire cut EDM. Representative fracture surface for uniaxial tension region (*120 mm×30 mm*), plain strain region (*120 mm×80 mm*) and biaxial tension region (*120 mm×120 mm*) is shown in Fig. 5.8.

The overall morphology of fracture surface appears to be rough and uneven which is shown in Fig. 5.8 (a, c & e). In uniaxial tension region, the SEM fractograph (Fig. 5.8 (b)) indicates healthy population of unidirectional dimples of varying size and shapes. It is a clear indication of shear failure. However, in plane strain region, the shallow type of small size equiaxed dimples is observed. Small dimples are formed when numerous nucleating sites are activated and adjacent microvoids join (coalesce) before they have an opportunity to grow to a larger size as shown in Fig. 5.8 (d). This is a clear indication of ductile failure due to excessive tensile stresses. In case of a biaxial tension region, similar fracture has been seen as shown in Fig 5.8 (e & f).

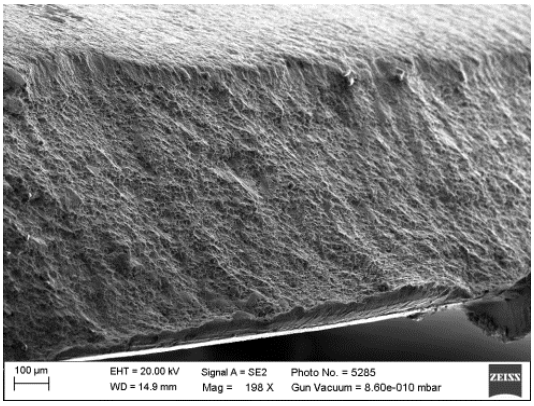

(a) 200 X Magnification

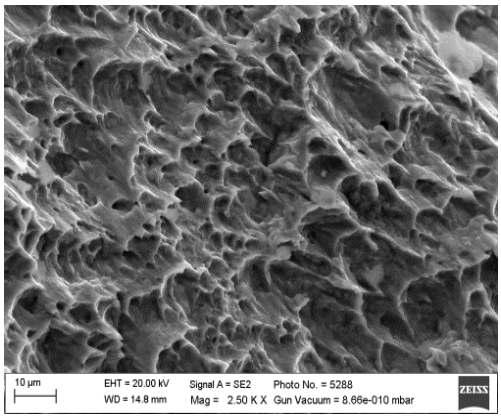

(b) 2500 X Magnification

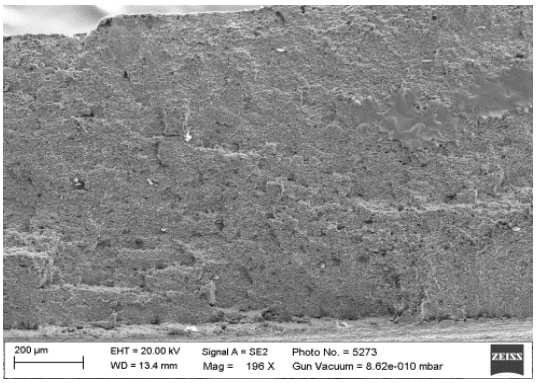

(c) 200 X Magnification

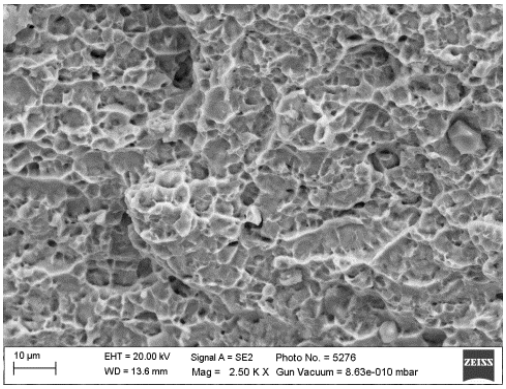

(d) 2500 X Magnification

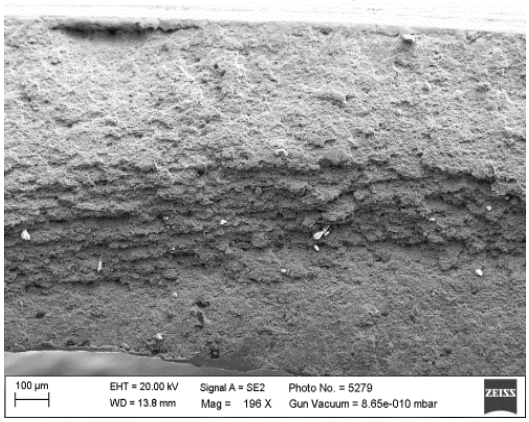

(e) 200 X Magnification

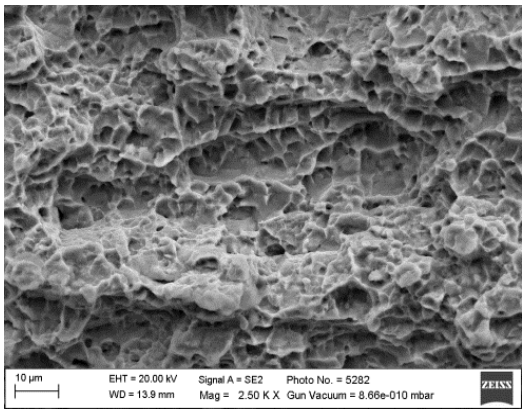

(f) 2500 X Magnification

Fig.5.8: Representative SEM images (a & b) uniaxial tension region (*120 mm×30 mm*) (c & d) plane strain region (*120 mm×80 mm)* (e & f) biaxial tension region (*120 mm × 120 mm)*

5.4 Theoretical Analysis for Forming Limit Curve

Experimental FLDs are time consuming and expensive, especially at elevated temperature, resulting in a great interest in employing theoretical models to simulate FLCs (*Djavanroodi & Derogar, 2010*). Consequently, considerable effort has been made to construct reliable forming limit prediction models from the perspective of theoretical calculations. The most widely used mathematical model is Marciniak-Kuczynski (M-K) theory (*Banabic, 2010*).

M-K model is based on the hypothesis of the existence of imperfections in sheet metal. According to Marciniak's hypothesis, sheet metal has geometrical (thickness variation) and structural imperfections (inclusions, gaps). In the sheet metal forming process, these imperfections progressively evolve and the plastic deformation of the sheet metal is almost completely localized in them, leading to the necking of the sheet metal (*Banabic, 2010*).

M-K model has been intensively used and developed by researchers due to the advantages it offers. It has an intuitive physical background; it correctly predicts the influence of different process or material parameters on the limit strains; the predictions are precise enough; the model can be easily coupled with FE analysis. The main drawbacks of this model are: the prediction results are very sensitive to the material models used, as well as to the values of the non-homogeneity parameter (*Sansot Panich et al., 2013*). In the present work, various material models have been incorporated in M-K theory for theoretical FLCs prediction.

This initial inhomogeneity factor is considered due to geometric and physical causes. It is considered in the direction perpendicular to the maximum principal stress. This means, there is a linear groove before deformation occurs on the sheet surface. The zone outside the groove is considered as zone *A* and the groove is considered as zone *B,* as shown in Fig. 5.9. A Cartesian coordinate system is aligned with the symmetry axes: the *x*-axis is along the rolling direction of sheet, and the *y*-axis is along the transverse direction of sheet This initial imperfection can be defined by a thickness ratio as per Equation (5.1).

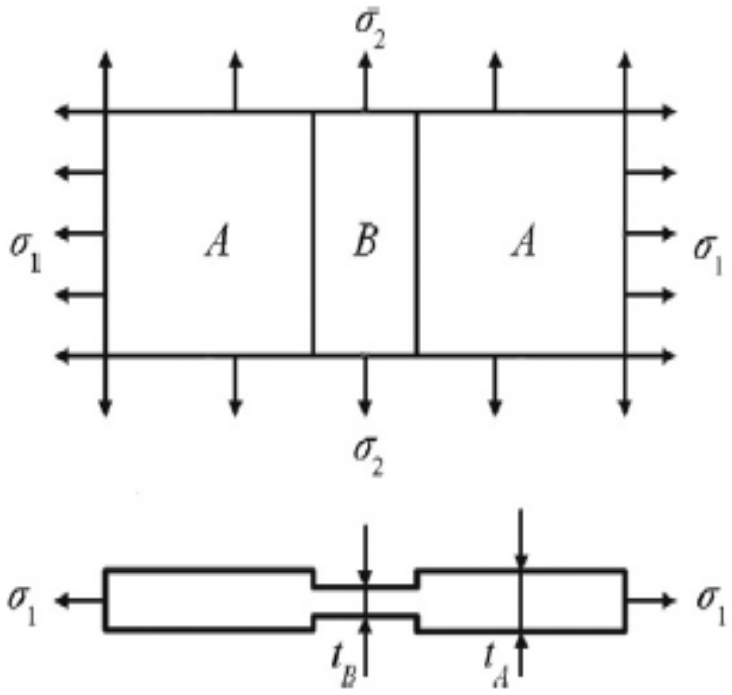

Fig.5.9: Geometric imperfection of the Marciniak Kuczinsky (M-K) model

$$f_0 = \frac{h_0^B}{h_0^A} < 1 \tag{5.1}$$

where, h_0^A, h_0^B are the initial thicknesses of zone *A* and zone *B*, respectively. f_0 is a inhomogeneity parameter of the M-K model. The boundary of the sheet (assumed to be far away from the groove) is subjected to monotonic proportional straining parallel to the symmetry axes.

$$\rho^A = \frac{\varepsilon_y^A}{\varepsilon_x^A} \tag{5.2}$$

where, $\varepsilon_x, \varepsilon_y$ are components of strain along the coordinate axes. The ε_x is major strain and ε_y is minor strain. The value of f_0 is varied until the theoretically predicted FLC curve agrees best with the experimental curve at the plane strain condition, i.e., for $\rho = 0$. As deformation increases, the thickness of zone *B* reduces continuously and faster than that of region *A*. Hence, it has to bear increasingly higher stresses than those in zone *A*. There will be a point when the region *B* has deformed substantially more than region *A*, signaling the start of necking. The failure criterion is thus:

$$\frac{d\overline{\varepsilon_A}}{d\overline{\varepsilon_B}} < N \tag{5.3}$$

where, $d\overline{\varepsilon_A}, d\overline{\varepsilon_B}$ denote the equivalent strains in the respective regions. From a computational point of view, the constant *N* should be a small number so as to ensure that region *B* has deformed sufficiently more than region *A*. Then it can be said with certainty that necking would have occurred. The common range of *N* value is taken as 0.15 to 0.20 (*Banabic, 2010*). For the present study, *N* is chosen as 0.15 which ensures substantial deformation of sheet before necking.

5.4.1 Formulation of Marciniak Kuczynski (M-K) model

The ratio of stresses and strains is defined as per Equation (5.4)

$$\alpha = \frac{\sigma_y}{\sigma_x}, \rho = \frac{\varepsilon_y}{\varepsilon_x} = \frac{d\varepsilon_y}{d\varepsilon_x} \tag{5.4}$$

Here, *x* is the rolling direction and *y* is the transverse direction. The effective stress and strain are defined as per Equation (5.5)

$$\bar{\sigma}\bar{\varepsilon} = \sigma_x\varepsilon_x + \sigma_y\varepsilon_y \ = \sigma_x\varepsilon_x(1+\alpha\rho) \tag{5.5}$$

The associative flow rule is given by Equation (5.6)

$$d\varepsilon_{ij} = d\lambda \frac{\partial\bar{\sigma}}{\partial\sigma_{ij}} \tag{5.6}$$

Using the associative flow rule and the constant volume condition given by $d\varepsilon_x + d\varepsilon_y + d\varepsilon_z = 0$, Equations for $d\varepsilon_x, d\varepsilon_y, d\varepsilon_z$ are obtained.

The M-K model incorporates a compatibility condition

$$d\varepsilon_y^A = d\varepsilon_y^B \tag{5.7}$$

Furthermore, the sheet metal being deformed will always be in equilibrium. This is represented by the force balance Equation:

$$\varphi_A C\left(\varepsilon = \overline{\varepsilon^A} + \overline{d\varepsilon^A}, \dot{\varepsilon} = d\varepsilon^A\right) = f\varphi_B C\left(\varepsilon = \overline{\varepsilon^B} + \overline{d\varepsilon^B}, \dot{\varepsilon} = d\varepsilon^B\right) \tag{5.8}$$

where, C is the function representing the required constitutive model, $\varphi = \frac{\sigma_x}{\bar{\sigma}}$ and $f = \frac{t_A}{t_B}$ and t_A, t_B denote the instantaneous thicknesses of regions *A* and *B*. This ratio can be found by using the Equation

$$f = f_0 \exp\left(\varepsilon_Z^A - \varepsilon_Z^B\right) \tag{5.9}$$

The value of f_0 is arbitrary chosen for FLC prediction. This value is varied across a range of 0.85 to 0.999, to ensure that at some value the predicted FLC matches the experimental results at the plain strain condition (*Butuc et al., 2003*). The value of ρ is varied from -0.45 till 0.95 to get all the points on the FLC (*Moshksar & Mansorzadeh, 2003*). The variation of ρ is done so as to find the forming limit along different strain paths that the sheet metal can possible endure during the actual forming process. Small strain increments of $d\varepsilon_x^B$ are imposed in the groove region. Iteratively, assuming a value for $d\varepsilon_x^A$, the values of $d\varepsilon_y^A, d\varepsilon_y^B, \overline{d\varepsilon^A}, \overline{d\varepsilon^B}$, are computed and the equality of the force balance equation is checked. If the equality is satisfied, the ratio $\frac{d\varepsilon_A}{d\varepsilon_B}$ is calculated. Further if this ratio is lower than the limit of *0.15* that has been levied on the constant *N*, the process is stopped and the most recent values of the major and minor strains of region *A* are taken to denote the coordinates of a point lying on the FLC. If the ratio $\frac{d\varepsilon_A}{d\varepsilon_B}$ is less than *0.15*, additional increments of strain are imposed on region *B* till the straining limit is achieved. Fig.5.10 shows a flow chart depicting the steps of the algorithm used for predicting theoretical FLCs.

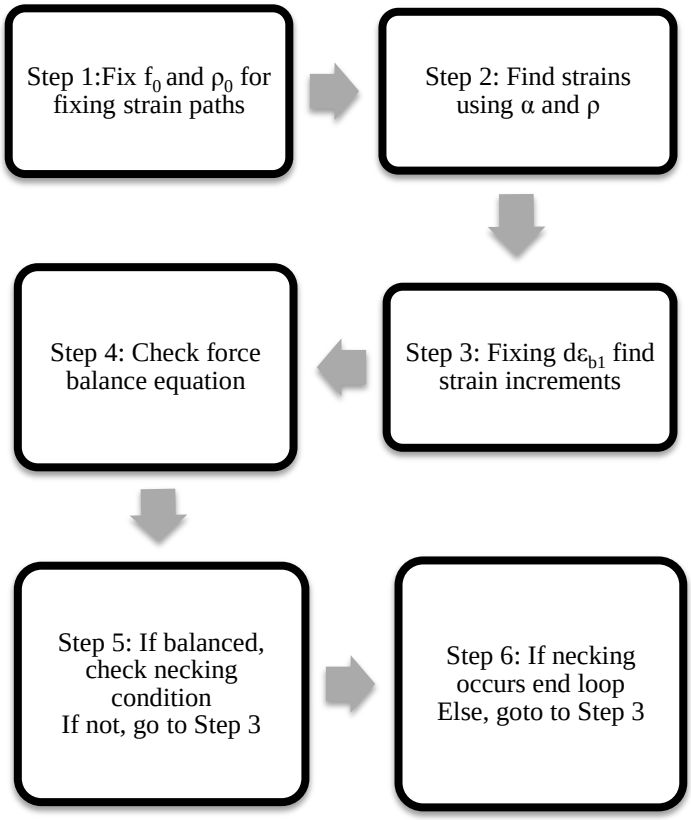

Fig.5.10: Flow chart of algorithm for plotting theoretical FLCs

5.5 Results and Discussion

The procedure used to predict FLCs using the M-K theory will have to assume a value for the parameter f_0, which denotes the initial thickness ratio of the regions *A* and *B*. The fact that the MK model uses this initial thickness defect to explain the forming limit makes this parameter a crucial one (*Sansot Panich, 2013*). Moreover, the value of f_0 can take any value based on thickness of the sheet, surface quality of sheet, grain size and material properties (*Siguang et al., 1998*). This makes it impossible to judge which will ensure correct predictions of the FLC. This is ensured by matching the FLCs with experimentally obtained forming limits at the plane strain condition. The value of f_0 which matches the experimental results will be used to make the predictions.

For all combinations of yield criterion and constitutive models considered in this study, the values of f_0 was varied across a wide range. The final f_0 values are listed in Table 5.1. It can be observed from Table 5.1, the constitutive models seem to be the only factor that determines the value of this parameter. This is further strengthened by the fact that this is not restricted to one class of yield criteria. This observation related to f_0 value is a very intriguing and not so easily controvertible fact.

Table 5.1: Final f_0 values used for the various theoretical FLC predictions

	Yield Criteria				
Constitutive Models	Hill 1948	Barlat 1989	Barlat 1996	Barlat 2000	Hill 1993
m-FB	0.995	0.995	0.995	0.995	0.995
JC	0.990	0.990	0.99	0.990	0.990
m-Arr.	0.995	0.995	0.996	0.996	0.996
m-ZA	0.960	0.960	0.960	0.960	0.960
MTS	0.960	0.960	0.960	0.960	0.960

The effect of changing the value of f_0 for a particular combination of yield criterion and hardening rule also follows a general trend. As the value of f_0 is decreased, the FLC's shape remains the same but the whole plot is displaced in the negative y direction. Fig. 5.11 shows representative one such situation using Barlat 1989 yield criterion with *m-Arr*. constitutive model. The f_0 value denotes the extent to which the groove region is thinner than the normal sheet region. Lower the value of f_0, thinner the groove region will be. This will make the groove more prone to necking as a result of increase in deformation rate in comparison to a thicker groove. This results in lower forming limits, which is characterized by the FLC traversing in the negative y direction.

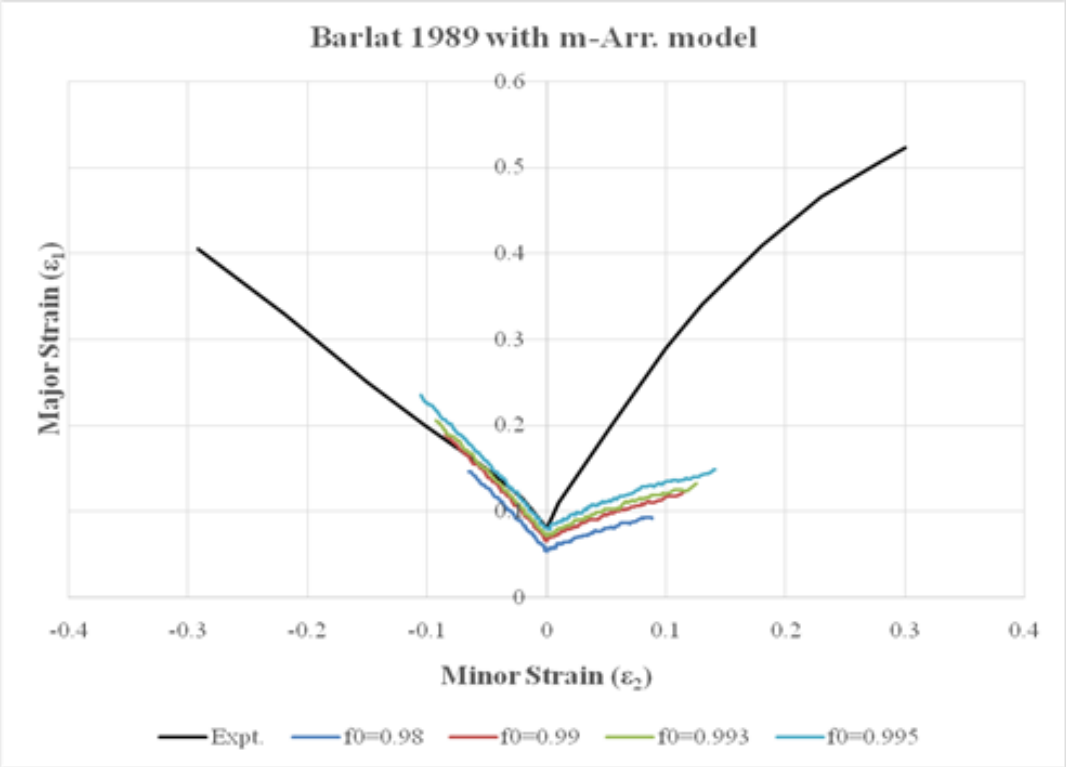

Fig.5.11: Variation of f_0 value for FLC prediction

The final prediction of theoretical FLCs using various yield criteria with variation of hardening models are shown in Fig. 5.12 (a, b, c, d & e). It can be seen that the predicted FLCs do not seem to vary much with change in constitutive model for a particular yield criterion. This was further analyzed by calculating the Fréchet distances between the predictions, the results of which are given in Table 5.2. The Fréchet distance is a measure of similarity between two curves, *P* and *Q*. It is defined as the minimum cord-length sufficient to join a point traveling forward along *P* and one traveling forward along *Q*, although the rate of travel for either point may not necessarily be uniform (*Alt & Godau, 1995*). This correlation study has been done by assuming the *m-FB* prediction as the base case and finding the similarity between this and the FLCs predicted by the other constitutive models. This gives a more quantitative reasoning of the above conclusion.

It can be seen from Fig. 5.12 (a & b), Hill 1948 and Barlat 1989 yield criteria predict the left part of FLC (uniaxial state region) better than the right part (Biaxial state region). This effect of poor prediction of biaxial region can be seen in the yield loci of these criteria as well. This is because; these criteria are modeled to predict the uniaxial state region better and do not capture the biaxial region. Although, Barlat 1996 yield locus predict biaxial behavior of Ti-6Al-4V alloy very well, but the forming limit curve obtained using this criterion does not conform to the experimental results in the right hand side of the FLC as shown in Fig. 5.12 (c).

Furthermore, Barlat 2000 yield criterion also predicts uniaxial and biaxial state of stress very well, but unexpectedly its FLCs prediction is poor in the right hand side of the FLC portion as shown in Fig. 5.12 (d). In the left hand side, all the constitutive models' predictions are in well agreement with experimental data points. On the other hand, in right hand side FLC prediction, all the constitutive models underestimate the experimental data points. However, the theoretical FLC based on the MTS model is close to the experimental FLC. Therefore, Barlat 2000 yield criterion with MTS constitutive model is better option for theoretical FLC prediction. The reason for this behavior might be a stress asymmetry which is not considered in Barlat 2000 yield criterion.

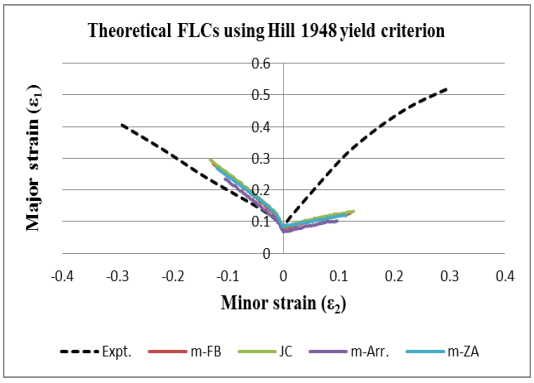

(a) Hill 1948

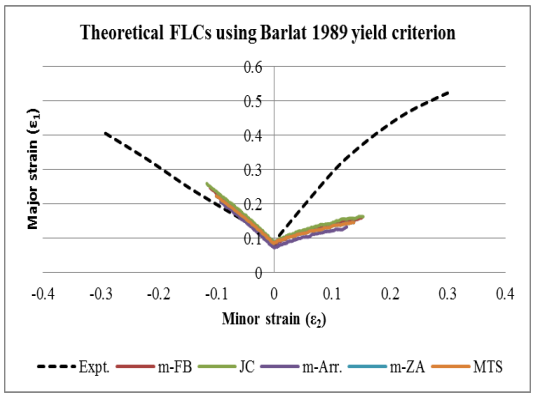

(b) Barlat 1989

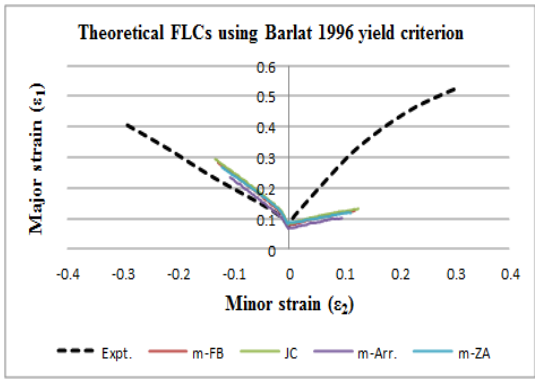

(c) Barlat 1996

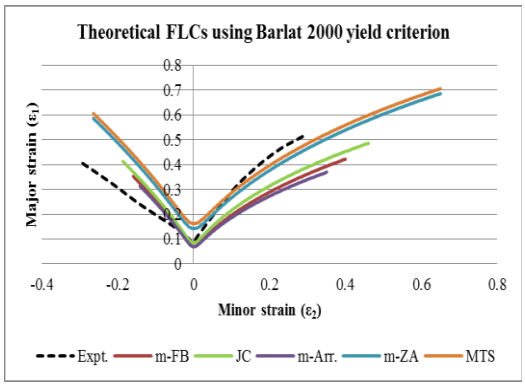

(d) Barlat 2000

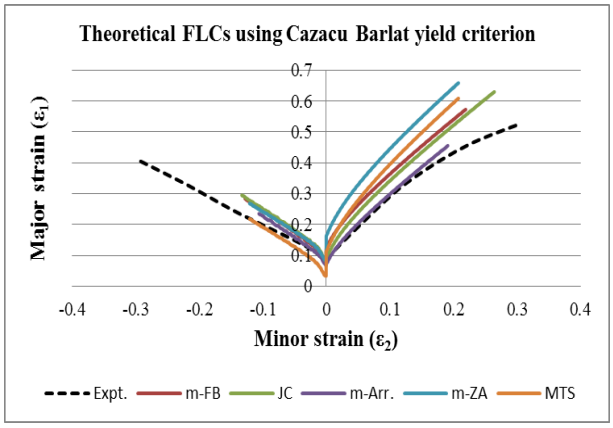

(e) Cazacu Barlat

Fig.5.12: Theoretical FLC using various yield criteria

Table 5.2: Fréchet Distance between FLC predictions

FLC prediction considered	*JC*	*m-Arr.*	*m-ZA*	*MTS*
Hill 1948	0.0125	0.0132	0.0192	0.0192
Barlat 1989	0.0132	0.0125	0.0231	0.0212
Barlat 1996	0.0121	0.0186	0.0175	0.0185
Barlat 2000	0.0121	0.0185	0.0176	0.0186
Hill 1993	0.0321	0.0332	0.0542	0.0442

Cazacu Barlat yield criterion considers stress asymmetry effect which is predominant in Ti-6Al-4V alloy at elevated temperature (*Odenberger et al., 2013*). The FLC prediction of Cazacu Barlat yield criterion with all the constitutive models are very well in agreement with the experimental FLC as shown in Fig. 5.12 (e). But, *m-Arr*. constitutive model prediction is better when compared with other constitutive models. The main reason might be that the flow stress prediction capability of *m-Arr*. model is better than the other considered constitutive models. One interesting observation is seen from Fig 5.12 (e), even though the physical based constitutive models (*m-ZA* and *MTS*) considers physical aspects of a material but it overestimate the FLC points in the right hand region. However, phenomenological based constitutive model performance is better in FLC prediction.

Based on the above discussion on theoretical FLCs prediction using M-K theory, it can be concluded that yield criteria effect are more predominant in theoretical FLCs prediction than the constitutive model effect. However, f_0 value is solely dependent on constitutive model. Thus, it can be concluded that the best yield criteria (Cazacu Barlat)

along with constitutive model which has lower error percentage (*m-Arr*.) is suitable for theoretical FLC prediction using M-K theory.

5.6 Summary

This chapter involves comparison of experimentally determined and theoretically predicted FLC using M-K theory with various yield criteria and constitutive models. The Cazacu Barlat yield criterion with *m-Arr.* constitutive model best predicts the FLC for Ti-6Al-4V alloy at 400^0C.

The experimental and theoretical FLC findings need to be validated with Finite Element (FE) analysis of sheet metal forming. The next chapter presents FE analysis of deep drawing and stretching process using various material models.

CHAPTER 6: FINITE ELEMENT ANALYSIS OF SHEET METAL FORMING PROCESS

This chapter presents various aspects of FE analysis for deep drawing and stretching processes using DYNAFORM software. The important qualitative aspects of deep drawing and stretching processes have been investigated using FE analysis and compared with experimental and theoretical results.

6.1 Introduction to Finite Element Analysis for Sheet metal Forming Process

Nowadays, several FE analysis codes are available for sheet metal forming analysis. FE analysis comprises many non-linearities due to structural and geometrical issues. It also involves complex contact interactions between moving and stationary parts. Therefore, explicit codes have been extensively used for sheet metal forming processes. (*Nielsen & Brian, 1997).*

In the present study, FE analysis has been done using a commercially available software DYNAFORM version *5.6.1* with *LSDYNA* version *971* solver. Fig. 6.1 summarizes the overall steps used in DYNAFORM software for finite element simulations.

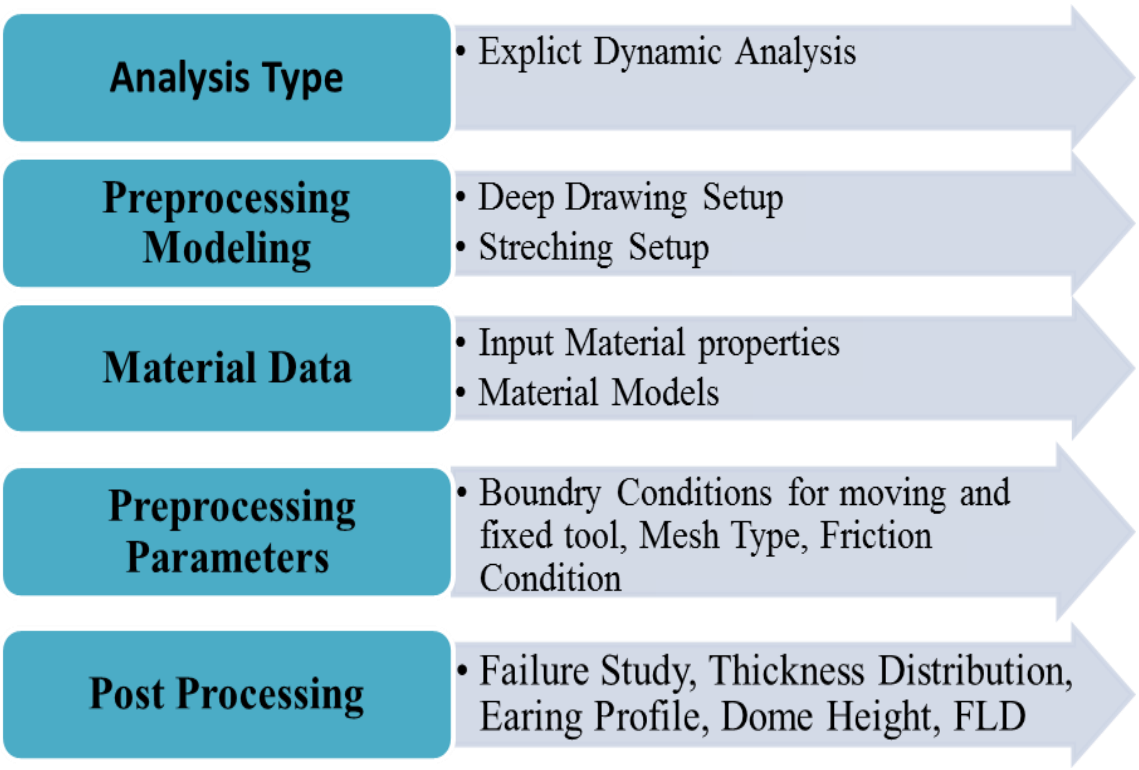

Fig.6.1: Schematic representation of step used in FE analysis

Few important points related to preprocessing in DYNAFORM software are discussed below.

(I) Selection of element type

The sheet metal forming process is considered as a plane stress problem. For plane stress condition generally shell element has better choice (*Chung & Shah, 1992*). The following are some important shell elements available in DYNAFORM software.

- Selective reduced Hughes-Liu shell (SRHL)
- Selective reduced co-rotational Hughes-Liu shell (SRCOHL)
- Hughes-Liu shell (HL)

- Englemann-Whirley shell (EW)
- Co-rotational Hughes-Liu shell (COHL)
- Belystchko-Lin-Tsay shell (BLT)
- Belyschko-Wong-Chiang shell (BWC)

The detailed description about each element is available in LSDYNA user manual (*LSDYNA keyword user manual, 2007*). For the present FE analysis, the blank and the tool components have been meshed using *Belytschko–Tsay shell elements* (*BLT*) as it takes less computational time, around 30–50% less than other elements like Hughes and Liu (*Nielsen & Brian, 1997*).

(II) Mesh adaptivity

Metal forming simulations are considered as large deformation problems. Therefore, the elements may undergo excessive deformation which leads to abrupt increase in aspect ratio of the element. Such increase in aspect ratio of the element increases the stiffness in one direction and decreases in another which further affects the accuracy of the simulation. Also, mesh size affects the time step calculation by taking smallest length into account and as the time step decreases the time required to solve the non-linear problem increases to a large extent. Therefore in order to resolve such a problem adaptive meshing is better option (*Crisfield, 1997*). Adaptive meshing divides the element into a number of parts when the aspect ratio becomes excessively large and maintains the stiffness properties balanced in both direction and thereby improving the results of finite element (FE) simulations (*Keum et al., 2001*). Fig. 6.2 shows mesh adaptivity after certain deformation in the blank.

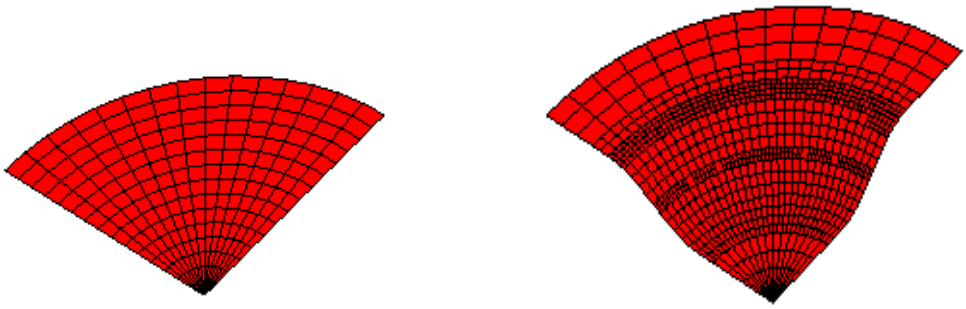

(a) (b)

Fig.6.2: Mesh adaptivity (a) blank (b) after some deformation

(III) Mass scaling

Sheet metal forming simulations are highly nonlinear in nature and it takes a lot of computational time to get the desired output. In industries, it is desirable to reduce the simulation time to get the required results. Therefore, few methods are available in the commercial FE analysis software for increasing of simulation speed. Specifically, mass scaling method is popularly used to speed the FE analysis (*Lars Olovsson et al. 2005*).

For a shell element the time step size is calculated using Equation (6.1). From this relation it is clear that the time step size can be changed by changing the element length (L), Young's modulus (E) and density (ρ). But changing L will change the mesh density and deteriorates the results; changing E is not recommended as it greatly affects the material stiffness. The last option is changing the density which may not have a significant effect on analysis results (*Lars et al., 2005*). This process of changing density to increase the time step and to minimize the computational time is called as mass scaling.

$$\Delta t_c = \frac{L}{c} \qquad (6.1)$$

where, $c = \sqrt{\frac{E}{\rho(1-\vartheta^2)}}$

6.2 Pre-processing of Deep Drawing Process

The input model consist of die, blank, blank holder and punch have been constructed in pre-processor. The punch, die, blank holder has been considered as rigid body in the FE analysis of deep drawing process. The fine meshing has been done on the surface of die, bank holder and punch. Blank has been considered as a deformable body and undergoes excessive deformation in deep drawing process. Therefore, adaptive meshing has been used for the blank material. It is very difficult to consider the thermal interaction between die, blank, blank holder force and punch. Additionally, calculation various thermal material at interaction of various tools in deep drawing process is very difficult and tedious task (*Takuda et al., 2003*). Therefore for the present study, isothermal models have been considered. The complete axisymmetric model in the pre-processor is shown in Fig. 6.3. In order to simplify FE model, only quarter geometry is modeled since the material properties, geometry and loading are considered to be symmetric along mutually perpendicular axes. The simulations have been carried out on a system with the configuration: Intel Xeon *CPU E3-1270 V2, 3.50 GHz, 16GB Ram and 64-bit Windows-7* Operating System.

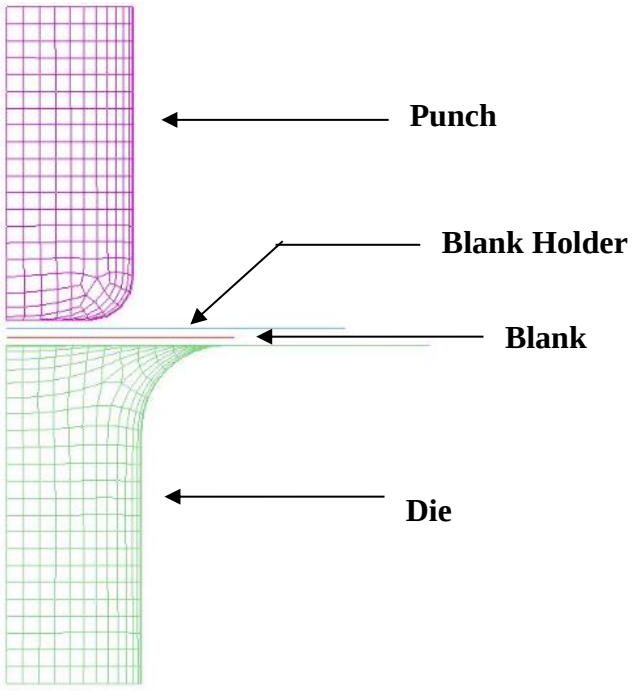

Fig.6.3: Axisymmetric model for deep drawing process

The blank and the tool components have been meshed using Belytschko–Tsay shell elements. The material properties required for FE analysis are mentioned in Table 6.1. In addition to this, few physical material properties need to give as input for FE analysis. These physical properties are taken from material properties handbook for titanium alloys (*Boyer et al., 1994*). The required physical propriety for FE analysis is mentioned in Table 6.2 and Table 6.3. Selective mass scaling has been used for FE simulations. The various developed anisotropic yield criteria namely; Hill 1948, Barlat 1989, Barlat 1996, Barlat 2000 and Cazacu Barlat have been assigned to blank material.

The accuracy of FE analysis in deep drawing process is significantly dependent on selection of friction coefficient value (*Tekkaya AE, 2000*). It is very difficult to calculate friction coefficient value experimentally (*Altan, 2003*). Inverse approach is one of the commonly used approach to determine friction coefficient value using FE analysis (*Singh*

et al., 2010). The methodology has been adopted by varying the coefficient of friction values and superimposing experimental and simulated plot of punch load vs. punch displacement. Fig. 6.4 shows representative punch load vs. punch displacement graph by varying the coefficient of friction value at 400^0C. Similarly, coefficient of friction values have been calculated at various temperatures, as presented in Table 6.4. It has been observed from Table 6.4, coefficient of friction values are increased with temperature. However, the variation in the values are negligible, it indicate the effectiveness of Molykote lubricant at elevated temperatures.

Table 6.1: Material properties as an input for FE analysis

Temp. (^{0}C)	$n_{avg.}$	m	r_0	r_{45}	r_{90}	$\sigma_{yavg.}$ (MPa)	$\sigma_{utavg.}$
RT	0.0358	0.001	0.46	1.43	0.29	860	935
50	0.0382	0.003	0.48	1.42	0.30	855	924
100	0.0413	0.006	0.52	1.39	0.34	823	901
150	0.0463	0.009	0.56	1.37	0.36	773	831
200	0.0571	0.010	0.60	1.61	0.56	709	801
250	0.0598	0.010	0.79	1.18	0.70	684	744
300	0.0642	0.011	0.75	1.15	0.48	663	741
350	0.0695	0.012	0.71	1.07	0.53	657	726
400	0.0702	0.012	0.60	1.26	0.51	655	721

Table 6.2: Physical properties for Ti-6Al-4V alloy at room temperature

Melting point (T_m)	1655^0C
Density (ρ)	4.428 gm/cm^3
Thermal conductivity (K)	7 W/m*K
Specific heat capacity (C)	580 J/kg*K
Thermal coefficient of linear expansion (α)	$9.0*10^{-6}$ /^{0}C

Table 6.3: Physical properties for Ti-6Al-4V alloy at various temperatures

Temp. (^{0}C)	Modulus of Elasticity (E) (GPa)	Possion's ratio (v)
RT	105	0.23
50	102.44	0.23
100	99.83	0.23
150	97.67	0.23
200	94.7	0.23
250	92.45	0.23
300	89.39	0.23
350	86.78	0.23
400	84.1	0.23

Table 6.4: Variation of coefficient of friction value with temperature

Temperature (^{0}C)	150	200	250	300	350	400
Coefficient of friction	0.05	0.05	0.07	0.07	0.08	0.09

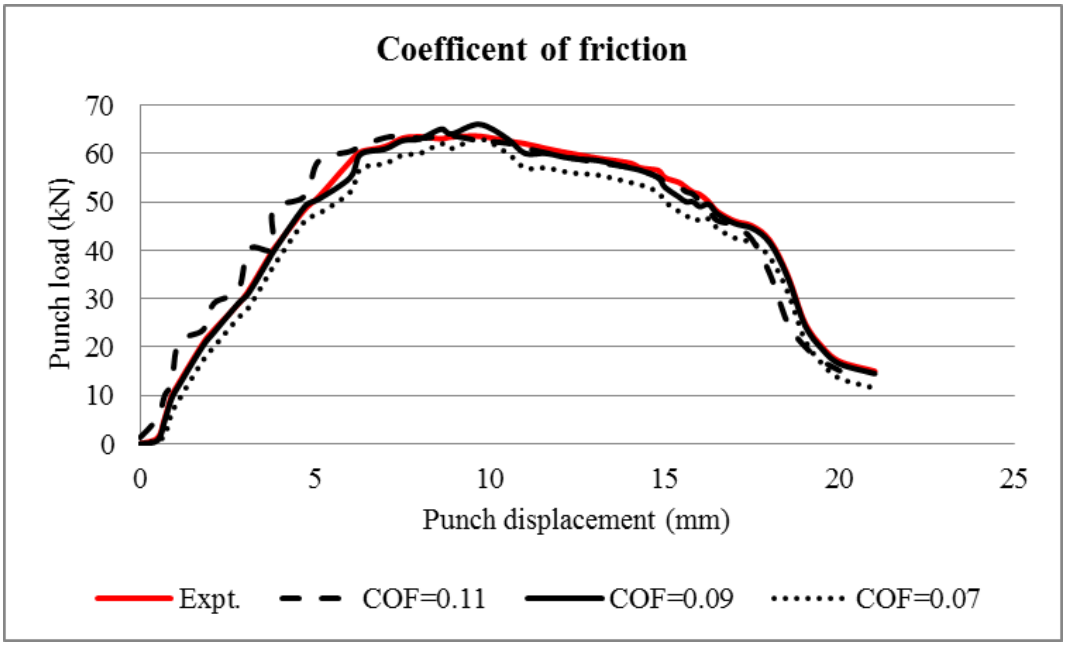

Fig.6.4: Representative experimental and FE validation of punch load vs. punch disp. at 400^0C

In the deep drawing simulations, selection of punch speed and blank holding pressure are crucial parameters. The simulation time is greatly dependent on punch speed. For initial check, four various punch speeds have been considered (10, 100, 500 and 1000 *mm/min*). It has been observed that effect of punch speed on thickness distribution is very negligible. Similarly, it has negligible influence on punch vs. load displacement curve. However, one cannot speed up the analysis arbitrarily and infinitely; after a certain point all simulation accuracy is lost and the results become unusable (*Nielsen & Brian, 1997*). After punch speeds of 500 *mm/min* extreme dynamic effects make the results unacceptable due to the presence of very large vibrations in blank material. In the present study, for the safer side, all the deep drawing simulations have been carried out at *100 mm/min* punch speed.

It is possible to assign punch speed in several ways. There are various ways to give punch speed in DYNAFORM software such as constant speed, sinusoidal, trapezoidal or random. The commonly used punch speed is constant speed (*Hol, 2009*). Although, it seems easier to assign a constant speed at first, undesired dynamic effects arise in the simulation due to the rapid strike of the punch on the blank (deformable body). After the collision, the blank starts to vibrate forcefully and the precision of the simulation is diminished due to these unrealistic vibrations (*Lars et al., 2005*). However, in reality the tools firstly accelerate from a stationary position to a maximum speed, and then decelerate until stopping again. This stroke controlled velocity function decreases the vibration of the blank at the first contact, making the simulation more successful, realistic and accurate (*Nielsen, 1997*). Therefore, trapezoidal punch speed option is used for deep drawing simulations. Generally, blank holding pressure is considered as 2% of the yield strength of material.

6.3 Finite Element Analysis of Deep Drawing Process

6.3.1 Failure Study

The fracture can be distinguished in two ways; initial fracture (punch corner region) and final fracture (chipping of material). The representative initial and final fracture is shown in Fig. 6.5 and Fig. 6.6 respectively. The failure strain has been observed in the punch corner region which indicates that the fracture may appear at the beginning of an experimental drawing process. This failure has been observed for larger diameter blank (above 52 mm) at 50^0C and 100^0C because very low *n* value and due to more punch load

requirement the extent of thinning is more. Hence, failure has been appeared in the neck region.

Furthermore, simulation of *56 mm* and above diameter cups at 400^0C shows excessively high Von Misses stresses in the upper region of the cup as shown in Fig. 6.6. The Von Misses stresses should not exceed mean flow stress as it may lead to fracture in the material. Hence it can be interpreted that the fracture can take place in this area.

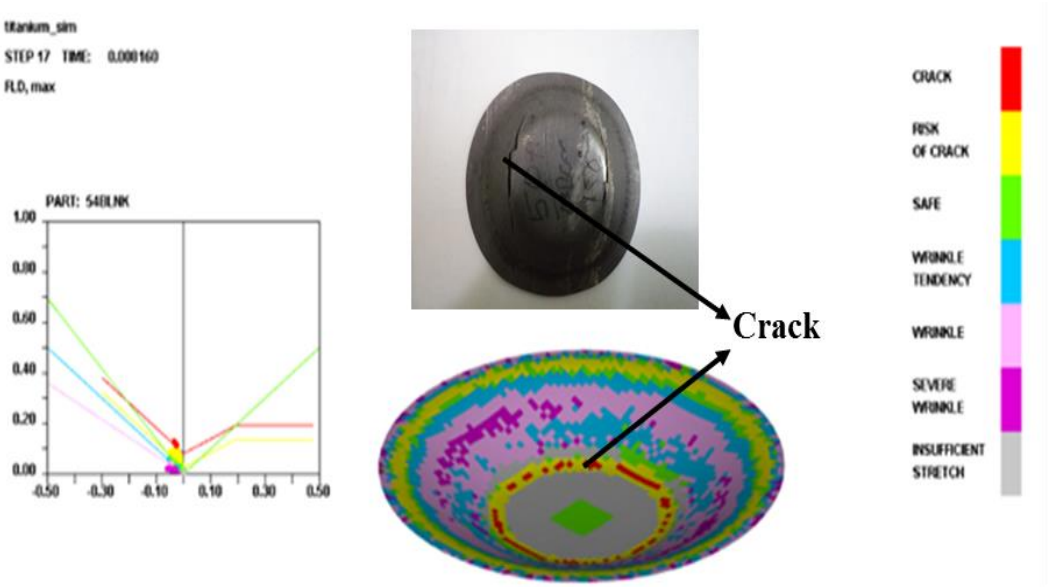

Fig.6.5: Comparison of neck failure at experimentation and FE analysis

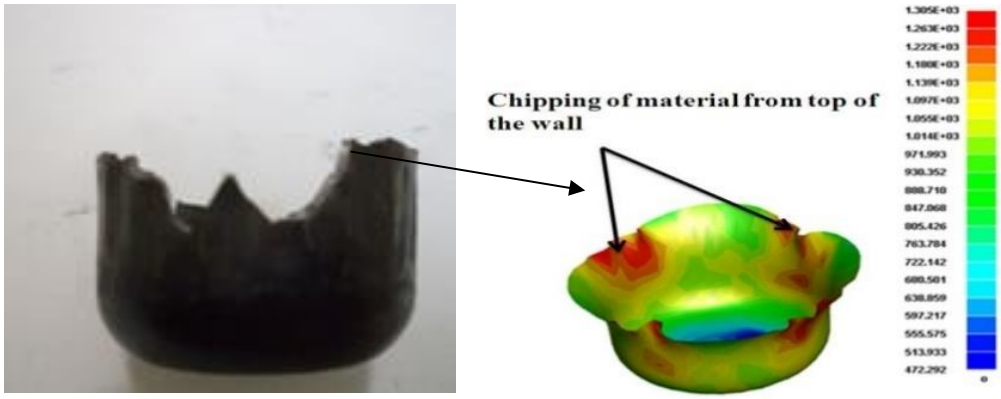

Fig.6.6: Comparison of chipping of material at experimentation and FE analysis

6.3.2 Thickness Distribution

Thickness distribution is one of the important qualitative aspect of deep drawn cups. FE analysis has been carried out for all the possible blank diameters with variation of temperature from 150^0C to 400^0C at interval of 50^0C. The representative successfully drawn cups using all the yield criteria at 400^0C is shown in Fig. 6.7. Fig. 6.8 shows representative thickness distribution using various yield criteria at 400^0C and 52 mm blank diameter. Table 6.5 presented average absolute error between experimental thickness distribution and all simulated cups using various yield criteria.

It has been clearly indicated that, Hill 1948 and Barlat 1989 yield criteria thickness prediction is very poor compared to other yield criteria. The average absolute error is almost 8%. Barlat 1989 yield criterion prediction is better than Hill 1948 yield criterion, specifically in the wall region thickness prediction. Nevertheless, these yield criteria are popularly used in FE analysis of sheet metal forming processes because of less number of mechanical parameters requires and their easy determination (*Nielsen KB, 1997*).

The accuracy of the thickness distribution can be further improved using advanced yield criteria. Even though Barlat 1996 yield criterion predicts yielding behavior of Ti-6Al-4V alloy accurately, but thickness prediction is poor compared with Barlat 2000 and Cazacu Barlat yield criteria. Excessive thickness reduction is observed in case of neck region using Barlat 1996 yield criterion. Further accuracy in thickness distribution is obtained using Barlat 2000 and Cazacu Barlat yield criteria. Both the yield criteria prediction is better than the other yield criteria. Particularly, in wall region, more deviation in thickness distribution has been observed by using Barlat 2000 yield criterion. Cazacu Barlat yield criterion prediction is better than the Barlat 2000 yield criterion. The

thickness in the neck region and wall region is very well predicted using Cazacu Barlat yield criterion.

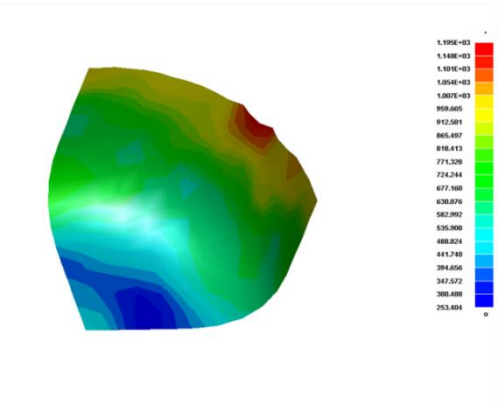

(a) Hill 1948

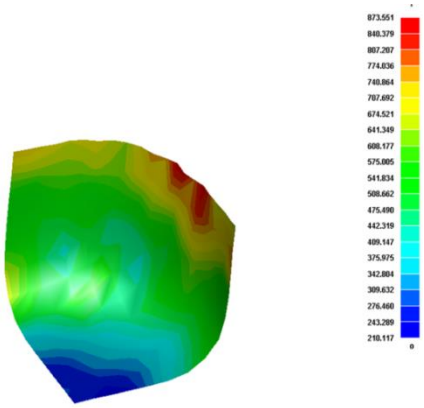

(b) Barlat 1989

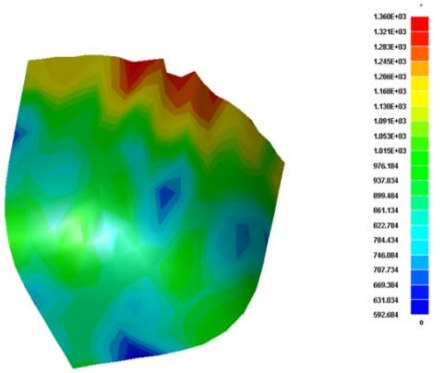

(c) Barlat 1996

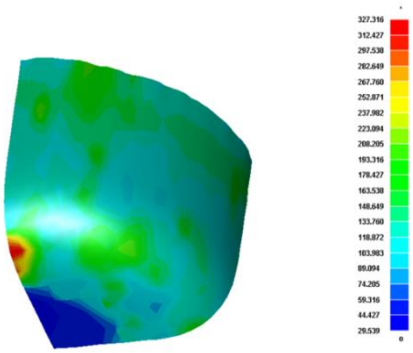

(d) Barlat 2000

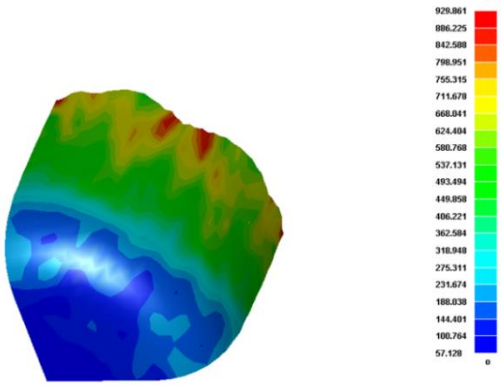

(e) Cazacu Barlat

Fig.6.7: Representative successfully drawn cups at 400^0C using various yield criteria

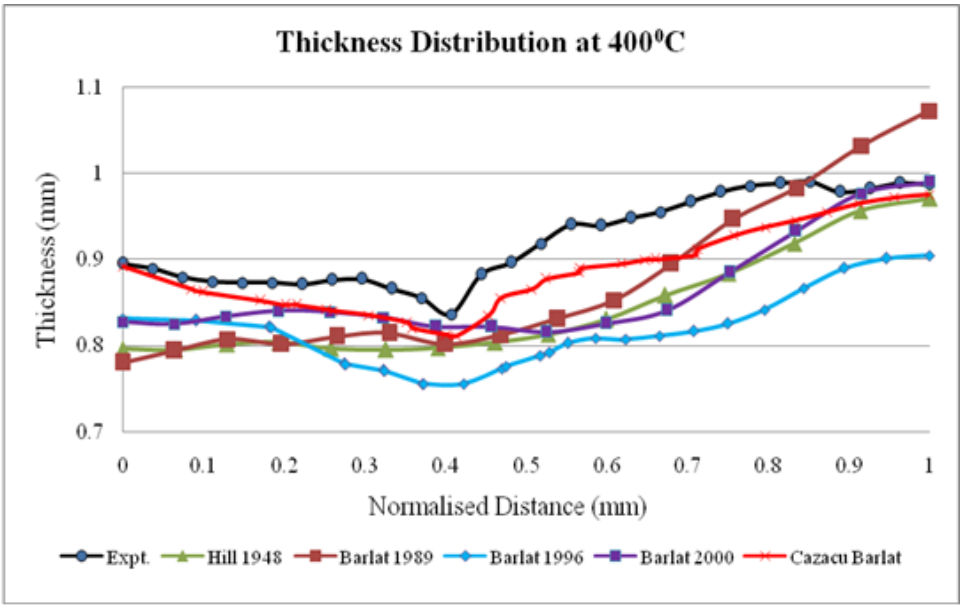

Fig.6.8: Representative thickness distribution using various yield criteria at 400^0C

Table 6.5: Average absolute error for experimental thickness

Material Model	Hill 1948	Barlat 1989	Barlat 1996	Barlat 2000	Cazacu Barlat
Average Relative Error (%)	8.3	8.1	5.98	2.8	1.6
Standard Deviation of error	0.236	0.283	0.213	0.142	0.098

6.3.3 Earing Profile

Earing in deep drawing for anisotropic metals is a pronounced phenomenon. Accurate prediction of earing profile is an important aspect to asesss the quality of deep drawn cup (*Saxena & Dixit, 2009*). This necessitates comparison of yield models based on earing prediction in deep drawing, as shown in Fig. 6.9. Earing is poorly predicted by Hill 1948, Barlat 1996 and Barlat 2000 yield models. On the other hand, Barlat 1989 predicts the earing tendency in simulated cups. However, prediction capability is poor compared with Cazacu Barlat yield criterion.

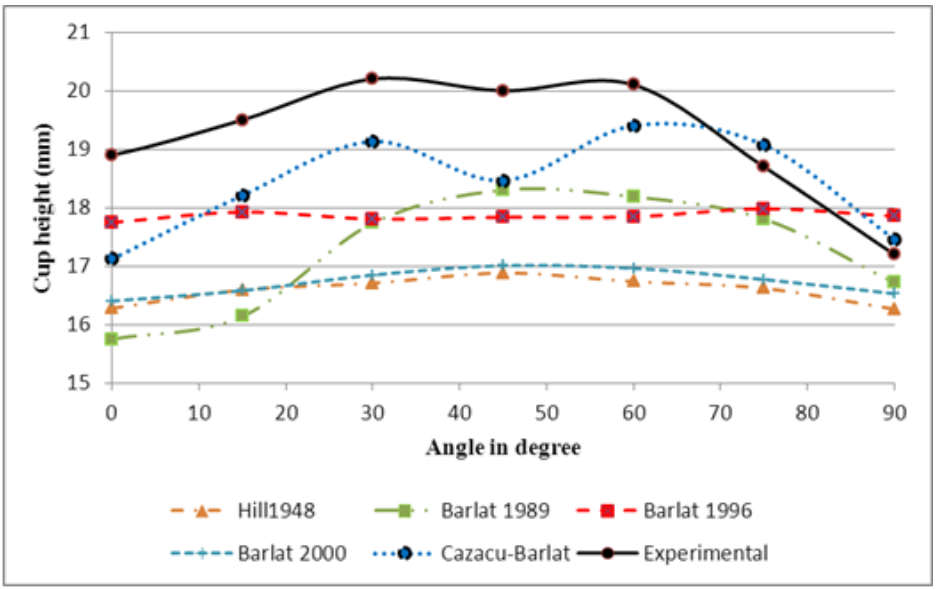

Fig.6.9: Representative earing profile of experimental and simulated cup at 400^0C

The yield model capability can also be assessed based on the complexity involved for determination of material constants and simulation time taken for FE analysis (B*anabic*, *2010*). Table 6.6 shows comparison of simulation time required for different anisotropic yield models. Hill 1948 and Barlat 1989 yield criteria have less material parameters which can be determined by performing simple uniaxial tension tests. Also, the simulation time taken for these models is relatively lesser than that of other models.

Table 6.6: Total CPU time taken for simulation

Yield Criterion	Time (sec)
Hill 1948	7166
Barlat 1989	8769
Barlat 1996	82722
Barlat 2000	76014
CazacuBarlat	37398

On the other hand, advanced yield models like Barlat 1996 and Barlat 2000 and Cazacu Barlat yield models needs different mechanical tests to be carried out like biaxial tensile test, compression test etc. which makes them complicated for their application in FE simulation. Moreover, the simulation time required for these models are very large compared to Hill 1948 and Barlat 1989 yield models. It should be noticed that simulation time for Cazacu Barlat yield model is less as compared to Barlat 1996 and Barlat 2000 with better accuracy. Therefore, considering these qualitative parameters of deep drawn cups, Cazacu Barlat yield criterion is well suited for deep drawing of Ti-6Al-4V alloy at elevated temperatures.

6.4 Finite Element Analysis of Stretching Process

In the previous chapter, FLC has been determined using experimental and theoretical method (M-K theory) using various yield criteria and constitutive models. M-K theory involves complex mathematics and required rigorous development of numerical code for FLC prediction (*Siguang et al.,1998*). The implementation of FE analysis in sheet metal forming processes reduces unnecessary experimental try outs and rigorous development of theoretical codes for forming limit prediction (*Chung & Shah, 1992*). In this section, FE analysis of stretching process has been done and various forming aspects namely; dome height, thickness distribution, failure points in FLC has been investigated.

The main difference between preprocessing of deep drawing process and stretching process is punch type. The Nakazima test is used for FLD prediction. Therefore, spherical punch is modeled in FE analysis. In addition to this circular draw bead has been constructed below the stretched specimen. The draw bead is not allowed a material to

flow into a die cavity. The fixed contact type constrain is given between draw bead and blank material. The input models like die, blank, blank holder, draw bead and spherical punch have been constructed in pre-processor. The remaining details are same as the preprocessing modeling of deep drawing process. In the stretching process the width of the blank is varied as per dimensions given in Fig. 5.4. The size of the blank is rectangular therefore quarter geometry is not possible to use in FE analysis. The complete model in the pre-processor is shown in Fig. 6.10.

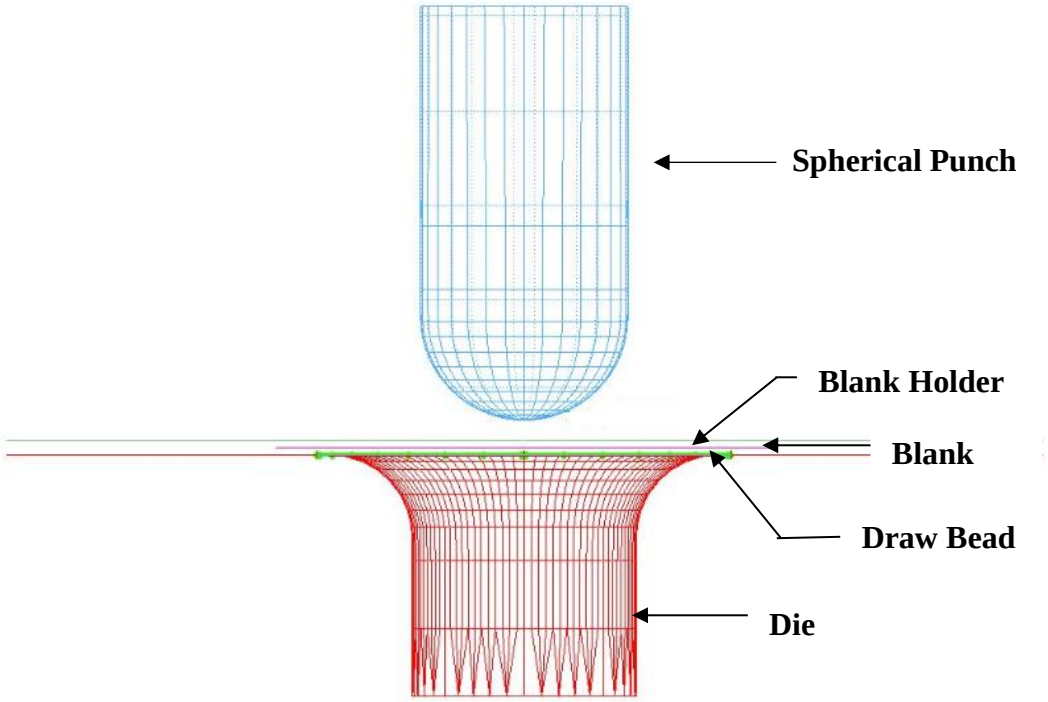

Fig.6.10: Preprocessing model of stretching setup

6.4.1 Thickness Distribution

The representative thickness distribution of successfully stretched specimens is shown in Fig. 6.11 (a, b & c). The thickness profile is considered from one end of the stretched corner to another end of the stretched corner. Table 6.7 shows average absolute

error for thickness distribution. As expected, minimum thickness has been observed at center portion of stretched specimens. It can be seen from Fig. 6.11 and Table 6.7, Hill 1948 yield criterion prediction is very poor compared with experimental thickness distribution. The excessive reduction in the thickness has been observed using Hill 1948 yield criterion Moreover, Barlat 1989 and Barlat 1996 prediction is poorer than the other yield criteria. Cazacu Barlat yield criterion prediction is in better agreement with experimental thickness distribution.

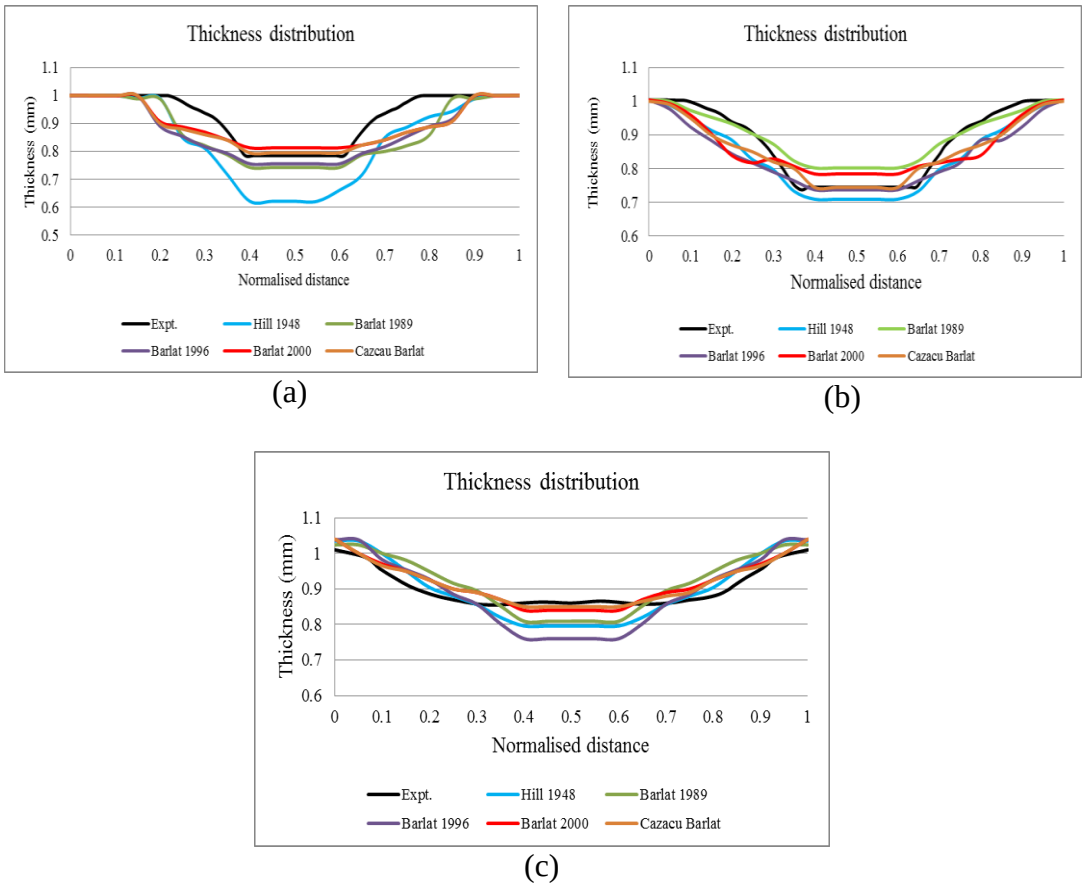

Fig.6.11: Representative thickness distribution of successfully stretched specimens

(a) *120 mm × 120 mm* (b) *120 mm × 80 mm* (c) *120 mm × 30 mm*

Table 6.7: Average absolute error for experimental thickness

Material Model	Hill 1948	Barlat 1989	Barlat 1996	Barlat 2000	Cazacu Barlat
Average Relative Error (%)	8.76	5.90	5.87	2.92	2.02
Standard Deviation of error	2.52	1.89	1.88	1.58	1.20

Additionally, accurate prediction of thickness at dome is one of the important parameters in stretching process. The maximum deformation is observed at dome in stretching process. Excessive deformation at dome initiates the failure in the stretching process (*Goodwin, 1968*). Therefore, it is vital to capture thickness at dome Fig. 6.12 shows representative thickness value at dome at various width specimens. The thickness at dome is poorly predicted by Hill 1948. Barlat 1989 and Barlat 1996 thickness at dome prediction is slightely better than the Hill 1948 yield criterion. However, further accuracy is obtained with Barlat 2000 and Cazacu Barlat yield criteria. Among all the considered yield criteria, Cazacu Barlat FE analysis capture deformation very well for Ti-6Al-4V alloy at elevated temperatures.

6.4.2 Limiting Dome Height

One of the important parameter in stretching process is Limiting Dome Height (LDH) calculation. It shows ability of material to form before fracture (*Brammar & Harris,*

1975). The LDH has been validated through FE analysis using various yield criteria as shown in Fig.6.13.

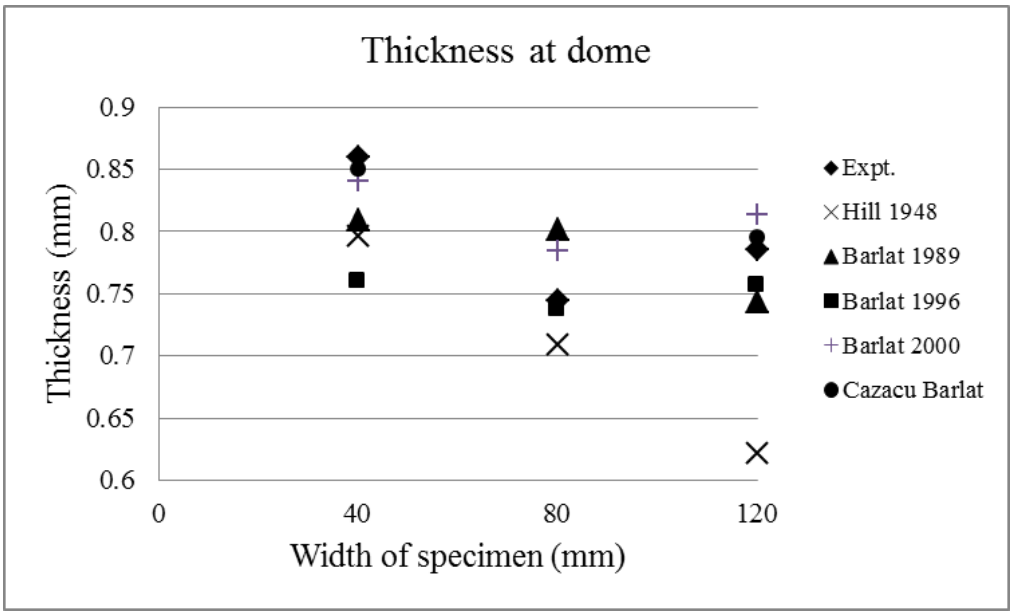

Fig.6.12: Representative thickness at dome using various yield criteria

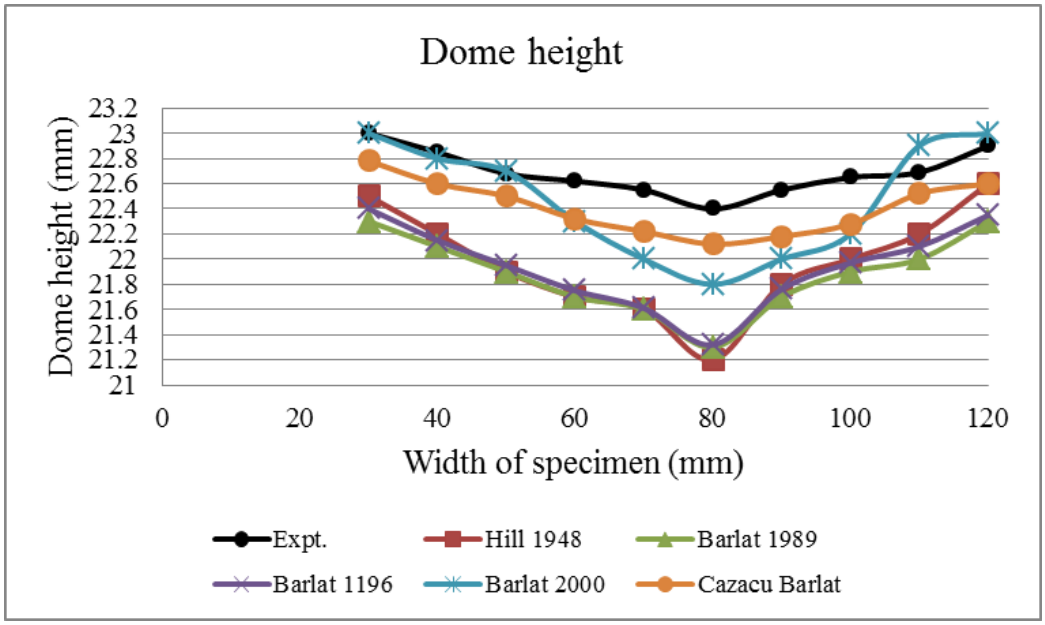

Fig.6.13: LDH using various yield criteria

The dome height is minimum at plane strain condition (*Ghosh, 1975*). The similar observation has been seen in FE analysis of dome height prediction. FE analysis of LDH

predictions are poorly predicted using Hill 1948, Barlat 1989 and Barlat 1996 yield criteria. Both the yield criteria under estimate the dome height calculation. It indicates the incapability of these two yield criteria to capture the deformation accurately. Moreover, Barlat 2000 and Cazacu Barlat yield criteria prediction is more accurate but, these yield criteria also underestimate the dome height prediction. In Barlat 2000, more deformation has been observed in plane strain condition. Among all these yield criteria, Cazacu Barlat yield criteria suits very well for dome height prediction. However, it slightly underestimate the dome height calculations.

6.4.3 Forming Limit Curve

The representative simulated stretched specimens at plane strain condition using various yield criteria is shown in Fig. 6.14. The failure strains from simulated FLDs have been determined. The failure strains have been considered as a basis for compassion with experimental and best theoretical FLC (Cazacu Barlat yield criterion + *m-Arr.* constitutive model).

It can be seen from Fig. 6. 15 (a & b), failure points are very well inside the experimental and theoretical FLC. Specifically in biaxial state stress region (right side) of FLD. It indicates incapability of these two yield criteria for failure strain prediction in biaxial region. The similar observation has been seen in case of yield locus prediction. On the other hand, Barlat 1996 yield criterion also underestimate the failure points in the right hand side of the FLC as shown in Fig. 6.15 (c). Barlat 2000 and Cazacu Barlat yield criteria failure predictions are very well close to the experimental and theoretical FLCs as shown in Fig. 6.15 (d). It indicates suitability of these yield criteria in FLCs prediction.

Further accuracy in FLC prediction can be obtained by incorporating M-K theory in FE analysis.

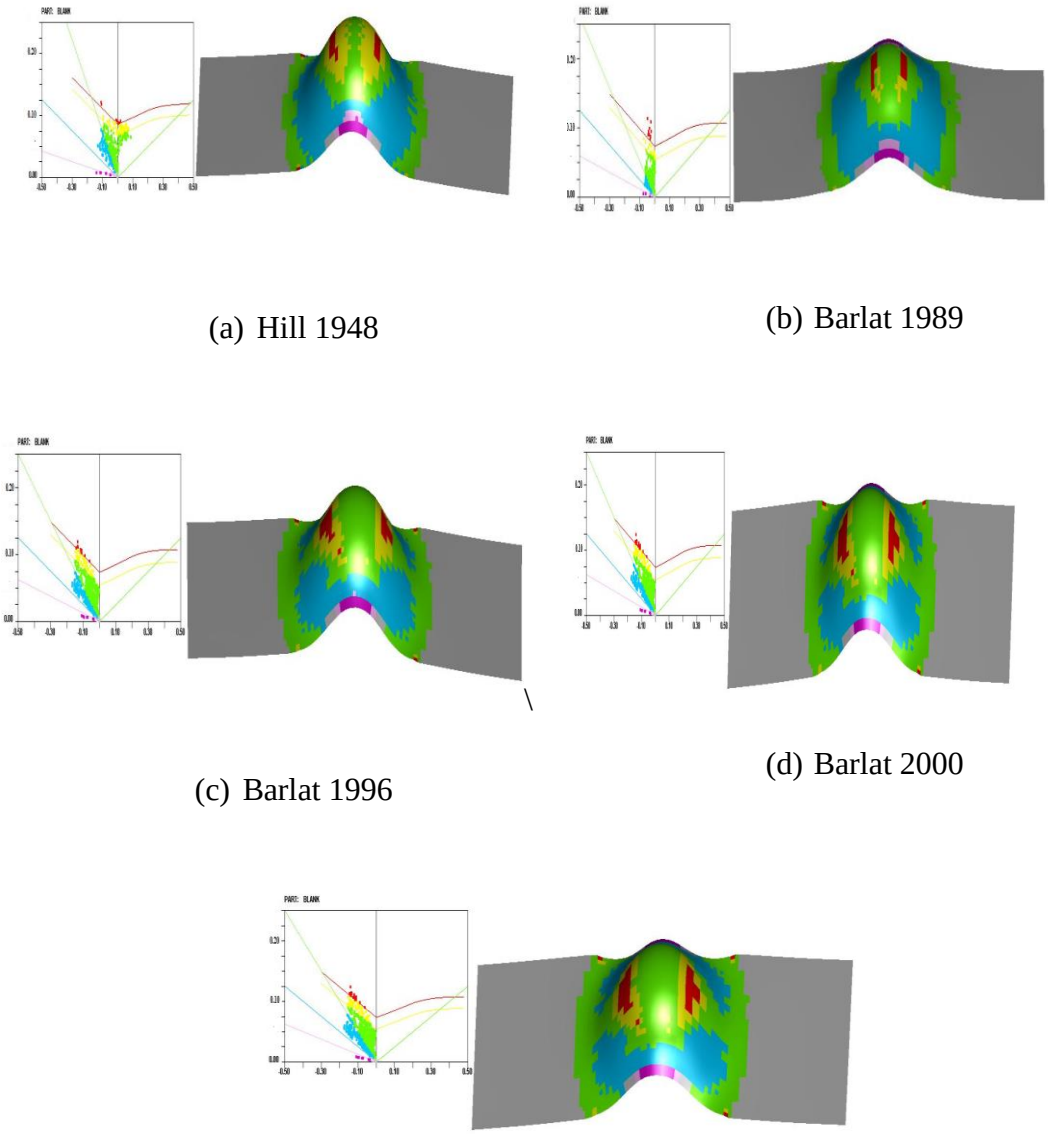

(a) Hill 1948

(b) Barlat 1989

(c) Barlat 1996

(d) Barlat 2000

(e) Cazacu Barla

Fig.6.14: Representative simulated specimens at plane strain condition

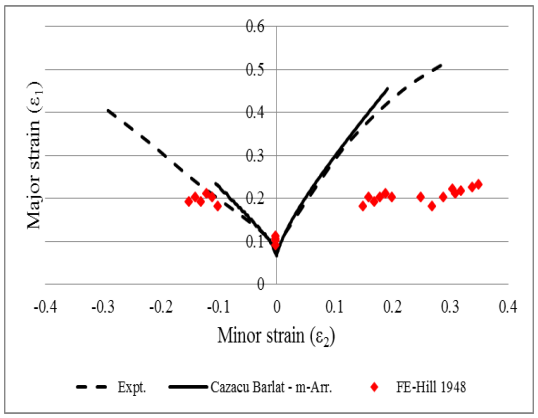

(a) Hill 1948

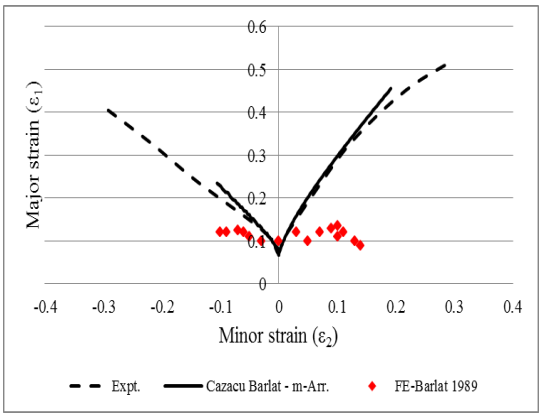

(b) Barlat 1989

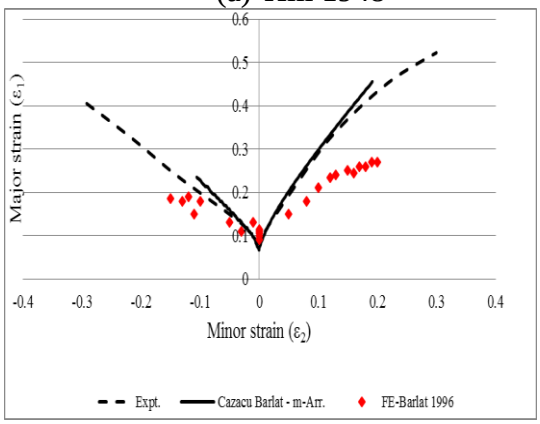

(c) Barlat 1996

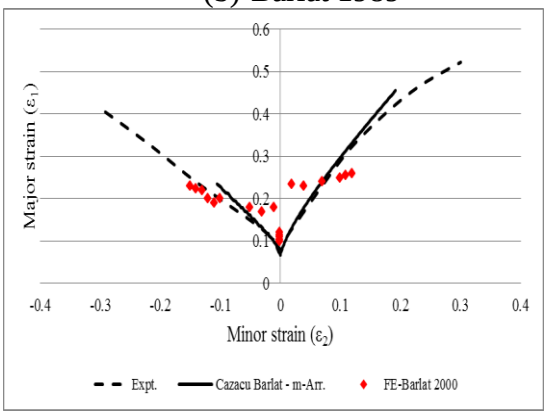

(d) Barlat 2000

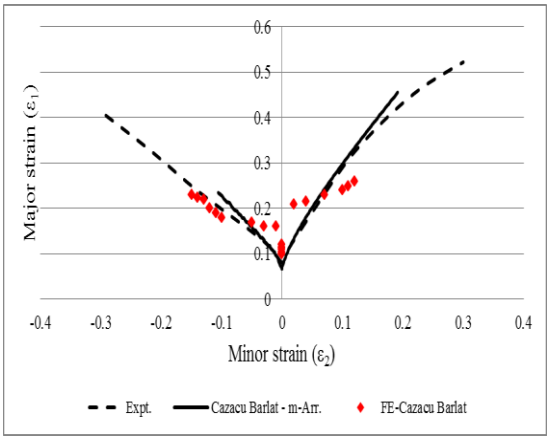

(e) Cazacu Barlat

Fig.6.15: Failure strain in simulated FLDs using various yield criteria

6.5 Summary

This chapter covers FE analysis of deep drawing and stretching process at elevated temperatures using DYNAFORM software. The developed material models are incorporated in FE analysis. The failure study, thickness distribution and earing profile of deep drawn cups have been compared with experimental results. Additionally, thickness distribution, dome height estimation and FLCs have been determined using FE analysis. Based on the observations, Cazacu Barlat yield criterion FE analysis is very well suited for Ti-6Al-4V alloy at elevated temperatures.

The next chapter discusses the conclusions and contributions from the present research work.

CHAPTER 7: CONCLUSIONS

In this thesis work, experimental and numerical investigations on forming behavior of Ti-6Al-4V alloy at elevated temperatures have been carried out. The important conclusions from this study are presented as follows:

7.1 Salient Conclusions

- The material properties and flow stress behavior of Ti-6Al-4V alloy have been comprehensively investigated based on uniaxial tensile tests from room temperature to 400^0C at an interval of 50^0C with wide range of slow strain rates (10^{-5}, 10^{-4}, 10^{-3}, 10^{-2} s^{-1}). The failed tensile test specimens have been comprehensively examined using SEM at elevated temperatures. The fractography studies of tensile fracture surface revealed a healthy population of microvoids and shallow dimples of varying size and shape, which indicated predominantly ductile type of fracture.
- Forming behavior of Ti-6Al-4V alloy has been investigated using circular deep drawing process from room temperature to 400^0C at an interval of 50^0C.
  - It has been observed that Ti-6Al-4V alloy is difficult to draw up to 150^0C and within the experimental range the maximum LDR of 1.86 is obtained at 400^0C. The obtained LDR is much lesser than the other structural alloys, which indicated the poor formability of Ti-6Al-4V at elevated temperatures.
  - Failure in the deep drawn cups has been identified in two regions namely, neck and upper wall. The fractography studies in the neck region revealed a healthy population of shallow type equiaxed dimples of varying size and shape,

indicating ductile type of failure due to excessive tensile stresses. However, in the wall region, unidirectional dimples have been observed, which indicate ductile type of failure due to excessive shear stresses.

- The quality of successfully drawn cups has been evaluated based on thickness distribution and earing profile. The uniform thickness distribution is obtained at higher temperature with optimum blank diameter and a predominant earing tendency with four ears has been observed in all the deep drawn cups at elevated temperatures.

- Forming Limit Curve (FLC) has been determined experimentally for Ti-6Al-4V alloy at 400^0C. The various formability aspects such as Limiting Dome Height (LDH) diagram, thickness distribution of stretched specimens and fractography study have been evaluated.

  - LDH diagram has been constructed for Ti-6Al-4V alloy at 400^0C. It has been observed that the dome height is minimum at plane strain condition and it increases in the region of uniaxial and biaxial state of stress region. Additionally, thickness distribution of successfully stretched specimens has been measured from one end to another end. The more thickness reduction has been observed in case of biaxial and plane strain region compared with uniaxial state region.

  - Fractography studies in the uniaxial tension region (*120 mm × 30 mm*) revealed unidirectional dimples, indicating ductile failure due to excessive stresses. However, in plane strain (*120 mm × 80 mm*) and biaxial tension region (*120 mm × 120 mm*), shallow type of equiaxed dimples have been observed which indicates ductile failure due to excessive normal stresses.

- For theoretical and numerical analysis, various advanced anisotropic yield criteria namely; Hill 1948, Barlat 1989, Barlat 1996, Barlat 2000 and Cazacu Barlat and different constitutive models viz., *m-FB*, *JC*, *m-Arr*., *m-ZA* and *MTS* have been developed for Ti-6Al-4V alloy.
  - The performance of the yield criteria has been investigated based on the yield locus, planer distribution of uniaxial yield stress and anisotropic coefficient. Based on the observations, Cazacu Barlat yield criterion is found to be the most suited model for Ti-6Al-4V alloy among the developed anisotropic yield criteria, since anisotropy in yielding and stress asymmetry resulted in excellent validation of yield function with experimental data points.
  - The constitutive models have been evaluated based on the statistical measures namely, correlation coefficient (R), average absolute error (Δ), its standard deviation (S), number of material constants and complexity involved in determination of these constants. Among all the considered models, *m-Arr.* model is the best in predicting the flow behavior of Ti-6Al-4V alloy. However, considering the fact that physical based models are more preferred over phenomenological models, *MTS* model is preferred for prediction of flow stress of Ti-6Al-4V alloy.
- Theoretical FLCs have been determined using Marciniak Kuczynski (M-K) theory incorporating the developed yield criteria and constitutive models.
  - The value of the thickness imperfection factor f_0 is determined solely by the constitutive models. In predicting FLCs, the effect of yield model is more pronounced than the effect of constitutive model on it.

- The Cazacu Barlat yield criterion with *m-Arr.* constitutive model is found to be the best in predicting the theoretical FLC of Ti-6Al-4V alloy at 400^0C

- Finite element (FE) analysis of deep drawing and stretching process has been carried out using DYNAFORM software with LS-Dyna solver. The various developed anisotropic yield criteria have been implemented in FE analysis. The important formability aspects such as thickness distribution, earing profile, LDH and FLC have been evaluated. FE analysis with Cazacu Barlat yield criterion is found to be in the best agreement with the experimental and theoretical results of forming behavior of Ti-6Al-4V alloy at elevated temperatures.

7.2 Specific Contributions to the Research

Through this thesis on the forming behavior of Ti-6Al-4V alloy at elevated temperatures, the following contributions have been made towards the frontiers of state-of-art research on high strength light weight alloys:

- Determination of material properties and flow stress behavior
- Experimental results of LDR, thickness distribution, earing profile, and FLC
- Development of various yield criteria and constitutive models
- Determination of theoretical FLC using Marciniak Kuczynski (M-K) theory
- FE model development and analysis of deep drawing and stretching process
- Comparison of experimental, theoretical and FE results

7.3 Further Scope of Work

Few directions for enhancing this research further are as follows:

- The formability study can be extended for Ti-6Al-4V alloy above 400^0C with inert and protective environment.
- The various constitutive models can be incorporated through user subroutine code in FE analysis. Additionally, M-K theory can be incorporated in FE analysis.
- Stress based and damage based FLDs can be developed at elevated temperatures.

REFERENCES

Adamus J, Lacki P, (2011). Forming of the titanium elements by bending. Computational Material Science, 50 (4): 1305-1309.

Alt H, Godau M, (1995). Computing the fréchet distance between two polygonal curves. Journal of Computational Geometry & Applications, 5 (1-2): 75-91.

Altan T, (2003). Advanced methods of simulation in tubehydroforming – research progress and case studies. Proceedings of the THF Conference, Stuttgart, 111-116.

Aly EI-Domiaty, (1992). The effect of strain, strain rate and temperature on formability of Ti–6Al–4V alloy. Journal of Material Processing Technology, 32:243–251.

Atkinson M, (1996). Accurate determination of biaxial stress–strain relationships from hydraulic bulging tests of sheet metals. International Journal Mechanical Science, 39 (7):761–769.

Banabic D, (2010). Sheet metal forming process: constitutive modeling and numerical simulations. Springer, Heidelberg.

Banabic D, Vulcan M, Siegert K, (2005). Bulge testing under constant and variable strain rates of superplastic aluminium alloys. CIRP Annuals Manufacturing Technology, 1:205–218.

Banerjee B (2007). The Mechanical Threshold Stress model for various tempratures of AISI 4340 steel. International Journal of Solids and Structures 44 (2007) 834–859.

Barlat F, Richmond O, (1987). Prediction of tri-component plane stress yield surfaces and associated flow and failure behaviour of strongly textured FCC polycrystalline sheets. Journal of Materials Science and Engineering, 91:15–29.

Barlat F, Lian J, (1989). Plastic behaviour and strechability of sheet metals Part I: a yield function for orthotropic sheets under plane stress condition. International Journal of Plasticity, 5: 51–56.

Barlat F et al., (1997_a). Yield function development for aluminum alloy sheets. Journal of Mechanics and Physics of Solids, 45 (11/12): 1727-1763.

Barlat F, et al., (1997_b). Yielding description for solution strengthened aluminium alloys. International Journal of Plasticity, 13:185–401.

Barlat F, et al., (2003). Plane stress yield function for aluminium alloy sheets – Part 1: Theory. International Journal of Plasticity, 19:297–319.

Barlat F, (2007). Materials processing and design: Modeling, simulation and applications. Proceedings of the NUMIFORM 2007 Conference, Porto, 3–22.

Beal Joseph D, Boyer Rodney, Daniel Sanders, (2006). The Boeing Company, Forming of Titanium and Titanium Alloys. ASM Handbook.14B: Metalworking: Sheet Forming.

Beddoes J, Bibby MJ, (1999). Principles of Metal Manufacturing Processes. Arnold, London.

Boehler JP, Demmerle S, Koss S, (1994). A new direct biaxial testing machine for anisotropic materials. Journal of Experimental Mechanics. 34:1–9.

Bolt, P, Lamboo N, Rozier P, (2001). Feasibility of warm drawing of aluminum products. Journal of Materials Processing Technology, 115:118–121.

Bong HJ, Barlat F, et al., (2013) Formability of austenitic and ferritic stainless steels at warm forming temperature. International Journal of Mechanical Sciences, 75:94–109.

Boyer, R, Welsch, G, Collings, EW, (1994). Materials Properties Handbook: Titanium alloys, ASM International.

Brammar IS, Harris DA, (1975). Production and Properties of Sheet Steel and Aluminum Alloys for Forming Applications. Journal of the Institute of Metals, 20 (2): 85–100.

Brozzo P, De Luca B, Rendina R, (1972). A new method for the prediction of the formability limits of metal sheets. Proceedings of the 7th Biannual Congress of the IDDRG, Amsterdam.

Butuca MC, et al., (2002). A more general model for forming limit diagrams prediction. Journal of Materials Processing Technology, 125–126: 213–218.

Butuc MC, Gracio JJ, Da Rocha AB, (2003). A theoretical study on forming limit diagrams prediction. International Journal of Material Processing. Techology, 142:714–724.

Cazacu O, Plunkett B, Barlat F, (2006). Orthotropic yield criterion for hexagonal close packedmetals. International Journal of Plasticity, 22:1171–1194.

Chen FK, Chiu KH, (2005). Stamping formability of pure titanium sheets. Journal of Material Processing Technology, 170:181–186.

Chung K, Shah K, (1992). Finite element simulation of sheet metal forming for planar anisotropic metals. International Journal of Plasticity, 8:453–476.

Cole, G.S., Sherman, A.M. (1995) Lightweight materials for automotive applications. Mater. Charact 35:3–9.

Crisfield MA, (1997). Non-linear finite element analysis of solids and structures. Advanced Topics, J. Wiley & Sons, New York.

Davis JR, (Edited by) (2004). Tensile Testing, Second Edition, ASM International.

Djavanroodi F, Derogar A, (2010). Experimental and numerical evaluation of forming limit diagram for Ti6Al4V titanium and Al6061-T6 aluminum alloys sheets. Materials and Design, 31:4866–4875.

Drucker DC, (1949). Relations of experiments to mathematical theories of plasticity. Journal of Applied Mechanics, 16:349–357.

Dziallach S, Bleck W, Blumbach M, Hallfeldt T, (2007). Sheet metal testing and flow curve determination under multi-axial conditions. Advance Engineering Material, 9(11):987–994.

El-Khaldi F, Lambriks M, (2002). New requirements in forming simulation. In: Proceedings of the NUMISHEET 2002, Jesu Island, South Korea, 97-104.

El-Khaldy, et al., (1992). Industrial validation of finite element simulation of drawn auto-body parts, in: Proceedings of the IDDRG Biannial Congress, Shenyang, China, 120-127.

Fang Gang, et al., (2012). Comparative analysis between stress and strain based forming limit diagrams for aluminum alloy sheet Transactions of Nonferrous Metals Society of China 22: 343−349.

Filip R, Kubiak K, Ziaja W, Sieniawski J, (2003). The effect of microstructure on the mechanical properties of two-phase titanium alloys. Journal of Material Processing Technology,133:84–89.

Findley WN, Michno MJ, (1976). A historical perspective of yield surface investigations for Metals. International Journal of Non-Linear Mechanics 11:59–80.

Gao CY, Zhang LC, Yan HX, (2011). A new constitutive model for HCP metals. Material Science and Engineering A, 528:4445–4452.

Geiger M, Hubnatter W, Merklein M, (2005). Specimen for anovel concept of the biaxial tension test. Journal of Material Processing Technology, 167:177–183.

Ghosh AK, (1975). The effect of lateral drawing-in on stretch formability. Metals Engineering Quarterly, 15:53–64.

Ghosh AK, Hecker SS, Keeler SP, (1985). Sheet metal forming and testing. In: Dieter FE (ed) Workability testing technique. ASM, Metals Park, OH, 135–195.

Goodwin GM, (1968). Application of strain analysis to sheet metal forming problems in the press shop. SAE Technical Paper, 60: 764–774.

Goto DM, et al., (2000). The Mechanical Threshold Stress Constitutive-Strength Model Description of HY-100 Steel 31 (8): 985-989.

Green DE, et al., (2004). Experimental investigation of the biaxial behaviour of an aluminum sheet International Journal of Plasticity, 20 (8-9):1677–1706.

Gupta AK, Anirudh VK, Singh SK, (2013). Constitutive Models to Predict Flow Stress in Austenitic Stainless Steel 316 at Elevated Temperatures. Materials & Design, 43: 410-418.

Gupta AK, Singh SK, Reddy S, Hariharan G, (2012). Prediction of flow stress in dynamic strain aging regime of austenitic stainless steel 316 using artificial neuralnetwork. Materials and Design,35:589–595.

Gutscher G, Wu HC, Ngaile G, Altan T, (2004). Determination of flow stress for sheet metal forming using the viscous pressure bulge (VPB) test. Journal of Material Processing Technology, 146: 1–7.

Hannon A, Tiernan P, (2008). A review of planar biaxial tensile test systems for sheet metal. Journal of materials processing technology, 198:1–13.

Hecker S, (1972). A simple forming limit curve technique and results on aluminum alloys. Proceedings of the IDDRG Congress, Amsterdam, 5.1–5.8.

Hill R, (1950). The mathematical theory of plasticity. Clarendon, Oxford.

Hill R, (1952). On discontinuous plastic states with special reference to localized necking in thin sheets. Journal of the Mechanics and Physics of Solids, 1:19–30.

Hol J, (2009). Optimization of the stretch forming process using the finite element method, Master Thesis, University of Twente.

Hollomon JH, (1945). Tensile deformation. Trans. AIME 162:268-290.

Holmedal B, (2007). On the formulation of the mechanical threshold stress model. Acta Materialia, 55:2739–2746.

Hora P, Tong L, (1994). Prediction methods for ductile sheet metal failure using FE simulation. In: Barata da Rocha A (ed) Proceedings of the IDDRG Congress, Porto, 363–375.

Hosford W, Canddell R, (2014). Metal forming mechanics and metallurgy. 3rd ed. Cambridge University Press, Cambridge, 52–75.

Hosford WF, (1972). A generalized isotropic yield criterion. Journal of Applied Mechanics, 39:607–609.

Jones C, (2001). Biaxial testing of polymer composites. Mater. World, 9 (11): 19–21.

Keefe AC, Carman, GP, Jardine P, (1998). Torsional behavior of shape memory alloys. Journal of Smart Structure Materials, 3324:58–67.

Keeler SP, (1965). Determination of forming limits in automotive stampings. SAE Technical Paper, 42: 683–691.

Keeler SP, Brazier WG, (1977). Relationship Between Laboratory Material Characterization and Press-Shop Formability, Proceedings, Union Carbide Corporation, 517–530.

Keum, YT, Ghoo BY, Waginer RH, (2001). 3-Dimensional finite element analysis of non-isothermal forming processes for non-ferrous sheets. Simulation of Materials Processing: Theory, Methods and Applications, A.A. Balkema, Lisse, 813–818.

Khan AS, Suh YS, Kazmi R, (2004). Quasi-static and dynamic loading responses and constitutive modeling of titanium alloys. International Journal of Plasticity, 20:2233–2248.

Khan AS, Kazmi R, Farrokh B, (2007). Multiaxial and non-proportional loading responses, anisotropy and modeling of Ti–6Al–4V titanium alloy over wideranges of strain rates and temperatures. International Journal of Plasticity, 23:931–950.

Koç M, Altan T, (2001_a). An overall review of the tube hydroforming (THF) technology. Journal of Material Processing Technology, 108(3):384–393.

Koç M, Aueulan Y, Altan T, (2001_b). On the characteristics of tubular materials for hydroforming - experimentation and analysis. International Journal of Machine Tools Manufacturing, 2001, 41(5):761–772.

Koç M, Eren Billur, Ömer Necati Cora, (2011). An experimental study on the comparative assessment of hydraulic bulge test analysis methods. Materials and Design, 32:272–281.

Lange K., (1985). Handbook of metal forming. McGraw-Hill publications, New York.

Lankford WI, Snyder SC, Bauscher JA, (1950). New Criteria for Predicting the Press Performance of Deep-drawing Sheets. Trans. ASM, 42 :1196-1232.

Lars Olovsson, Kjell Simonsson, Mattias Unosson, (2005). Selective mass scaling for explicit finite element analyses. International Journal for Numerical Methods in Engineering, 63(10):1436–1445.

Lee WS, Lin CF, (1998). Plastic deformation and fracture behaviour of Ti–6Al–4V alloy loaded with high strain rate under various temperatures. Mater Science and Enginnering A, 241:48–59.

Leu, DK, Wu J, (2004). A Simplified Approach to Estimate Limiting Drawing Ratio and Maximum Drawing Load in Cup Drawing. Journal of Engineering Materials and Technology, 126: 116-122.

Li D, Ghosh A, (2004). Biaxial warm forming behavior of aluminum sheet alloys. Journal of Material Processing Technolology, 145:281–293.

Liang RQ, Khan AS, (1999). A critical review of experimental results and constitutive models for BCC and FCC metals over a wide range of strain rates and temperatures. International Journal of Plasticity, 15:963–980.

Lin SB, Ding JL, (1995). Experimental study of the plastic yielding of rolled sheet metals with the cruciform plate specimen. International Journal of Plasticity, 11(5):583–604.

Lin YC, Chen MS, Zhang J, (2008). Constitutive modeling for elevated temperature flow behavior of 42CrMo steel. Computational Material Science,424: 470–477.

Lin YC, Chen MS, Zhong J, (2009). Effects of deformation temperatures on stress/strain distribution and microstructure evolution of deformed 42CrMo steel. Materials and Design, 30:908–913.

Lin YC, Chen XM, (2011). A critical review of experimental results and constitutive descriptions for metals and alloys in hot working. Materials and Design, 32:1733–1759.

Liu C, Huang Y, Stout MG, (1997). On the asymmetric yield surface of plastically orthotropic materials: A phenomenological study. Acta Materialia, 45:2397–2406.

Lütjering G, Williams JC, (2003). Titanium. Springer-Verlag Berlin Heidelberg.

Makinde A, Thibodeau L, Neale KW, (1992). Development of a apparatus for biaxial testing for cruciform specimens. Journal of Experimental Mechanics, 32:138–144.

Makinouchi A, (1996). Sheet metal forming simulation in industry, Journal of. Material .Processing. Technolology. 60: 19–26.

Marciniak Z, Kuckzynski K, (1967). Limit strains in the process of stretch-forming sheet metal. International Journal of Mechanical Sciences, 9:609–620.

Marciniak Z, Duncan, JL, Hu SJ, (2002). Mechanics of Sheet Metal Forming, 2nd Edition, Butterworth-Heinemann, Oxford.

Medellín CH et al., (2013). Analysis of the allowable deep drawing height of rectangular steel parts. International Journal of Advance Manufacturing Technology, 66(1–4):371–380.

Moshksar MM, Mansorzadeh S, (2003). Determination of the forming limit diagram for Al 3105 sheet Journal of Materials Processing Technology, 141: 138–142.

Nakazima K, Kikuma T, Hasuka K, (1971). Study on the formability of steel sheets. Yawata Technical Report No. 284, 678–680.

Narayanasamy R, Sathiya Narayanan C, (2007). Experimental analysis and evaluation of forming limit diagram for interstitial free steels. Materials and Design 28: 1490–1512.

Naumenko VP, Atkins AG, (2006). Engineering assessment of ductile tearing in uniaxial and biaxial tension. International Journal of Fatigue, 28:494–503.

Nemat Nasser S, et al., (2001). Dynamic response of conventional and hot iso-statically pressed Ti–6Al–4V alloys: experiments and modeling. Journal of Mechanics of Materials, 33:425–439.

Nguyen DT, Kim YS, Jung DW, (2012). Flow stress equations of Ti-6Al-4V titanium alloy sheet at elevated temperatures. International Journal of Precision Engineering and Manufacturing, 13(5): 747–751.

Nielsen KB, (1997). Sheet metal forming simulation using explicit finite element methods. 3rd edition, Aalborg University, Denmark.

Novotny S, Geiger M, (2003). Process design for hydroforming of lightweight metal sheets at elevated temperatures. Journal of Materials Processing Technology, 138: 594–599.

Odenberger Eva Lis, (2005). Material characterization for analyses of titanium sheet metal forming. Sweden: Luleå University of Technology.

Odenberger EL, Schill M, Oldenburg M, (2013). Thermo-mechanical sheet metal forming of aero engine components in Ti–6Al–4V—PART 2: Constitutive modelling and validation. International Journal of Material Forming, 6:403–416.

Olsen TY, (1920). Machines for ductility testing. Proceedings of the American Society for Testing and Materials 20:398–403.

Picu R, Majorell A, (2002). Mechanical behavior of Ti–6Al–4V at high and moderate temperatures—Part II: constitutive modeling. Material Science and Engineering A, 2:306–316.

Pöhlandt K, Banabic D, Lange K, (2002). Equi-biaxial anisotropy coefficient used to describe the plastic behavior of sheet metal. Proceedings of the ESAFORM Conference, Krakow,723–727.

Poondla N, Srivatsan TS, Patnaik A, Petraroli M, (2009). A study of the microstructure and hardness of two titanium alloys: Commercially pure and Ti–6Al–4V. Journal of Alloys and Compounds, 486:162–167.

Ramaekers, J, (1999). A Relation between the Limit-Drawing Ratio LDR and the Material Properties: Strain-Hardening Exponent (n) and Anisotropy Factor (R), Advanced Technology of Plasticity, Proceedings of the 6th ICTP, 2: 1997-1404.

Rees DW, (1995). Plastic flow in the elliptical bulge test. International Journal of Mechanical Sciences, 37(4):373–389.

Sansot Panich, et al., (2013). Experimental and theoretical formability analysis using strain and stress based forming limit diagram for advanced high strength steels. Materials and Design, 51: 756–66.

Saxena Ravindra, Dixit PM, (2009). Finite element simulation of earing defect in deep drawing, International Journal of Advanced manufacturing Technology, 45 (3-4): 219-233.

Schuler, (1998). Metal Forming Handbook. Springer Berlin Heidelberg.

Seshacharyulu T, Medeiros SC, Frazier WG, et al., (2000). Hot working of commercial Ti–6Al–4V with an equiaxed α–β microstructure: materials modeling considerations. Mater Science and Engineering A, 284:184–194.

Shin H, Kim JB, (2010). A phenomenological constitutive equation to describe various flow stress behaviors of materials in wide strain rate and temperature regimes. Journal of Engineering Materials and Technology, 132:021009, doi: 10.1115/1.4000225.

Siguang XU, Klaus J, Weinmann, (1998). Prediction of forming limit curves of sheet metals using Hill's 1993 user-friendly yield criterion of anisotropic materials. Journal of Mechanical Sciences, 40 (9): 913- 925.

Singh SK, Ravi Kumar D, (2008). Effect of process parameters on product surface finish and thickness variation in hydro-mechanical deep drawing. Journal of Material Processing Technology, 204:169–178.

Singh SK, et al., (2010). Understanding formability of extra-deep drawing steel at elevated temperature using finite element simulation. Materials and Design, 31:4478–4484.

Swift HW, (1952). Plastic instability under plane stress. Journal of the Mechanics and Physics of Solids, 1:1–18.

Takuda H, Mori K, et al., (2003). Finite element analysis of the formability of an austenitic stainless steel sheet in warm deep drawing. Journal of Material Processing Technology, 143:242–248.

Taylan, Soo-Ik Oh, Gegel H.L., (1983). Metal forming: fundamentals and applications. American Society for Metals, Vol.1 of ASM series in metal processing.

Tekkaya AE, (2000). State-of-the-Art of Simulation of Sheet Metal Forming. Journal of Materials Processing Technology, 103 (1):15-23.

Toussaint F, Tabourot L, Ducher F, (2008). Experimental and numerical analysis of the forming process of a CP titanium. Journal of Material Processing Technology, 197(1-3): 10-16.

Thomas W, Altan T (1998). Application of computer modelling in manufacturing of automotive stampings. Journal of Steel Res. 69 (4/5) :181–187.

Van den Boogaard AH, Huétink J, (2006). Simulation of aluminium sheet forming at elevated temperatures. Computer Methods in Applied Mechanics and Engineering, 195:6691–6709.

Weilong H, Wang ZR, (2002). Anisotropic Characteristics of Material and basic Selecting Rules with Different Sheet Metal Forming Processes. Journal of Materials Processing Technology, 127: 374-381.

Xiang-Dong W, Wan M, Xian-Bin Z, (2005). Biaxial tensile testing of cruciform specimen under complex loading. Journal of Material Processing Technology, 168:181–183.

Xiao YH, Guo C, (2011). Constitutive modelling for high temperature behavior of 1Cr12Ni3Mo2VNbN martensitic steel. Materials Science and Engineering A, 528:5081–5087.

Xiaoqiang Li, et al., (2014). Constitutive modeling and the effects of strain-rate and temperature on the formability of Ti–6Al–4V alloy sheet Materials and Design, 55:325–334.

Yong Y, et al., (2002). Design of a cruciform biaxial tensile specimen for limit strain analysis by FEM. Journal of Material Processing Technology, 123:67–79.

Yoon JW, et al., (1999). A general elasto-plastic finite element formulation based on incremental deformation theory for planar anisotropy and its application to sheet metal forming. International Journal of Plasticity, 15:35–67.

Yoon JW, Barlat F, (2006). Modeling and simulation of the forming of aluminium sheet alloys. In: Semiatin SL (ed) ASM handbook, Vol 14B, Metalworking: Sheet forming. ASM International, Materials Park, OH, 792–826.

Yu MH, (2002). Advances in strength theories for materials under complex stress state in the 20th century. Applied Mechanics Reviews, 55:198–218.

Zerilli PJ, Armstrong RW, (1987). Dislocation-mechanics-based constitutive relations for material dynamics calculations. Journal of Applied Physics,61:1816–1825.

Zerilli FJ, Armstrong RW, (1995). High strain rate effects on polymer, metaland ceramic matrix composites and other advanced materials. ASME, NewYork.

Zhang SH, et al., (2007). Deep-drawing of magnesium alloy sheets at warm temperatures. Journal of Materials Processing Technology, 185:147–151.

Zyczkowski M, (1981). Combined loadings in the theory of plasticity. Polish Scientific Publishers, Warsaw.

LIST OF PUBLICATIONS

(I) International Journals:

Published:

1. Nitin Kotkunde, Hansoge Nitin Krishnamurthy, Pavan Puranik, Amit Kumar Gupta, Swadesh Kumar Singh. Microstructure study and constitutive modeling of Ti–6Al–4V alloy at elevated temperatures, Journal of Materials and Design 2014; 54: 96–103.
2. Nitin Kotkunde, Aditya D. Deole, Amit Kumar Gupta, Swadesh Kumar Singh. Comparative study of constitutive modeling for Ti–6Al–4V alloy at low strain rates and elevated temperatures, Journal of Materials & Design 2014; 55: 999-1005.
3. Nitin Kotkunde, Aditya D. Deole, Amit Kumar Gupta, Swadesh Kumar Singh. Failure and formability studies in warm deep drawing of Ti-6Al-4V alloy, Journal of Materials & Design 2014; 60: 540–547.
4. Nitin Kotkunde, Aditya D. Deole, Amit Kumar Gupta, Swadesh Kumar Singh, Experimental and numerical investigation of anisotropic yield criteria for warm deep drawing of Ti–6Al–4V alloy, Materials and Design 63 (2014) 336–344.
5. Nitin Kotkunde, Aditya D Deole, Amit Kumar Gupta, Swadesh Kumar Singh, Analysis of Thickness Strain Prediction in Warm Deep Drawing of Ti-6Al-4V Alloy, Journal of Advanced Materials Research 979 (2014) 52-56.

Under review:

6. Nitin Kotkunde, Geetha Krishna, Shyam Krishna Shenoy, Amit Kumar Gupta, Swadesh Kumar Singh, Experimental and Theoretical investigation of forming limit

diagram for Ti-6Al-4V alloy at warm condition, Under review in International Journal of Material Forming, Springer publication.

7. Nitin Kotkunde, Sashank Srinivasan, Geetha Krishna, Amit Kumar Gupta, Swadesh Kumar Singh, Influence of Material Models on Theoretical Forming Limit Diagram Prediction for Ti-6Al-4V Alloy at Warm Condition, Under review in Transactions of Nonferrous Metals Society of China, Elsevier publication.
8. Nitin Kotkunde, Abhijeet Arote, Amit Kumar Gupta, Swadesh Kumar Singh, Experimental and Finite Element Investigations of Forming Behavior in Ti-6Al-4V alloy at Elevated Temperature, Under review in Journal of Manufacturing Processes, Elsevier publication.

(II) Book Chapter

1. Nitin Kotkunde, Aditya D. Deole, Amit Kumar Gupta, Swadesh Kumar Singh. Numerical Analysis of Warm Deep Drawing for Ti–6Al–4V Alloy, Accepted in Advances in Material Forming and Joining, 2015, Springer publication.

(III) International Conferences

Published

1. Nitin Kotkunde, Amit Kumar Gupta, Nitin Krishnamurthy, Pavan Puranik, Swadesh Kumar Singh. Flow stress prediction of Ti-6Al-4V Alloy using Modified Johnson-Cook Model. Third Asian Conference on Mechanics of Functional Materials and Structures (ACMFMS) December 5-8, 2012, IIT-Delhi, New Delhi, pp. 799-802.

2. Nitin Kotkunde, Amit Kumar Gupta, Nitin Krishnamurthy, Pavan Puranik, Swadesh Kumar Singh. Study of Flow Stress Analysis for Ti-6Al-4V Alloy using Modified Zerilli-Armstrong Model. International Conference on Advances in Materials Processing and Characterisation (AMPC) February 6-8, 2013, Anna University, Chennai, pp. 933-939.
3. Nitin Kotkunde, , Nitin Krishnamurthy ,Amit Kumar Gupta, Swadesh Kumar Singh. Development of Modified Arrhenius Model for Ti-6al-4V Alloy to Predict the Flow Stress. 3rd International conference on Material Processing and Characterization (ICMPC), March 2013, pp. 83-87.
4. Nitin Kotkunde, Aditya Deole, Amit Kumar Gupta, Swadesh Kumar Singh. Development of Constitutive models for Ti–6Al–4V alloy over wide ranges of strain rates and temperatures. International conference on Precision, Meso, Micro and Nano Engineering (COPEN 8), December, 2013 NIT Calicat, pp. 1011-1016.
5. Nitin Kotkunde, Aditya Deole, Amit Kumar Gupta, Swadesh Kumar Singh. A comparative study on Modified Johnson Cook and Fields–Backofen constitutive models to predict flow behavior of Ti-6Al-4V alloy sheet at elevated temperature. International conference on Computer Aided Engineering, December, 2013, IIT Madras, Chennai, pp. 419-423.
6. Nitin Kotkunde, Aditya D. Deole, A.K Gupta, S.K Singh. Effect of Process Parameters on Deep Drawing of Ti-6Al-4V Alloy Using Finite Element analysis. 9th International conference and workshop on numerical simulations of 3D sheet metal forming processes (NUMISHEET-2014), AIP Conference preceding 1567, Melbourne, Australia, Jan., 2014, pp. 1065-1068.
7. Nitin Kotkunde, Amit Kumar Gupta, Swadesh Kumar Singh, " Experimental and Finite Element Studies of Warm Deep Drawing of Ti-6Al-4V Alloy" Advances in Materials and Processing Technology (AMPT) Conference, Nov, 2014, Dubai.

8. Nitin Kotkunde, Sachin Rane, Amit Kumar Gupta, Swadesh Kumar Singh, “Analysis of warm deep drawing of Ti-6Al-4V” 5th International and 26th AIMTDR, IIT Guwahati, Assam India, Dec, 2014, pp 496-501.
9. Nitin Kotkunde, Amit Kumar Gupta, Swadesh Kumar Singh, " Experimental and Numerical Studies of Warm Formability for Ti-6Al-4V Alloy" 23rd International Conference on processing and fabrication of Advanced Materials, December, 2014, IIT Roorkee, pp 1064-1074.
10. Swadesh Kumar Singh, Nitin Kothkunde, Geetha Krishna and Amit Kumar Gupta, Analysis of Formin Limit Curve for Ti-6Al-4V alloy at warm condition. 26th International Symposium on Plasticity 2015 and Its Current Applications, Montego Bay, Jamaica, Jan., 2015 pp 172-174.
11. Nitin Kotkunde, Amit Kumar Gupta, Analysis of Forming Limit Diagram for Ti-6Al-4V Alloy. 5th International conference on Material Processing and Characterization (ICMPC), Accepted for Materials today proceeding (Elsevier publisher).

BRIEF BIOGRAPHY OF THE SUPERVISOR

Name of the supervisor	Dr. Amit Kumar Gupta
Qualifications	PhD
Designation and Address	Associate Professor, Mechanical Engineering Department, BITS-Pilani, Hyderabad Campus.
Experience (years)	8
Number of Publications	International Journals : 40 Book Chapter : 1 International Conferences : 49
No. of Ph.D. students supervised	1

BRIEF BIOGRAPHY OF THE CANDIDATE

Name of the candidate	Nitin Ramesh Kotkunde
ID No	2012PHXF542H
Designation and Address	Lecturer, Mechanical Engineering Department, BITS-Pilani, Hyderabad Campus.
Number of Publications	International Journals : 5 Book Chapter : 1 International Conferences : 11